SPONSORED BY

Celanese

The chemistry inside innovation™

2022 Combined UHMWPE, PEEK, & POLYMER IMPLANT ADDITIVE Manufacturing Conference

JUNE 23-24, 2022

"Unione Industriale" Congress Center, Torino Italy

Hosted by the University of Torino and Drexel University

ADDITIONAL SPONSORS

EVONIK Leading Beyond Chemistry

Invibio BIOMATERIAL SOLUTIONS

KUMOVIS a 3D Systems company

MITSUBISHI CHEMICAL ADVANCED MATERIALS

Orthoplastics A VIANT COMPANY science making a material difference

SEQENS

2022 Combined UHMWPE, PEEK, & POLYMER IMPLANT ADDITIVE Manufacturing Conference

Thursday & Friday, June 23-24, 2022
"Unione Industriale" Congress Center
Torino, Italy

The purpose of the meeting is to bring together engineers, scientists, regulators, and clinicians from academia, industry, and government to present leading edge research on advancements in medical grade UHMWPE, PEEK, and the rapidly growing field of polymer implant additive manufacturing technology. In addition to UHMWPE and PEEK, the Combined Meeting will also broadly showcase point-of-care additive manufacturing of implantable polymers.

Scientific and Organizing Committee and Invited Speakers:

Co-Presidents: Pierangiola Bracco, Ph.D. and Steven Kurtz, Ph.D.
PD Dr. mult. Florian Thieringer, MHBA
Hannah Spece, Ph.D.
Ebru Oral, Ph.D.
Orhun Muratoglu, Ph.D.
Mark Allen
Sebastian Pammer

Organizer: Hannah Spece, Ph.D.

Sponsorship

We are pleased to announce that Celanese will be supporting the 2022 Combined Meeting as a Platinum Sponsor. We also welcome the sponsorship of Orthoplastics, Kumovis, Invibio and Evonik as Silver Sponsors; and Mitsubishi Chemical Advanced Materials and Seqens as Bronze Sponsors.

2022 Combined
UHMWPE, PEEK,& POLYMER IMPLANT ADDITIVE
Manufacturing Conference

CONFERENCE
AGENDA

Thursday, June 23, 2022 | Day One

7:00 AM	**On Site Registration Opens**
8:30 AM	**Opening Remarks** Steven Kurtz, Ph.D.
8:45 AM	**Welcome** Amanda Dresch, Celanese
	SESSION I: Clinical Performance and New Applications of Polyethylene Biomaterials Session Co-Moderators: Anuj Bellare & Pierangiola Bracco
8:50 AM	**Invited Talk 1: Advanced Manufacturing of Drug Eluting, Ethyl Vinyl Acetate Implants** Presenter: Amanda Dresch
9:15 AM	**Podium Talk 1: Systematic Review of Vitamin E HXLPE Clinical Performance** Presenter: Hannah Spece, Ph.D.
9:30 AM	**Podium Talk 2: Effect of accelerated aging on UHMWPE stabilized by Vitamin E and Tetracycline Antibiotic** Presenter: Veronika Gajdošová, Ph.D.
9:45 AM	**Podium Talk 3: Tribological Behavior of a Total Lumbar Disc Replacement in Clean, Aggressive, and Impingement Loading Conditions** Presenter: Ryan Siskey, M.S.
10:00 AM	**Morning Coffee Break**
10:45 AM	**Podium Talk 4: Performance of PEEK Telescopic Crowns** Presenter: Andreas Schwitalla, DDS

11:00 AM	**Podium Talk 5: Czech-Italian-Spanish database of explanted UHMWPE liners: Evaluation of oxidative degradation, structure changes and micromechanical properties of the explanted polymer components of total joint replacements** Presenter: Miroslav Slouf, Ph.D.
11:15 AM	**Rapid Fire Talks: 5 minute presentations of selected UHMWPE and Implant Polymer posters – no discussion until poster session**
12:00 PM	**Buffet Lunch and POSTER SESSION**
	SESSION II: Advances in Processing, Crosslinking, and Additives Session Co-Moderators: Steve Kurtz & Francisco Medel
1:30 PM	**Invited Talk 2: Advances in Therapeutic HXLPE** **Presenter: Ebru Oral, Ph.D.**
2:00 PM	**Podium Talk 6: Development and Clinical Introduction of Chemically Crosslinked HXLPE** Presenter: Orhun Muratoglu, Ph.D.
2:15 PM	**Podium Talk 7: A New Bulk Lamellar Polyethylene Morphology Induced Using High-Rate Pressurization** Presenter: Anuj Bellare, Ph.D.
2:30 PM	**Podium Talk 8: Static fracture and cyclic fatigue resistance of split-dose irradiated AOX TM UHMWPE** Presenter: Leandra Bowsman
2:45 PM	**Podium Talk 9: The efficacy of antibiotic-eluting materials in a two stage model of periprosthetic joint infection** Presenter: Ebru Oral, Ph.D.
3:00 PM	**Afternoon Coffee Break**

3:00 PM **Afternoon Coffee Break**
SESSION III: In Vivo Performance and Clinical Applications of Polymer Biomaterials

Session Co-Moderators: Miroslav Slouf & Pierangiola Bracco

3:45 PM **Invited Talk 3: Drug Delivery Via Composite Implant Manufacturing**
Presenter: Mark Allen

4:15 PM **Podium Talk 10: Bioresorbable Polymers in Additive Manufacturing: How Material Characteristics and Printing Process Parameters Impact Medical Device Performance?**
Presenter: Cécile Boudot, Ph.D.

4:30 PM **Podium Talk 11: Evaluation of debris generated from the mechanical testing of continuous carbon fibre reinforced PEEK plates**
Presenter: Shiling Zhang, Ph.D.

4:45 PM **Day 1 Meeting Adjourns**

6:00 PM **Transition to Gala Dinner**
Museo Egizio (Egyptian Museum)

2022 Combined
UHMWPE, PEEK,& POLYMER IMPLANT ADDITIVE
Manufacturing Conference

CONFERENCE
AGENDA

Friday, June 24, 2022 | Day Two

8:30 AM **On Site Registration Opens**
SESSION IV: Properties and Behavior of PAEK Biomaterials

Session Co-Moderators: Steve Kurtz & Oana Ghita

9:00 AM **Invited Talk 4: Clinical Experience and Design Considerations for Trauma and Extremity Plates Made From Continuous Carbon Fiber Reinforced PEEK**
Presenters: Jo Wilson, Ph.D.
Bradley Cowan
Sherri Gambill

9:30 AM **Invited Talk 5: PEKK is the Innovative Material for Printed Medical Implants**
Presenter: Alexandra Ngawa Zenang

10:00 AM **Invited Talk 6: Osseointegration Evaluation of VESTAKEEP® Fusion using a Preclinical Sheep Model**
Presenters: Mahrokh Dadsetan, Ph.D.
Philip Engel, Ph.D.

10:30 AM **Podium Talk 12: Contamination- and Distortion-Free Solidification of PEEK on a Non-adherent Substrate for 3D Printing Medical Products**
Presenter: Uwe Popp

10:45 AM **Morning Coffee Break**

11:30 AM **Podium Talk 13: Additive manufacturing of PEEK cranial implants: Powder Bed Fusion or Material Extrusion?**
Presenter: Yaan Liu, Ph.D.

11:45 AM **Podium Talk 14: Biomechanically Tuning the Strength and Stiffness of an Open Pillar Implant Interface**
Presenter: Greg Causey, Ph.D.

12:00 PM	**Podium Talk 15: 3D Direct-Printed PEEK Has Longer High-Cycle Fatigue Life to Machined 3D Printed PEEK** Presenter: Leandra Bowsman
12:15 PM	**Rapid Fire Talks: 5 minute presentations of selected PAEK and AM posters – no discussion until poster session**
12:45 PM	**Buffet Lunch and POSTER SESSION**
	SESSION VI: Point of Care 3D Printing Session Co-Moderators: Dave Schroeder & Ryan Siskey
2:15 PM	**Invited Talk 7: MDR-compliant Medical Device Production System for PEEK CMF-implants** Presenter: Sebastian Pammer
2:45 PM	**Invited Talk 8: Point of Care 3D Printing of PEEK Implants: The University Hospital Basel Perspective** Presenter: PD Dr. mult. Florian Thieringer, MHBA
3:15 PM	**Invited Talk 9: Regulatory Considerations for POC 3D Printing of Medical Devices** Presenter: Matthew DiPrima, Ph.D.
3:45 PM	**Afternoon Coffee Break**
	SESSION VI: Advances in 3D Printed Biomaterials and Composites Session Co-Moderators: Florian Theiringer & Ryan Siskey
4:30 PM	**Podium Talk 16: Optimizing Flexural Strength of CF-PEKK for Fracture Fixation** Presenter: Aliza Rabinowitz

4:45 PM **Podium Talk 17: Extraordinary Interfacial Behaviors of Osteofab™ (Powder Bed Fusion of PEKK (PolyEtherKetoneKetone) Polymer) Orthopedic Devices - Anti-Microbial and Bone Apposing Effects Observed in the Absence of Surface Modification – an Overview**
Presenter: Tony DeCarmine

5:00 PM **Podium Talk 18: 3D-Printed Silicon Nitride-PEEK Composite Promotes In Vitro Osteogenic Activity and Mineralization**
Presenter: Paul DeSantis, M.S.

5:15 PM **Closing Remarks**
Steven Kurtz, Ph.D.

5:30 PM **Meeting Adjourns**

2022 Combined
UHMWPE, PEEK,& POLYMER IMPLANT ADDITIVE
Manufacturing Conference

POSTER
PRESENTATIONS

Title: Will cement in your cup cause dramatic failure? A Geometric Analysis of Polyethylene Liners Exposed to Acrylic-based Bone Cement
Presenter: Zoe Thompson

Title: Migration of the femoral component and clinical outcomes after total knee replacement: a narrative review
Presenter: Domenico Alesi

Title: Causes of stiffness after total knee arthroplasty: a systematic review
Presenter: Domenico Alesi

Title: Retrieval Analysis and Comparison Between Blended and Diffused Vitamin E HXLPE Components for TKA
Presenter: Tabitha Derr

Title: Fatigue Crack Propagation Assessment of Unfilled and Carbon Fiber Reinforced PEEK using a Compliance Approach
Presenter: Clare Rimnac, Ph.D.

Title: Enhanced Pre-Clinical Wear Simulation of an All-Polymer Total Knee Replacement
Presenter: Raelene Cowie, Ph.D.

Title: In Vitro Wear Performance of X-ray Cross-Linked Vitamin E Blended Polyethylene
Presenter: Rainer Bargon, Ph.D.

Title: Experimental and Computational Modelling Assessment of Edge Loaded Marathon Total Hip Replacement Liners
Presenter: Nicholas Cooper

Title: Evaluation of mechanical properties of PEEK filled materials and nanoscale observations
Presenter: Ryan Siskey, M.S.

Title: Additive Manufactured PEEK Scaffold: Understanding the AM Process Capability
Presenter: Chaozong Liu, Ph.D.

Title: Adjustment of simulation models for essential work of fracture tests of polymeric materials intended for biomedical applications
Presenter: Francisco Javier Pascual Aranzana

Title: Application of a Composite Silicon Nitride-PEKK Coating to a Titanium Alloy Substrate to Provide Enhanced Infection Resistance and Tissue Integration
Presenter: Ryan Bock, Ph.D.

SPECIAL THANKS

to all the sponsors & attendees at the 2022 Conference!

2022 Combined UHMWPE, PEEK, & POLYMER IMPLANT ADDITIVE Manufacturing Conference

In Vivo Performance of Vitamin E-Doped Polyethylene Implants: A Systematic Review

Hannah Spece[1], Ron Yarbrough[2], Steven M. Kurtz[1]

[1] Drexel University, Philadelphia, PA
[2] 3Spine Inc., Chattanooga, TN

hgs29@drexel.edu

Introduction:
Vitamin E stabilization was introduced to improve the oxidative stability, wear resistance, and mechanical properties of highly crosslinked polyethylene (HXLPE) used in total joint arthroplasty (TJA). Existing reviews for vitamin E-stabilized polyethylene (VEPE) often report that VEPE demonstrates wear resistance superior to conventional ultrahigh molecular weight polyethylene (UHMWPE) and may lead to decreased risk for osteolysis and implant loosening. Given the limited scope of some previous reviews and the recent increase in VEPE-related studies, an updated review of the literature is warranted.

The aim of this systematic review is to provide an overview of *in vivo* performance for vitamin E UHMWPE and comparison with non-stabilized UHMWPE published in the literature. We also aimed to determine whether the use of VEPE has expanded beyond lower extremity arthroplasty devices and if there are reports of VEPE in spinal or upper extremity implants.

Methods and Materials:
The Preferred Reporting Items for Systematic Review and Meta-Analyses (PRISMA) guidelines were used. A systematic review of the literature was performed using PubMed and Embase on May 18, 2022, using search terms: (UHMWPE OR polyethylene OR HXLPE) AND (vitamin E OR "alpha-tocopherol" OR "α-tocopherol") AND (implant* OR Arthroplasty OR "Joint replacement" OR prosthesis OR orthopaedic OR orthopedic OR spinal OR spine OR "upper extremity" OR shoulder OR elbow OR histolog*). The database searches resulted in 253 studies from PubMed, 381 from Embase, and 1 from source bibliographies, totaling 370 unique papers. Following title/abstract screening and assessment of full texts according to inclusion/exclusion criteria, 48 studies were included for review.

Results:
We reviewed 39 cohort studies, 5 case studies, and 4 retrieval analyses. For the cohort and retrieval studies, most (n = 28/43) compared VEPE with a control group of either conventional UHMWPE or HXLPE. The number of implants in the cohort studies ranged from 34 to 53842 (range 17 to 5069 for VEPE alone) with follow-up time ranging from 2 to 11 years. For THA studies, average wear rate measured as femoral head penetration ranged from 0.0 to 0.38 mm/year. Steady-state wear rate, with early creep-dominated penetration excluded, tended to be much lower. Most VEPE wear rates were < 0.1 mm/year, the threshold below which osteolysis is not expected to occur. For all studies that compared VE-stabilized and non-stabilized polyethylene, outcomes including material wear, patient reported outcomes, and rates of osteolysis for VEPE were as good or better than the control group. Reports of polyethylene-related complications were infrequent but included component wear and fracture, most of which were reported as single instances. No revisions due to osteolysis and no adverse outcomes related to VEPE were reported.

Across the literature, we found no studies regarding the use of VEPE in spinal applications. For upper extremities we found one report of *in vivo* performance for shoulder arthroplasty.

Conclusion:
Overall, the literature for vitamin E-stabilized HXLPE indicated positive clinical results and supports its safety and efficacy for use in total joint arthroplasty, with much of the research reporting lower wear rates than for conventional UHMWPE and non-stablized HXLPE. Adoption of VEPE for spinal and small joint applications is still limited.

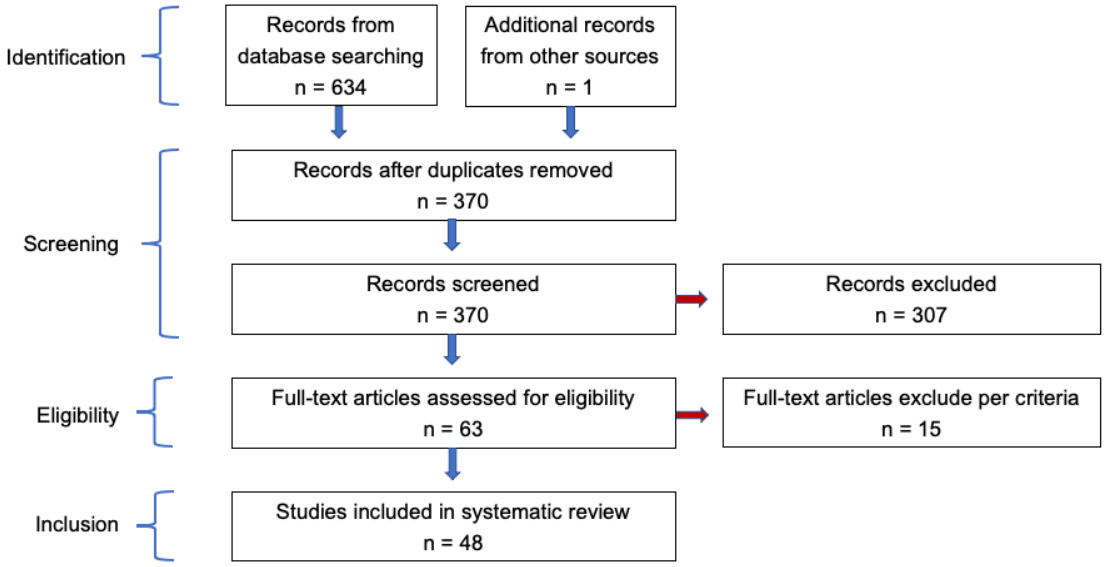
Identification
Records from database searching n = 634
Additional records from other sources n = 1
Screening
Records after duplicates removed n = 370
Records screened n = 370
Records excluded n = 307
Eligibility
Full-text articles assessed for eligibility n = 63
Full-text articles exclude per criteria n = 15
Inclusion
Studies included in systematic review n = 48

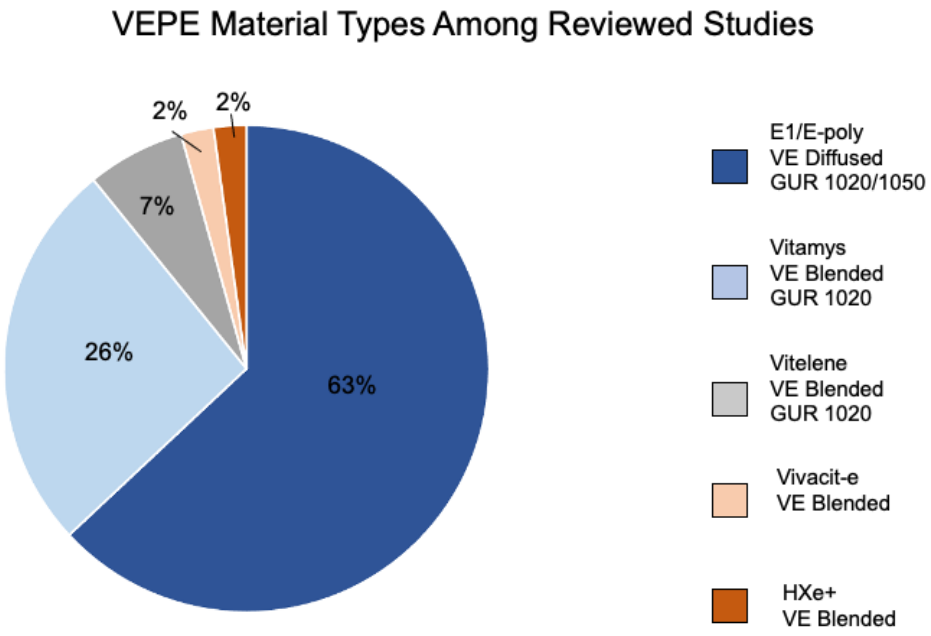
VEPE Material Types Among Reviewed Studies
2%
2%
7%
26%
63%
E1/E-poly VE Diffused GUR 1020/1050
Vitamys VE Blended GUR 1020
Vitelene VE Blended GUR 1020
Vivacit-e VE Blended
HXe+ VE Blended

Effect of accelerated aging on UHMWPE stabilized by Vitamin E and Tetracycline Antibiotic

Gajdosova V[1], Slouf, M[1], Hodan J[1], Michalkova D[1], Gohs U[2], Fulin P[3], Pokorny D[3]
[1]Institute of Macromolecular Chemistry AS CR, Heyrovsky Sq. 2, 162 06 Prague 6, Czech Republic
[2]Institute of Polymer Research Dresden, Hohe Strasse 6, 01 069 Dresden, Germany
[3]1st Orthopedics Clinic of the 1st Faculty of Medicine UK, Hospital Motol, V Uvalu 84, 156 06 Prague 5, Czech Republic
gajdosova@imc.cas.cz

Introduction: UHMWPE wear and oxidative degradation are the most important reasons of total joint replacement failures from the point of view of materials science [1]. The wear resistance is usually increased by radiation-induced crosslinking combined with thermal treatment. The oxidation resistance can be increased by addition of biocompatible stabilizers (α-tocopherol, i.e. vitamin E or tetracycline antibiotic) [1,2]. In this contribution, we introduce the effect of novel stabilization system on the accelerated aged samples.

Methods and Materials: Samples were prepared from UHMWPE powder (M_w = 3×10^6 g/mol; bought from Sigma-Aldrich), which was dry mixed with 0.15 wt. % of stabilizer(s) and compression molded (hot press at 190 °C). For each sample, the first part was unmodified (NN samples), while the other two parts were irradiated with accelerated electrons (100 kGy) and annealed (AN samples; hot press at 110°C/10min) or remelted (RM samples; hot press at 150°C/10min). Control samples were commercial Chirulen 1020 and Chirulen 1020E; all samples are summarized in Table 1. All samples were characterized by OIT (oxidation induction temperature from TGA measurements) and aged in 0.1% H_2O_2 aqueous solution at 70 °C (simulated in vivo aging). All samples were characterized by several microscale methods: LM, SEM, IR, DSC, TGA and microindentation.

Table 1. List of the prepared UHMWPE samples.

Sample ID	Description
Chirulen 1020	Control #1: medical grade UHMWPE
Chirulen 1020E	Control #2: like previous, with 0.1% vit.E
PE	Control #3: compression molded PE powder
PE+E	PE + 0.15% of vitamin E
PE+E+T (2:1)	PE + 0.15% of vit.E and tetracyclin (2:1)
PE+E+T (1:1)	PE + 0.15% of vit.E and tetracyclin (1:1)
PE+E+T (1:2)	PE + 0.15% of vit.E and tetracyclin (1:2)
PE+T	PE + 0.15% of tetracyclin

Results and discussion: Our previous work suggested that combination of vitamin E and tetracycline results in synergistic increase in UHMWPE oxidation resistance [3]. This effect was found to be reproducible, as documented in Fig. 1. Nevertheless, all previous experiments were based on thermooxidation (i.e. resistance of the stabilized samples to heating during TGA experiment).
In this contribution, we show that the synergistic stabilization effect is much weaker during simulated *in vivo* aging (UHMWPE samples submerged in 1% solution of H_2O_2 at 70 °C). This is shown schematically in Fig. 2. The figure is based on combined results from microscopic, spectroscopic and thermogravimetric measurements. The PE+E+T samples (see Table 1) exhibited just a very small increase in oxidation resistance during simulated *in vivo* aging with respect to PE+E sample (right part of Fig. 2). Moreover, PE+E+T and PE+T samples showed similar properties and no synergistic effect of E+T combination.

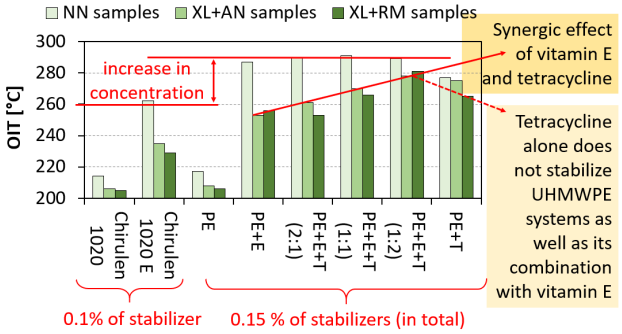

Figure 1. Resistance of the prepared UHMWPE systems to thermooxidation: a synergistic increase in oxidation induction temperature (OIT) for PE+E+T(1:2) sample.

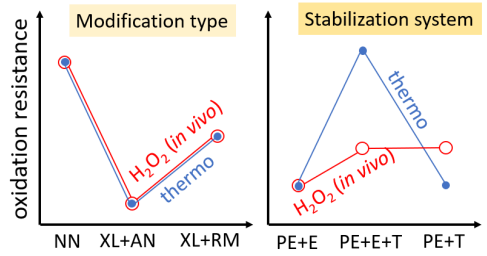

Figure 2. Final resistance of the prepared UHMWPE systems to thermooxidation (blue) and simulated *in vivo* oxidation (red): the semi-quantitative schemes summarize results of LM, SEM, IR and TGA experiments for different modification types (left) and stabilization systems (right).

Conclusions: We have demonstrated that the stabilization system based on the combination of vitamin E and tetracycline increased the UHMWPE thermooxidation resistance more than vitamin E or tetracycline alone. On the other hand, the improvement of oxidation resistance against the accelerated aging in H_2O_2 seemed to be minimal or negligible.

References

[1] Kurtz SM: UHMWPE biomaterials handbook (2016).
[2] Czech patent application CZ 2015-267 A3.
[3] Slouf M et al.: UHMWPE 2019, oral presentation.

Acknowledgement: TN01000008 (TA CR) and NU21-06-00084 (AZV CR).

Performance of PEEK Telescopic Crowns

Schwitalla, AD[1], Priester, M[2], Sütel, M[1], Müller, WD[1]
[1]Charité-Universitätsmedizin Berlin, corporate member of Freie Universität Berlin and Humboldt-Universität zu Berlin, Department of Prosthodontics, Geriatric Dentistry and Craniomandibular Disorders, Berlin, Germany
[2]Dental-Labor Werth & Priester Kassel GmbH & Co KG, Kassel, Germany
andreas.schwitalla@charite.de

Introduction: Telescopic crowns are universal retentive elements for oral rehabilitation of partially edentulous and edentulous patients with implant-supported prostheses. These are composed of the primary crown, which is anchored to a tooth or implant, and the secondary crown, which is integrated into the denture, with the secondary crown being placed on the primary crown. The vertical outer surface of the primary crown, which is parallel to the inner surface of the secondary crown, creates friction that holds the prosthesis in position in the mouth. A fundamental problem is the loss of friction over time. Forces between 3.5 and 7 N are considered sufficient. However, the values given in the literature vary between 0.08 up to 30 N. Values of 13.83 ± 7.82 N were measured for the combination of a primary crown made of zirconia ceramic with PEEK. The aim of the present study was to evaluate the retentive forces between primary and secondary crowns made of PEEK.

Methods and Materials: First, primary crowns were fabricated from PEEK and zirconia ceramic (ZrO_2). These were scanned to design the secondary crowns, which were machined from PEEK. In this way, two material combinations were obtained: ZrO_2 (primary crown) + PEEK (secondary crown) and PEEK (primary crown) + PEEK (secondary crown). Of these, 3 crown pairings were always tested simultaneously in a universal testing machine, with the secondary crowns being pulled off and put back on 10,000 times, corresponding to a lifetime of 13.68 years, at a speed of 10 mm/min and the retentive forces measured.

Results: The ZrO_2+PEEK material combination initially showed a retentive force of 16.46 N, which increased slightly to 24.45 N over the 10000 cycles. The retentive force of the material combination PEEK+PEEK also increased somewhat from 24.87 N initially to 28.23 N at the end of the test.
Surface roughness (Rz) decreased slightly on the PEEK primary crowns from 11.34 ± 0.78 µm to 0.99 ± 0.26 µm, with the roughness of the ZrO_2 primary crowns increasing slightly from 0.59 ± 0.17 µm to 0.87 ± 0.39 µm.

Discussion: The results show that PEEK is suitable for the fabrication of telescopic crowns. Due to its excellent wear behavior, there was no loss of retention force, rather the opposite was the case. With regard to the fabrication of tooth-supported telescopic crowns, it must of course be taken into account that the holding forces are not too high so as not to traumatize the periodontium during removal of the prosthesis. According to the literature, 41 N represents a certain threshold value. This value marks the lower range of forces that were necessary for tooth extractions.

Czech-Italian-Spanish database of explanted UHMWPE liners: Evaluation of oxidative degradation, structure changes and micromechanical properties of the explanted polymer components of total joint replacements

Slouf, M[1], Gajdosova V[1], Dybal J[1], Sticha R[2], Fulin P[2], Pokorny D[2],
Mateo J[3,4], Panisello JJ[3,4], Canales V[5], Medel F[6], Bistolfi A[7], Bracco P[8]
[1] Institute of Macromolecular Chemistry of the Czech Academy of Sciences, Prague, Czech Republic
[2] 1st Orthopedics Clinic of the 1st Faculty of Medicine UK, Hospital Motol, Prague, Czech Republic
[3]Department of Orthopaedic Surgery and Traumatology, Miguel Servet University Hospital, Zaragoza, Spain
[4] Department of Surgery, Medicine School, University of Zaragoza, Spain
[5]Department of Orthopaedic Surgery and Traumatology, Royo Villanova Hospital, Zaragoza, Spain
[6]Department of Mechanical Engineering-Institute of Engineering Research of Aragon, University of Zaragoza, Spain
[7] Cardinal Massaia Hospital, Department of Surgery, Orthopedics and Traumatology. Asti, Italy
[8] Chemistry Department and NIS Centre, University of Torino, Torino, Italy
slouf@imc.cas.cz

Introduction: Analysis of UHMWPE liners from revised total joint replacements (TJR) can yield valuable information for analysis of TJR failures [1]. We introduce the first results from the joint database of UHMWPE retrievals from three European teams located in the Czech Republic (CZ), Italy (IT), and Spain (ES).

Materials and methods: *The explanted UHMWPE components* come from CZ, IT and ES hospitals.
The three databases can be updated independently as they are separate XLSX files (MS Excel). The only requirement is that each database file must contain pre-defined columns with anonymized patient data, manufacturer data (irradiation, thermal treatment etc.), orthopedic evaluation (links to revision protocols), and material characterization (IR microspectroscopy and microindentation). At present the database contains >500 retrievals.
The IR microspectroscopy data (maximum and average values of oxidation index, OI, trans-vinylene index, VI, and crystallinity index, CI, ref. [2]) were evaluated from line profiles (IR spectra as a function of distance from articulating surface). The IR indexes are calculated in a standardized way by means of our package MPint (semi-automatic multiple peak integration; free Python package available at *https://pypi.org/projects/mpint*).
The final data analyses are made with freeware Python scripts and libraries for data processing [3]. The scripts can read arbitrary number of XLSX files (which makes our project flexible and extensible).

Results and discussion: In the first step, we verified if the standardized sample treatment, data collection protocols and IR microscopy evaluation from the three independent research groups in Czech Republic, Italy and Spain yielded reasonable and mutually compatible results. We employed the well-known correlation among oxidative degradation and increase in crystallinity due to cold crystallization [4]. The data from all three countries showed quite similar trends as documented in Fig. 1.
In the second step, we tested selected differences between different UHMWPE types. The negative effect of gamma sterilization on oxidative degradation is well-established. Our data confirmed that gamma-sterilized samples (gIRR) exhibited higher OI than samples sterilized chemically by formaldehyde (HCHO; old sterilization employed in Czech hospitals) and ethylene oxide (EtO), as evidenced in Fig. 2

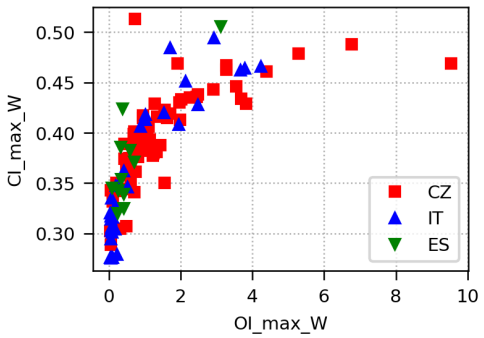

Figure 1. Correlation between maximal values of oxidation index (OI-max-W) and crystallinity (CI-max-W) from linear profiles starting at worn surfaces (W).

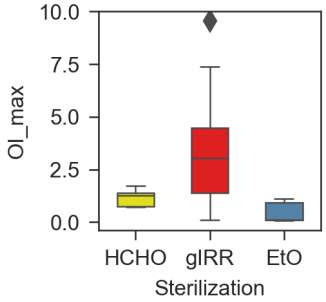

Figure 2. Different oxidative degradation (OI-max) of UHMWPE liners sterilized with formaldehyde (HCHO), gamma irradiation (gIRR) and ethylene oxide (EtO).

Conclusion: The international database of UHMWPE retrievals contains consistent data (Fig. 1) and starts to show reasonable trends (Fig. 2). The project is in active development and is open to partners from other countries.

Acknowledgement: Project NU21-06-00084 (AZV CR).

References:
[1] UHMWPE Biomaterials Handbook, Elsevier, 2016.
[2] *J Biomed Mater Res A* 89 (2009) 530–538.
[3] Python for Data Analysis, O'Reilly, 2018.
[4] *J Mech Behav Biomed Mater* 120 (2021) 104205.

Antibiotic-loaded Ultrahigh molecular weight polyethylene (UHMWPE)

Sashank Lekkala[1], Jaynie Criscione[1], Keith K. Wannomae[1], Amita Sekar[1,2], Ebru Oral[1,2]
[1]Harris Orthopaedic Laboratory, Massachusetts General Hospital, Boston, MA, [2]Department of Orthopaedic Surgery, Harvard Medical School, Boston, MA
eoral@mgh.harvard.edu

Disclosures: Sashank Lekkala (N), Jaynie Criscione (N), Keith K. Wannomae (N), Amita Sekar (N), Ebru Oral (1-Corin, Iconacy, Renovis, Arthrex, ConforMIS, Meril Healthcare, Exactech)

INTRODUCTION: Prosthetic joint infection (PJI) is one of the major causes of revision surgery. Patients with PJI have an increased risk of recurrent infection, and higher mortality and morbidity rates [1,2]. Current gold standard treatment involves two-stage revision where all the infected implants are removed and replaced with an antibiotic loaded bone cement spacer for at least six to eight weeks, followed by reimplantation of new components. These spacers often elute less than minimum inhibitory concentration (MIC) of common PJI bacteria after one week [3]. We showed in our seminal work that vancomycin and rifampin-eluting UHMWPE can be efficacious against planktonic and biofilm-forming Staphylococci [4]. Our aim here is to investigate the thermal and chemical stability of common antibiotics to determine their suitability for incorporation into UHMWPE as a local drug delivery device.

METHODS: Twelve different antibiotics (**Table 1**) were characterized using thermogravimetric analysis at molding temperatures of UHMWPE. 0.5-5 mg of the drug was loaded on a platinum pan (n=3 each) and the temperature was ramped up from room temperature to 250°C at 5°C/min and held at 250°C for 3 minutes. Weight loss was recorded. The drugs were blended at 7% and 10% w/w with 1020 GUR UHMWPE followed by compression molding. Six 3x5x20 mm^3 strips were cut and eluted in 1.7 ml de-ionized water and the eluent was collected at multiple timepoints (6 hours, 1 day, 2 days, 3 days, 1 week, 2 weeks, 3 weeks). The eluent concentration was determined using UV spectroscopy. The concentrations of gentamicin sulfate and tobramycin sulfate were assessed by tagging with o-phthaldialdehyde and quantifying the resultant fluorescence [5]. ^{1}H nuclear magnetic resonance (NMR) was used to determine the stability of the drugs after molding by comparing the spectra of the eluent in D_2O to that of the unprocessed drug. Energy dispersive X-ray analysis (EDX) was used to visualize the drug domain morphology in UHMWPE.

RESULTS: Eight of the antibiotics (labelled green in **Table 1**) lost less than 2% weight from 110ºC until 200°C. Five lost greater than 2% weight below 110°C due to dehydration (labeled yellow in **Table 1**), these were dehydrated before incorporation into UHMWPE. Elution from all the 7% w/w drug loaded UHMWPEs showed a burst release until 3 days followed by decreasing release rate until 21 days (**Figure 1**). NMR spectra of the drug and eluent agreed well except for minocycline hydrochloride, gentamicin sulfate and vancomycin hydrochloride (not shown), which showed some changes. EDX revealed that the drug domains are eccentric clusters except for gentamicin sulfate and tobramycin sulfate which had largely spherical domains (not shown here).

DISCUSSION: We screened for 8 antibiotics that are thermally stable for incorporation into UHMWPE (**Table 1**). NMR results showed that minocycline hydrochloride degraded substantially during molding despite showing low weight loss during TGA until 190ºC. Among the antibiotics molded into UHMWPE, linezolid, and ciprofloxacin-loaded UHMWPEs showed the highest release rates (**Figure 1**), potentially due to percolation from interconnected drug domains (not shown here).

SIGNIFICANCE/CLINICAL RELEVANCE: Sustained local delivery of antibiotics is a more efficient way to treat infection than systemic administration due to high concentration at the infection site. This work supports the possible use of UHMWPE joint replacement components as delivery devices for antibiotics.

REFERENCES: [1] Kubista et al. Int. Orthop. **36**, 65–71 (2012); [2] Lentino et al. Clin. Infect. Dis. **36**, 1157–1161 (2003); [3] Jill et al. J. Bone Jt. Surg. **93**(22), 2049-2056 (2011); [4] Suhardi et al. Nature Biomed Eng 1:80 (2017); [5] Gubernator et al. Int J Pharm. **327**(1-2), 104–109 (2006).

ACKNOWLEDGEMENTS: This work was supported by the National Institutes of Health Grant R01AR077023.

IMAGES AND TABLES:

Table 1. Dehydration and degradation characteristics of antibiotics assessed by TGA. Yellow indicates that the drug must be vacuum dried, green indicates <2% degradation, and red indicates >2% degradation.

Drug	% Weight loss until 110°C (dehydration)	% Weight loss, 110°C - 200°C (degradation)
Ciprofloxacin Hydrochloride	0.33±0.15	0.13±0.092
Clindamycin Hydrochloride	4.9±0.87	22±0.68
Colistin Sulfate Salt	9.9±2.1	0.62±0.052
Fusidic Acid	1.2±0.16	9.9±0.44
Gentamicin Sulfate	8.2±0.64	1.8±0.11
Linezolid	0.20±0.20	0.92±1.0
Meropenem Trihydrate	12±0.76	10±0.53
Minocycline Hydrochloride	8.5±0.094	2.9±0.13
Neomycin Sulfate	7.6±1.3	2.8±0.35
Rifampicin	0.34±0.34	0.22±0.16
Tobramycin Sulfate	7.0±3.9	1.3±0.17
Vancomycin Hydrochloride	7.6±3.4	1.8±0.10

Figure 1. Drug elution rates (mg/day) with time normalized to a 7% (top) and 10% (bottom) drug loaded 100cm^2 implant surface.

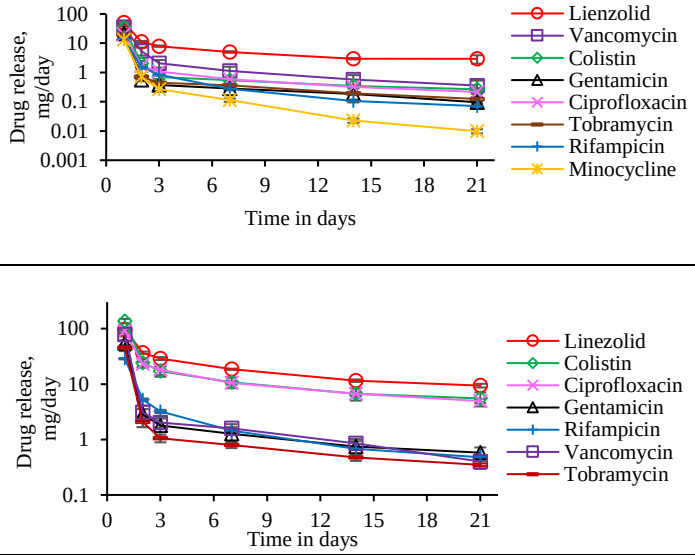

Clinical Introduction of a Chemically Crosslinked UHMWPE

Orhun Muratoglu, Ebru Oral, Brinda Badwe, Rachel Connolly, Keith Wannomae, Mehmet Asik, and Cecilia Nepple

Harris Orthopedic Laboratory, Massachusetts General Hospital, Harvard Medical School, Boston, MA

Ultra-high molecular weight polyethylene (UHMWPE) has undergone many iterations over the past two decades. In 1990s, UHMWPE particulate induced periprosthetic osteolysis and oxidation induced damage in UHMWPE implants were the dominant causes of revision in total joint patients. We addressed these by first eliminating air from packaging in gamma sterilized implants, followed by the clinical introduction of radiation crosslinked and thermally stabilized polyethylenes. More recently, added antioxidants further improved the oxidative stabilization of UHMWPE implants. These advances, particularly high levels of crosslinking, resulted in excellent clinical outcomes in total hips, knees, and shoulders. While all highly crosslinked UHMWPEs in clinical use are treated with ionizing radiation, chemical crosslinking with peroxides is also an option. We demonstrated that peroxide crosslinking (PRX) of UHMWPE is a viable technique and requires antioxidant stabilization. The technique comprises blending di-cumyl peroxide (DCP), vitamin-E and polyethylene followed by consolidation, during which UHMPE crosslinks. DCP undergoes thermal dissociation into peroxy free radicals that abstract protons from UHMWPE and lead to its crosslinking. The residual by-products of DCP are small molecules that are then removed by high temperature melting (HTM) of the consolidated blend. We optimized the formulation and the HTM cycle to reduce the concentration of the by-products to well below those that could raise toxicological concerns. The optimized formulation can be gamma sterilized without any stability concerns. Wear resistance is comparable to those of other clinically successful formulations. In addition, the PRX-HTM polyethylene has higher strength, ductility, and toughness than other crosslinked polyethylenes – these are properties that could improve long-term performance in high-demand patients. The FDA cleared the use of this technology in tibial knee inserts and patellae components in a specific total knee replacement implant system. As gamma radiation availability is becoming more scarce, peroxide crosslinked and high temperature melted UHMWPE will be a feasible option for continued clinical success of highly crosslinked UHMWPE implants.

A New Bulk Lamellar Polyethylene Morphology Induced Using High-Rate Pressurization

Bellare, A[1]
[1]Polymerix LLC, Boston, MA, USA
anuj@alum.mit.edu

Introduction: Over the last two decades, ultra-high molecular weight polyethylene (PE) components of total joint replacements have been crosslinked to increase wear resistance and have shown clinical success in minimizing wear particle induced osteolysis. Initially, post-radiation crosslinked UHMWPE (HXLPE) was thermally treated to remove free radicals trapped in lamellae to prevent long-term oxidative degradation. However, both ultimate tensile stress (UTS) and maximum strain-to-failure (MS) of HXLPE was lower than that of uncrosslinked PE. Inclusion of antioxidants made it unnecessary to conduct post-radiation thermal treatments which preserved the UTS but decreased the MS. The base morphology of PE induced by ram extrusion or compression molding of PE powder have led to a relatively uniform starting lamellar morphology with crystallinity ranging from 55-60% and lamellar thickness of approximately 25-30nm. Conventional high-pressure crystallization induces 70-80% crystallinity and 100-250nm lamellar thickness in PE. In this study, a new high pressure crystallization route is being introduced for the first time in which rapid pressurization can lead to quenching of the bulk material. Although thermal quenching has been performed on melted PE sheets using liquid nitrogen or ice water, its low thermal conductivity prevents it from affecting the bulk morphology, thereby relegating it to a surface phenomenon. Hydrostatic pressure does not have such constraints. This study compares the morphology of PE induced by rapid pressurization with both conventional high-pressure crystallization and compression molded PE, showing that pressure can be used to create relatively low crystallinity PE with a large number of thin lamellae with consequences for tensile properties.

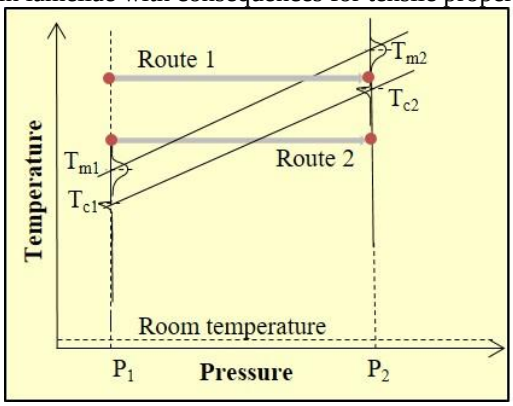

Figure 1. Phase diagram of PE superimposed with differential scanning calorimeter thermograms indicating melting temperature (Tm) and crystallization temperature Tc) for two pressures and showing Route 1 (high-pressure crystallization) and Route 2 (rapid pressurization)

Methods and Materials: Ram-extruded GUR 1050 (Celanese, Oberhausen, Germany) bars served as controls (CPE) and machined into 3" long cylinders of 0.5" diameter to snugly fit into a high pressure cell. Conventional high-pressure crystallization was conducted by heating the PE to 180˚C, applying 500 MPa pressure slowly over 5 minutes, cooling to room temperature under pressure followed by pressure release (HPPE) (Route 1 in Figure 1). Rapid pressurization was conducted by heating the PE to 140˚C and then rapidly (within 10 seconds) pressurizing to 500 MPa, slow cooling under pressure followed by pressure release (Route 2 in Figure 1) (RPPE). ASTM standard tensile tests using ASTM 638-Type V specimens were conducted (n=4 per group) to measure the UTS and MS. Small angle x-ray scattering (SAXS) and differential scanning calorimeter (DSC) were used to measure the crystallinity and lamellar thickness (n=3).

Results and Discussion: SAXS plots showed that RPPE had the highest scattering angle followed by CPE and HPPE, indicating that the RPPE had the smallest inter-lamellar spacing (Figure 2). Combined with DSC, lamellar thickness was calculated showing that RPPE had the thinnest lamellae and lowest crystallinity (Table 1) compared to CPE while HPPE had the thickest lamellae and highest crystallinity ($p<0.05$, ANOVA). As expected, HPPE had the lowest UTS and MS while there was no statistical difference between the UTS of CPE and PQPE ($p>0.05$, ANOVA). However, the MS of RPPE was much higher than for both CPE and HPPE. Considering that antioxidant containing PE, radiation crosslinked without thermal treatments, retains UTS but decreases MS, the RPPE shows promise as a starting material whose crosslinked counterpart could have a comparable or larger MS compared to uncrosslinked CPE. More comprehensive wear and mechanical properties investigation of RPPE will be required prior clinical application.

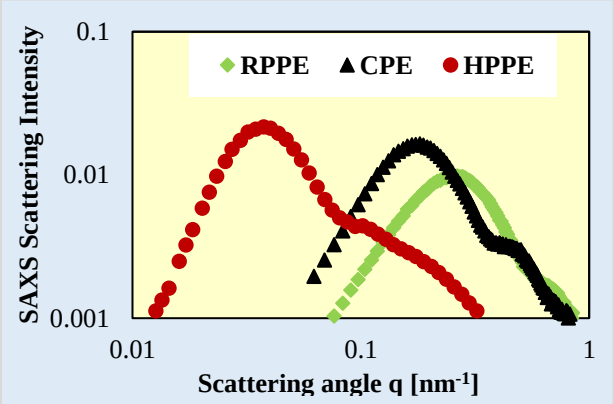

Figure 2. Log-log plot of SAXS scattering intensity versus Scattering angle for RPPE, CPE and HPPE, respectively.

ID	X(%)	L(nm)	UTS(MPa)	MS
CPE	51.8±0.8	23.8±0.3	50.5±4.3	9.9±0.4
HPPE	69.4±1.4	125.6±2.4	24.5±1.4	4.0±0.7
RPPE	44.7±3.1	20.6±0.7	50.2±1.7	21.9±0.8

Table 1. Crystallinity (X), Lamellar thickness (L), Ultimate tensile stress (UTS) and maximum strain (MS)(mm/mm) for CPE, HPPE and RPPE, respectively.

Static fracture and cyclic fatigue resistance of split-dose irradiated AOX™ UHMWPE

Bowsman, L[1], Rimnac, C[2], Bensusan, J[2], Aghazadeh, M[1], Quirindongo, R[1]
[1]DePuy Synthes, Warsaw, IN; [2]Case Western Reserve University, Cleveland OH, USA
LBowsman@its.jnj.com

Introduction: Radiation crosslinking of UHMWPE coupled with an antioxidant greatly decreases wear and deters in vivo oxidation [1]. However, fatigue crack propagation (FCP) resistance and static fracture (J-R) resistance can deteriorate with increasing levels of crosslinking [1-2]. Furthermore, small but discernable preferred chain orientation, or anisotropy, has been detected in both non-irradiated and gamma-irradiated ram extruded bars [3-4]. Thus, attention to the effects of radiation dose and potential processing-induced material anisotropy is important when evaluating new UHMWPE processing methods.
Objective: This study investigated the FCP resistance in the anteroposterior (A-P) and mediolateral (M-L) orientations and static J-R fracture resistance of Low, Mid, and High split-dose gamma-irradiated UHMWPE containing a hindered phenol antioxidant (AOX™).

Methods and Materials: Specimens were machined from ram extruded bars (GUR 1020 resin blended with AOX™) and underwent split-dose gamma-irradiation, i.e., an initial crosslinking dose prior to machining, followed by a secondary terminal crosslinking and sterilization dose after machining. Bars/test specimens were individually vacuum sealed in barrier packaging for both irradiation dose steps. Testing and analysis was conducted at CWRU.
Fatigue crack propagation: FCP tests were conducted on an Instron servo-hydraulic test machine, following ASTM E647 guidance. Bars received target first irradiation doses of 50 kGy (FD-Low), 55 kGy (FD-Mid), or 60 kGy (FD-High). Round compact tension specimens were machined so that crack propagation would occur in either the A-P or M-L orientation relative to a machined tibial component (Fig. 1). All specimens received a 40 kGy target second irradiation dose (Table 1). Three specimens for each dose-orientation combination were tested to failure. Specimens were razor sharpened (A-P specimens were sharpened from anterior to posterior) to a depth of 2 mm and allowed to stress relax a minimum of 16 hours prior to testing. All cycling used a sinusoidal waveform of 3 Hz and R ratio of 0.1 (minimum load/maximum load). The crack tip of the specimen was cooled with an air jet during loading. For every 0.2 mm of crack propagation, cycling was interrupted, and the crack length was measured. Fatigue crack growth rate (da/dn) and cyclic stress intensity factor (ΔK) were calculated and linear regression of the log-log data was used to determine the coefficient (C) and exponent (m) of the Paris relationship ($da/dn = C\Delta K^m$). The Paris regime was defined from a crack growth rate (da/dn) of 10^{-4} mm/cycle to 10^{-2} mm/cycle. $\Delta K_{inception}$ was estimated using visual inspection of the pooled da/dn v. ΔK curves for a treatment group.
Static fracture resistance (J-R curve): J-Integral tests were conducted in ambient air on an Instron closed-loop servo-hydraulic test machine using the multiple specimen test method (ASTM D6068). All bars were irradiated to a 55 kGy target initial dose, machined into notched three-point bend specimens, and irradiated to target second doses of 25 kGy (SD-Low), 30 kGy (SD-Mid), or 40 kGy (SD-High) (Table 1). For each dose, load v. displacement was recorded from 8-10 specimens that underwent stable crack extensions of different lengths at a displacement rate of 0.85 mm/s. Notches were pre-sharpened with a razor a minimum of 48 hours prior to testing. J (kJ/m^2) was determined from the load-deflection curves according to: $J = (2A)/(Bb)$, where A = area under the load-deflection curve, B = specimen thickness, and b = length of the unfractured ligament. J was corrected for indentation at the loading points. After unloading, the specimens were soaked in liquid nitrogen and then broken open at a high strain rate to demarcate the test crack extension. The crack extension, Δa, was determined from the fracture surface using high resolution digital photography and image analysis (ImageJ, NIH). J v. Δa was fit with a power law regression to describe the J-Integral v. crack growth resistance (J-R) curve ($J = C_1\Delta a^{C2}$).
Statistical analysis: Regression analysis was conducted to compare the Paris regime coefficient (C) and exponent (m) between pooled FCP da/dn v. ΔK curves: (1) same orientation, different total dosing (e.g., FD-Low A-P v. FD-Mid A-P); (2) different orientation, same dosing (e.g., FD-Low A-P v. FD-Low M-L); (3) orientation only, i.e., all doses A-P v. all doses M-L; and (4) single-dose (80 kGy) and FD-Low A-P and FD-Low M-L split-dose (90 kGy) (the latter was conducted using a historical comparison to the closest comparable single-dose condition) (Minitab 20). Regression analysis was also used to compare the coefficient (C_1) and exponent (C_2) between dosing combinations from the J-R curves (e.g., SD-Low v. SD-Mid). Significance was taken as $p < 0.05$.

Results: There was a significant difference in C and m between FD-Low v. FD-Mid and FD-Low v. FD-High dose combinations, with overall no difference between FD-Mid v. FD-High dose combinations of the same orientation (only C from the M-L group differed, Table 2). Further, there was no difference in C and/or m between orientations with equal dosing (e.g., Fig. 2). Comparing orientations overall (i.e., pooled A-P v. M-L), there was no difference in FCP behavior (Fig. 3). For all pooled data sets, $\Delta K_{inception}$ was estimated as 1.6 $MPa(m)^{1/2}$. For the 80 kGy single-dose historical material, $\Delta K_{inception}$ was 1.5 $MPa(m)^{1/2}$; there was a difference in C but not in m between the single-dose and split-dose materials (Fig. 4). For the J-R curve comparison, the exponent C_2 did not differ between dose combination groups; the coefficient C_1 only differed between SD-Low v. SD-High dose combinations (Fig. 5).

Discussion: In general, UHMWPE FCP and static J-R fracture resistance can be expected to decrease with an increase in total irradiation dose [1, 2]. The FCP and J-R findings in this study are consistent with this expectation, though the differences are small. The similar $\Delta K_{inception}$ among the dose-orientation combinations also suggests that there is comparable resistance to initial fatigue crack growth between the A-P and M-L directions. Overall, FCP behavior was not found to be sensitive to crack growth orientation. The comparable FCP behavior for the A-P and M-L orientations suggests that processing conditions produce a relatively homogenous material with respect to a finished tibial component. Though there were statistically significant differences found between some dose combinations for both cyclic and static fracture behavior, the differences were small and it is unlikely that these differences would result in clinically meaningfully different outcomes. Finally, despite a higher combined target irradiation dose of 90 kGy (FD-Low), this split-dose combination appears to have comparable or slightly better FCP resistance compared to a historical single-dose of 80 kGy; this may suggest an overall lower degree of crosslinking or better maintenance of % crystallinity due to split-dosing and warrants further investigation.

Limitations of this study include that crack propagation direction was assigned only for split-dose FCP tests and tests were conducted in ambient air. Finally, FCP and three-point bend specimens received different Low, Mid, and High irradiation doses at different points in the irradiation process (first v. second target doses), and ultimately different combined target doses.

References:

[1] UHMWPE Handbook, 3rd ed, 2015; [2] C Rimnac et al, 8th Int UHMWPE Meeting, 2017; [3] LG Malito et al, JMBBM, 2018; [4] A Bellare et al, Biomat, 1996.

Table 1. Split-dose gamma-irradiation of test specimens.

Test Specimen	Target 1st Dose (kGy)		Target 2nd Dose (kGy)		Combined Target Dose (kGy)	
Compact Tension	Low	50	40		FD-Low	90
	Mid	55			FD-Mid	95
	High	60			FD-High	100
Notched 3 Point Bend	55		Low	25	SD-Low	80
			Mid	30	SD-Mid	85
			High	40	SD-High	95

Table 2. Paris regime coefficient (C) and exponent (m) p-value comparisons from regression analysis of pooled A-P or M-L FCP da/dn v. ΔK curves.

	FD-Low v. FD-Mid	FD-Low v. FD-High	FD-Mid v. FD-High
A-P	C: p < 0.001 m: p = 0.012	C: p < 0.001 m: p = 0.005	C: p = 0.12 m: p = 0.81
M-L	C: p < 0.001 m: p = 0.028	C: p < 0.001 m: p < 0.001	C: p = 0.005 m: p = 0.062

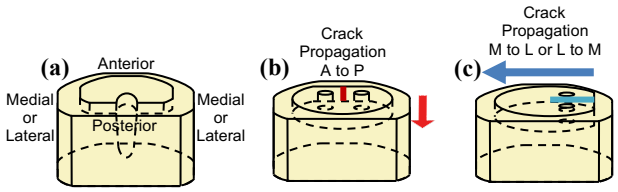

Figure 1. Machined (a) tibia and FCP specimens showing (b) A-P and (c) M-L crack propagation direction. Tibial components are symmetric, thus M-L crack propagation is not direction specific (i.e., M-L or L-M).

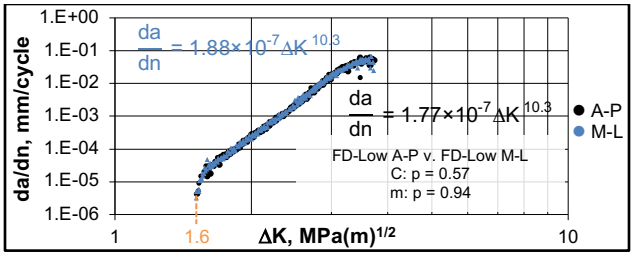

Figure 2. Representative pooled da/dn v. ΔK data for FD-Low A-P v. FD-Low M-L.

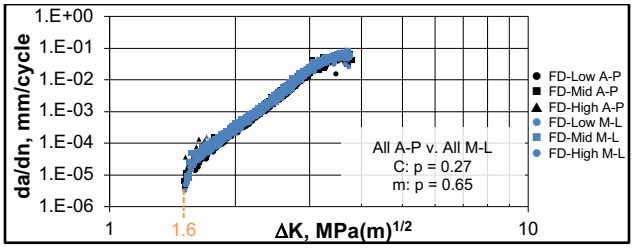

Figure 3. Pooled da/dn v. ΔK data for all dose-orientation combinations.

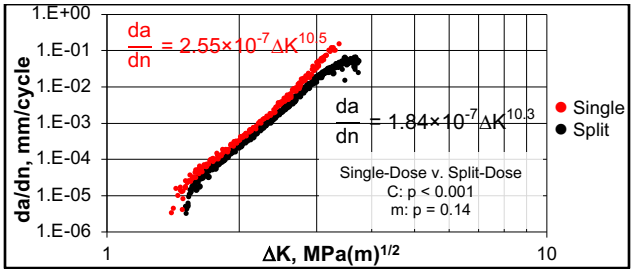

Figure 4. Pooled da/dn v. ΔK data for single-dose (80 kGy) and FD-Low A-P and FD-Low M-L split-dose (90 kGy).

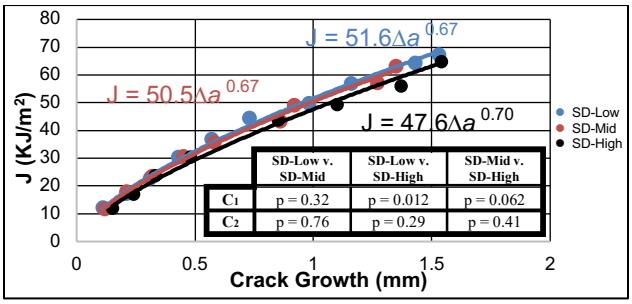

Figure 5. J-R curves for SD-Low, SD-Mid, and SD-High dose combinations.

Synergistic antibacterial activity of pain medication with antibiotics in Staphylococcal infection management

Peyton Tierney[1], Amita Sekar[1,2], Vikram Daesety[1], Darina Trendafilova[1], Kathryn Daffinee[3], Kerry LaPlante[3,4,5], Ebru Oral[1,2]
[1]Harris Orthopedic Laboratory, Massachusetts General Hospital, Boston, MA, [2]Department of Orthopedic Surgery, Harvard Medical School, Harvard University, Boston, MA, [3]Rhode Island Center of Innovation in Long-Term Services and Supports, Providence Veterans Affairs Medical Center, Providence, RI, [4] Kingston Infectious Diseases Research Program, College of Pharmacy, University of Rhode Island, Providence, RI, [5]Warren Alpert Medical School of Brown University, Division of Infectious Diseases, Providence, RI
ptierney3@mgh.harvard.edu

Disclosures: Peyton Tierney (N), Amita Sekar (N.), Vikram Daesety (N), Darina Trendafilova (N), Kathryn Daffinee (N), Kerry Laplante (3B-Nabriva, Melinta, Tetraphase, 5-Merck, Pfizer, Ocean Spray Cranberries, 8, 9-Society of Infectious Disease Pharmacists), Ebru Oral (1-Corin, Styker, Iconacy, Renovis, Arthrex, ConforMIS, Meril Healthcare, Exactech)

Introduction: Periprosthetic joint infections (PJI) are devastating complications associated with orthopedic surgeries. Staphylococcus aureus and Staphylococcus epidermidis are two of the chief causative microorganisms of these infections. As part of the common treatment for PJI, the patient is administered both antibiotics to help prevent infection and analgesics for pain management. A limitation of this treatment is that general antibiotics can engender resistance to the surviving bacteria if the local infection is not eradicated. Previously, we showed synergistic antimicrobial effects for gentamicin and ketorolac, a non-steroidal anti-inflammatory drug (NSAID)[1]. In this present study, we aim to explore synergism against Staphyloccoccal bacteria of antibiotics and analgesics/NSAIDs, which are commonly used in joint replacement surgeries.

Methods: All experiments were conducted on reference and clinical Staphylococci, representing both "low risk" (methicillin and gentamicin susceptible) and "high risk" (mecA-positive, gentamicin resistant) strains **[Table 1]**. For this study, the relationship between antibiotics and analgesics/NSAIDs was assessed for three common antibiotics: gentamicin sulfate, vancomycin hydrochloride, and tobramycin sulfate; and six common pain medications: ketorolac tromethamine, bupivacaine hydrochloride, lidocaine hydrochloride monohydrate, procaine hydrochloride, tetracaine hydrochloride, and tolfenamic acid . First, the minimum inhibitory concentration (MIC) was established for each antibiotic and analgesic independently for each strain of bacteria. Potential synergy was then assessed for each combination by performing a fractional inhibitory concentration (FIC) checkerboard assay[2]. Results were interpreted using the following equation: $\frac{A}{MIC\ A} + \frac{B}{MIC\ B} = FIC\ A + FIC\ B = FIC\ Index$, and classified according to FIC index as either synergistic (FIC <1), additive (1 < FIC < 2), indifferent (2 < FIC < 4), or antagonistic (FIC > 4)[2].

Results: MIC data for all antibiotic and analgesics/NSAIDs are displayed by strain in **Table 1**; these values were used as the basis for the FIC experiments. It was determined that for the combination of gentamicin and ketorolac, the FIC was <1 for all strains [**Table 2**]. When gentamicin was combined with either lidocaine, procaine, or tolfenamic acid, it was found that the 1<FIC<2 [**Table 2**]. For tobramycin, FIC was <1 when paired with ketorolac and tetracaine, and 1<FIC<2 when paired with bupivacaine, procaine, or lidocaine. Vancomycin yielded additive effects (1<FIC<2) when paired with any of the six analgesics/NSAIDs [**Table 3**]. There were a few exceptions to this, vancomycin shows synergy (FIC<1) when paired with either ketorolac, tetracaine, or tolfenamic acid for a few select strains [**Table 3**]. Additionally, there were a few instances where, when vancomycin when paired with bupivacaine, lidocaine, or tetracaine, resulted in 2<FIC<4, indicating indifference [data not shown].

Discussion: For the two aminoglycosides, gentamicin and tobramycin, ketorolac tromethamine and tetracaine hydrochloride were the analgesics that had consistent synergistic effects regardless of the strain of bacteria. There was a general trend in the behavior between the two aminoglycoside antibiotics with tobramycin exhibiting slightly stronger synergistic effects. The FIC for the combinations of ketorolac, tolfenamic acid, and tetracaine with vancomycin, the glycopeptide antibiotic, were the only pairings demonstrating synergy, however these were dependent on the strain of bacteria. Vancomycin was also the only antibiotic to demonstrate combinations yielding indifference or near antagonistic behavior.

Significance: These results serve as a basis for the exploration of the potential antibacterial interactions between antibiotics and analgesics/NSAIDs. Synergistic combinations can possibly be prescribed clinically as a more effective post-operative treatment, whereas combinations yielding indifference or antagonism should be avoided when possible. Further confirmation of this screening test using time-kill curves *in vitro* and efficacy testing *in vivo* can maximize treatment efficacy. Overall, understanding whether the combination of prescribed drugs produces synergistic or antagonistic antibacterial effects is vital to not only maximizing the regiment's efficacy, but also has an impact on mitigating antibiotic resistance.

References: 1. D.Gil et al. J Orthop Res 2018; 2. Adopted from CLSI M-27 Protocol

Acknowledgements: This work was supported by the National Institutes of Health Grant R01AR077023.

Table 1. Lists all strains of Staphylococcal bacteria tested in the study, describing their phenotypic characteristics. Additionally, displays the MIC of relevant drugs by strain.

	Bacterial Strain						
	S. aureus					S. epidermidis	
	12600	L1101	L1112	L1147	L1163	35984	L1116
Bacterial Characteristics	Reference	mecA positive; GISA	mecA positive; HVERSA	mecA negative; VISA	mecA positive; VISA	Reference	mecA positive; VISE
Gentamicin MIC (ug/mL)	1	>16	>16	>16	>16	8	>16
Vancomycin MIC (ug/mL)	0.5	8	4	4	4	2	8
Ketorolac MIC (mg/mL)	8	4	8	8	4	8	4
Bupivacaine MIC (mg/mL)	2	2-4	4	4	4	2	4
Lidocaine MIC (mg/mL)	16	16	32	32	32	16	64
Procaine MIC (mg/mL)	100	16-32	32	32	32	32	128
Tolfenamic Acid MIC (mg/mL)	0.0625	64	16	32	16	32	64
Tetracaine MIC (mg/mL)	1	1-2	1	1	1	1	1

Table 2. Displays average FIC index results for gentamycin-analgesics/NSAIDs experiments by bacterial strain. Results are color coded by classification.

	Gentamicin			
	S. aureus		S. epidermidis	
	12600	L1101	35984	L1116
Ketorolac	0.99	0.85	0.91	0.88
Bupivacaine	1.18	1.09	0.82	1.18
Lidocaine	1.79	1.04	1.22	1.08
Procaine	1.1	1.1	1.08	1.58
Tolfenamic Acid	1.11	1	1	1.1
Tetracaine	0.93	1.04	1	0.91

Table 3. Displays average FIC index results for vancomycin-analgesics/NSAIDS experiments by bacterial strain. Results are color coded by classification.

	Vancomycin			
	S. aureus		S. epidermidis	
	12600	L1101	35984	L1116
Ketorolac	1.38	0.75	0.94	1.16
Bupivacaine	1.16	1.08	1.04	1.08
Lidocaine	1.79	1.08	1.19	1.15
Procaine	1.19	1.08	1.04	1.17
Tolfenamic Acid	1.19	1.14	0.8	1.14
Tetracaine	1.19	0.92	1.44	1.07

Bioresorbable polymers in additive manufacturing: How material characteristics and printing process parameters impact medical device performance?

Cécile Boudot[1], Mahrokh Dadsetan[2], Thiago Borges[2]
[1]Evonik Operations GmbH, Darmstadt, Germany
[2]Evonik Industries, Medical Competence Center, Birmingham, USA

Bioresorbable polymers have been used in implantable medical device applications for decades and they are traditionally processed by injection molding. Recently, the emergence of additive manufacturing enabled production of complex part geometries with targeted degradation profiles leading to promising applications in regenerative medicine and tissue engineering. Evonik has recently developed several types of RESOMER® Filaments and RESOMER® PrintPowders to support additive manufacturing of bioresorbable implants using FFF Fused Filament Fabrication (FFF) and Selective Laser Sintering (SLS) technologies.

In this presentation, we have demonstrated that filament manufacturing for FFF based on bioresorbable polymers such as poly(lactide-co-glycolide) (PLGA), poly(L-lactide) (PLLA), polycaprolactone (PCL) and polydioxanone (PDO) required a precise control over material degradation and dimensions during the extrusion process. This allowed to achieve optimal printing process and to produce parts with almost similar mechanical properties as injection molding. In particular, it was shown that PCL and PDO polymers required an optimized cooling set up for production of parts with higher mechanical strength and elongation at break.

In the case of powder development for SLS, achieving a free-flowing powder with a precise particle size distribution range was critical and a flow aid was added to the polymer powder to improve powder flow properties. It has demonstrated that an optimal concentration of flow aid had a major impact on performance of SLS powder in printing operations. In addition, SLS printing required narrow setting of process parameters such as printing temperature, scanning speed and hatch distance to control the mechanical strength and porosity of the parts. In the case of PCL and PLLA polymer powders, it was shown that use of optimized printing parameters resulted in parts with mechanical properties in a similar range as for injection molding.

In summary, additive manufacturing has become an important tool in manufacturing of bioresorbable tissue engineering scaffolds and patient specific implants. Bioresorbable polymers utilized in additive manufacturing require to have tight specifications, good control of material degradation and optimal processing parameters to produce parts with consistent printing quality.

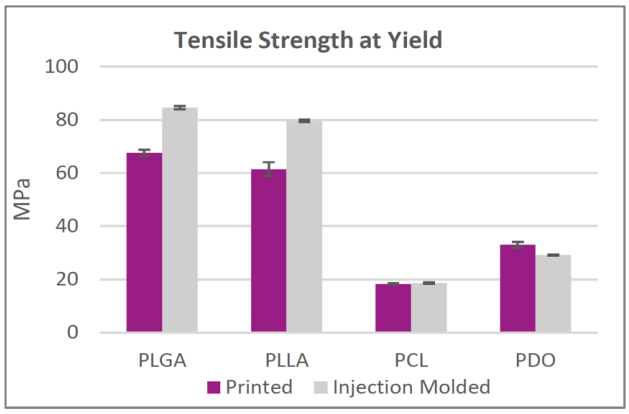

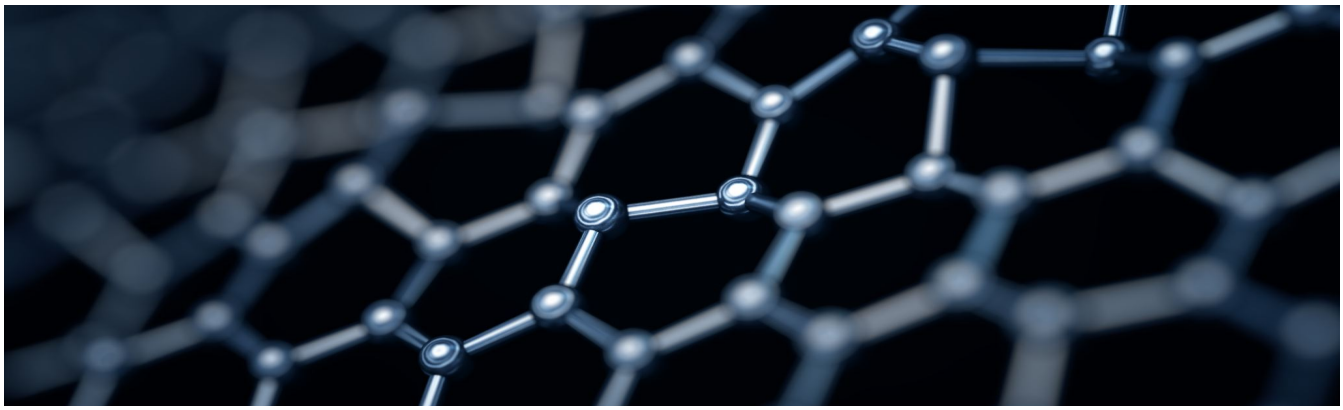

Evaluation of debris generated from the mechanical testing of continuous carbon fibre reinforced PEEK plates

Zhang, S[1]; Gambill S[1]; Swadener J[2]; Junaid S[2]; Leslie L[2]
[1]Invibio Ltd, Hillhouse International, Thornton-Cleveleys, Lancashire, UK, FY5 4QD
[2] Aston Institute of Materials Research (AIMR), Aston University, Birmingham, B4 7ET
shiling.zhang@invibio.com

Introduction:

Continuous carbon fibre reinforced Poly-Ether-Ether-Ketone (cCFR-PEEK) received first US Food and Drug Administration (FDA) clearance in 2005 and has been clinically used in orthopaedic fracture fixation since 2009 (1, 2). One of the most advantageous properties of cCFR-PEEK is its radiolucency, which has improved the visualisation of the fracture site in the surgery and postoperatively (3, 4). In addition, it is also reported to promote early callus formation and a faster healing process (5, 6). However, despite the reported advantages, concerns remain about this novel composite material. Within the past decade, debris has also been drawing growing attention by relevant stakeholders to ensure patients' safe recovery due to arising issues caused by debris. These issues include but are not limited to implant failure such as loosening, osteolysis, hypersensitivity, inflammation, toxicity, and carcinogenicity (7, 8). The aim of this study is to provide insight on the worst scenarios for plates made of this novel composite biomaterial: i.e., when the plates fail catastrophically, what is the debris morphology including the size distribution. In the meantime, we also intend to evaluate this novel cCFR-PEEK plate's biomechanical properties compared to a conventional Ti plate.

Methods and Materials:

Three groups of plates were studied under four-point bending configuration to mimic the overload conditions, PEEK-OPTIMA™ Ultra Reinforced plates (POUR), PEEK-OPTIMA™ Ultra Reinforced Image Contrast plates (POUR-IC), and conventional commercially pure Titanium plates (Ti). Ti plates were purchased from Animal Orthopaedics (UK), while POUR and POUR-IC plates were manufactured and provided by Invibio Ltd (UK). All tested plates were 3.5 mm 12-hole straight locking plates with a width of 13.5 mm and a length of 188.9 mm. The tested POUR, POUR-IC and Ti plates' mean thickness was 3.65 mm, 3.37 mm and 3.56 mm, respectively.

The tests were conducted as per the ASTM F382 requirements, based on the plate design and hole locations with n=3 for each of the composite plates and n=2 for the Ti plate. Testing was carried out on an Instron 3345 (Instron, UK) using a load cell of 5 kN capacity. The centre and loading spans were set to 30 mm, creating a support span of 90 mm. Each specimen positioned with the bone-side facing up, preloaded to 2 N and then subsequently loaded to failure at a rate of 2 mm/min. Failure was defined as a 20% drop in the detected load, or an increase in the detected load above the safety limit of the load cell, i.e., 4,900 N. Flexural strength and bending structural stiffness were calculated from the test data.

Following the four-point bend tests, debris from the specimen surfaces was collected using one carbon stub per tested specimen and observed under a scanning electron microscope (Hitachi TM 3000, UK) at a low-pressure mode for debris analysis. Based on ASTM F1877, SEM images of a minimum of 100 debris particles were taken. The debris morphology was then statistically summarised and analysed using Image J and R, where equivalent circular diameter, aspect ratio, and circularity were all characterised, and particle size distribution curves were plotted.

To ensure there was no existing contamination on the specimen surfaces, a specimen cleaning procedure was followed on all tested samples before the test. The specimen was first ultrasonically cleaned in soap solution for 5 minutes, followed by 5 minutes in ultra-clean deionised water for two times repeatedly. Specimens were then oven-dried at 120 °C for 15 minutes.

Each specimen was weighed gravimetrically on a UKAS calibrated analytical scale with an accuracy of 10 µg (Mettler Toledo, UK) before and after the overload bending test.

Results and discussion:

All tested composite plates, including both POUR and POUR-IC, failed by intra-laminar dominated fracture, with the only exception of one tested POUR plate where inter-laminate failure was more apparent, while Ti plate failed

due to excessive plastic deformation. In addition, POUR-IC plates revealed potentially better bone healing properties with a lowest structural stiffness (2.97±0.16 Nm^2) comparing to both POUR plate (3.45±0.18 Nm^2) and Ti plates (4.45±0.15 Nm^2). In terms of resistance to overload failure, both POUR and POUR-IC plates demonstrated higher flexural strength, with a value of 730.17±139.15 MPa and 682.54±7.56 MPa respectively, than Ti plate (660.14±11.96 MPa).

The amount of debris generated during the overload bending test is represented as a gravimetrical loss. Due to the difference in the failure mode, where Ti plate failure plastically, and POUR and POUR-IC failure inter-laminarly and intra-laminarly, there was no weight changes in Ti plate while POUR and POUR-IC plate showed an average loss of 3.02 mg and 0.15 mg, respectively. The debris generated accounted for 0.071% and 0.004% of the original tested plates and their standard deviations were 4.95 mg and 0.06 mg, respectively. It should be noted that that this test was carried out under dry conditions, where there was no exposure to physiological liquid; therefore, scenarios, such as corrosion from Ti plates, were not considered. Before this work, only Steinberg et al. (9) evaluated the quantity of debris through gravimetric measurement from wear test of a continuous CFR-PEEK diaphyseal plate. The authors self-assembled a plate and screws construct set-up in their study using Delrin rod as simulated bones. The construct was then tested in buffered saline solutions (PBS) at 300 N with R =0.1 for 1 million cycles. This is also one of the pioneer studies assessing the debris generated from continuous CFR-PEEK fracture fixation plates; however, the authors gave no quantitative results about the debris morphology. The results showed that Ti generated 8.95 mg debris, which is 5.9 times that of CFR-PEEK (1.51 mg) on testing conditions simulating the period when the fixation construct was in functioning in the patient. Therefore, if we assume the plate was implanted into the patient but unfortunately failed/broke, the overall quantity of debris from Ti would be 8.95 mg, i.e., around 2 times and 5.4 times than that of the POUR (4.51 mg) and POUR-IC (1.66mg) plates.

1288 and 871 debris were captured under SEM for POUR, which exceeds the requirement of a minimum of 100 debris for quantitative morphology observation. According to the particle distribution profile in Figure 1, most of the debris were less than 4 μm for both POUR and POUR-IC. The median size for POUR and POUR-IC were 2.33 μm and 3.02 μm, respectively. Similar shape parameters were also observed between POUR and POUR-IC plates, i.e., median Aspect Ratio (AR) of 1.613 and 1.664 and median roundness of 0.497 and 0.483. The shape of the debris ranged from small irregular granules to medium fibrous and large irregular flakes. Up to date, no research has studied the biological response of debris generated from cCFR-PEEK, but there are limited studies about discontinuous CFR-PEEK by S. Utzschneider, A. C. Paulus, V. Lorber et al.(10-13). Their research showed that CFR-PEEK (pan and pitch) of size 1.60-1.65 μm exhibited a similar increased inflammatory response than UHMWPE of the same size range. When the debris size came down to be 0.79 ± 0.3 μm, 1.22 ± 0.5 μm and 1.39 ± 0.3 μm for UHMWPE, CFR-PEEK pitch, and CFR-PEEK pan, respectively, the results showed elevated inflammatory responses of CFR-PEEK (pan and pitch) than that of UHMWPE. Then when the size ranges from 0.1 to 2 μm, the CFR-PEEK debris were all incorporated by macrophages without noticeable giant cell reaction while small particles of UHMWPE activated macrophages and larger ones were incorporated in giant cells. The morphology of the debris can impact largely differently on its biological responses and the explanation would be very complex. Further research is therefore needed to confirm the impact of the continuous CFR-PEEK debris that are of the same size could cause on the patient's recovery.

Conclusion:

This is the first time the debris generated from catastrophic failure of fracture fixation plate using a four-point bending configuration were characterised. As discussed above, the amount of debris from Ti (including both the catastrophic failure and in-patient service) is around 2 times and 5.4 times in comparison to POUR and POUR-IC, respectively. Therefore, POUR and POUR-IC would be a potentially better choice of materials to replace the current Ti in the fracture fixation plate.

However, further validation for this preliminary conclusion needs to be conducted; for example, we did not consider the impact of various scenarios such as pre-fatigue, pre-corrosion (for Ti plate), and physiological liquid when it broke.

No previous research has been conducted regarding the biological response on debris generated from continuous CFR-PEEK. Debris from discontinuous CFR-PEEK on the other hand had shown different responses based on its morphology. Further biological study is therefore needed to confirm the impact of the generated debris from our study on patients' recovery.

Acknowledgement:

PEEK-OPTIMA™ is a trademark of Invibio Limited.

This work was funded by Innovate UK through a Knowledge Transfer Partnership project, in conjunction between Aston University and Invibio Limited.

References:

1. FDA. 510(k) clearance - K052533 Kimba Spinal Implant. 2005.
2. Kojic N, Rangger C, Özgün C, Lojpur J, Mueller J, Folman Y, et al. Carbon-Fibre-Reinforced PEEK radiolucent intramedullary nail for humeral shaft fracture fixation: technical features and a pilot clinical study. Injury. 2017;48:S8-S11.
3. Perugia D, Guzzini M, Mazza D, Iorio C, Civitenga C, Ferretti A. Comparison between Carbon-Peek volar locking plates and titanium volar locking plates in the treatment of distal radius fractures. Injury. 2017;48:S24-S9.

4. Mitchell PM, Lee AK, Collinge CA, Ziran BH, Hartley KG, Jahangir AA. Early Comparative Outcomes of Carbon Fiber-Reinforced Polymer Plate in the Fixation of Distal Femur Fractures. J Orthop Trauma. 2018;32(8):386-90.
5. Byun SE, Vintimilla DR, Bedeir YH, Dean CS, Parry JA, Hak DJ, et al. Evaluation of callus formation in distal femur fractures after carbon fiber composite versus stainless steel plate fixation. European journal of orthopaedic surgery & traumatology : orthopedie traumatologie. 2020;30(6):1103-7.
6. Ziran BH, O'Pry EK, Harris RM. Carbon Fiber-Reinforced PEEK Versus Titanium Tibial Intramedullary Nailing: A Preliminary Analysis and Results. J Orthop Trauma. 2020;34(8):429-33.
7. Laing PG, Ferguson Jr. AB, Hodge ES. Tissue reaction in rabbit muscle exposed to metallic implants. Journal of biomedical materials research. 1967;1(1):135-49.
8. Geetha M, Singh AK, Asokamani R, Gogia AK. Ti based biomaterials, the ultimate choice for orthopaedic implants – A review. Progress in Materials Science. 2009;54(3):397-425.
9. Steinberg EL, Rath E, Shlaifer A, Chechik O, Maman E, Salai MJjotmbobm. Carbon fiber reinforced PEEK Optima—a composite material biomechanical properties and wear/debris characteristics of CF-PEEK composites for orthopedic trauma implants. 2013;17:221-8.
10. Utzschneider S, Becker F, Grupp TM, Sievers B, Paulus A, Gottschalk O, et al. Corrigendum to "Inflammatory response against different carbon fiber-reinforced PEEK wear particles compared with UHMWPE in vivo" [Acta Biomaterialia 6 (2010) 4296–4304]. Acta Biomaterialia. 2012;8(3):1396-8.
11. Utzschneider S, Becker F, Grupp TM, Sievers B, Paulus A, Gottschalk O, et al. Inflammatory response against different carbon fiber-reinforced PEEK wear particles compared with UHMWPE in vivo. 2010;6(11):4296-304.
12. Lorber V, Paulus AC, Buschmann A, Schmitt B, Grupp TM, Jansson V, et al. Elevated cytokine expression of different PEEK wear particles compared to UHMWPE in vivo. Journal of Materials Science: Materials in Medicine. 2014(1):141.
13. Paulus AC, Haßelt S, Jansson V, Giurea A, Neuhaus H, Grupp TM, et al. Histopathological Analysis of PEEK Wear Particle Effects on the Synovial Tissue of Patients. BioMed Research International, Vol 2016 (2016). 2016.

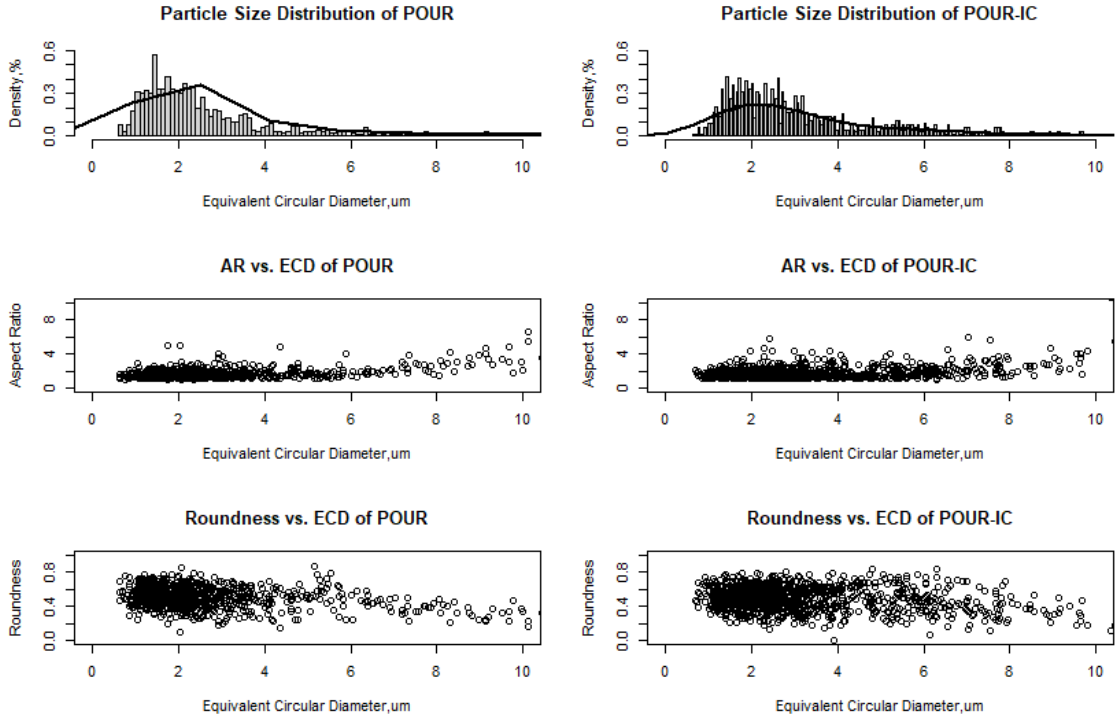

Figure 1 Particle Size distribution of debris generated during overload failures of POUR and POUR-IC plates

PEKK is the innovative material for printed medical implants

Ngawa Zenang, A
Seqens, Ecully, FR
Drug Delivery Solutions Department
alexandra.ngawazenang@seqens.com

Introduction:

Semi-crystalline Polyaryletherketone polymers (PAEKs) are widely used in orthopedic, trauma, spine and dental implants as biomaterials and are suitable for all conventional thermoplastic processing technologies, such as injection molding, extrusion, compression molding, or powder coating. For the past ten years, and this trend is accelerating, these polymers have been the subject of major efforts in Additive Manufacturing (AM) (Selective Laser Sintering (SLS) and Fused Filament Fabrication (FFF)), as this technology is perfectly suited to the needs of implantable medicine: offering customized devices for patients, allowing a more direct access for the patients and a significant time reduction. Within PAEKs for medical implants, PEEK is widely recognized (Victrex/Invibio, Solvay, Evonik) and used, benefiting from a solid history and an advanced ecosystem. Although PEKK is more recent (OPM and Seqens), it is actually the first polymer used in implants manufactured by SLS technology (OsteoFab® from OPM [1]). Recent advances and the spread of FFF technologies mean that the trend towards additive manufacturing is set to accelerate significantly. In addition to the excellent properties (thermomechanical, chemical resistance and tribological) of other PAEKs, PEKK has a better temperature resistance (higher Tg), a better tensile strength and in particular a better compressive strength. The presence of an additional ketone group gives PEKK a greater polarity and allows better acceptance of functional fillers, thus offering a wide choice of formulations in the context of specific optimization sought by manufacturers of implantable medical devices. PEKK is composed of ether (flexibilizing) and ketone (stiffening) groups. The more ketone groups there are, the higher the Tg and the better the mechanical properties. PEKK is a copolymer comprising both Terephthaloyl and Isophthaloyl units. This modularity allows fine tuning of the crystallization rate and melting point (Tg)

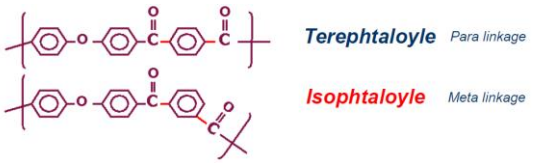

Figure 1: Distribution of Isophthaloyl and Terephthaloyl groups of PEKK

PEEK being a semi-crystalline linear homopolymer, it crystallizes much faster and is therefore naturally less suitable for FFF in AM.

PEKK is the easiest ultra-polymer to print. IMPEKK™ 3D (Implantable PEKK produced by Seqens) can be printed both in its amorphous form (with no or very limited crystallization and very high ductility) and in its crystalline form.

.

Methods, Materials and Results:

As illustrated in table 1, PEKK is an emerging material to be exploited in FFF with a potential to overcome the problems encountered with already existing materials.

	PEKK	PEEK	Comments
Compressive Strength (MPa) ISO 604	175	145	Many implantable medical devices, such as interbody fusion devices, work under compressive load
Polarity $\frac{[Ketone]}{[Ketone]+[Ether)}$%	66%	33%	PEKK displays an excellent acceptance of functional fillers (customization)
AM FFF	+++	+/++	PEKK copolymer ideally suited for FFF can be printed both amorphous or semi-crystalline
AM SLS	+++	Emerging	PEKK SLS already used for Medical Implants [1]
Processing Temperature (°C)	330 to 390 °C	390°C	

Table 1: Comparison of relevant properties of PAEK (PEEK & PEKK) polymers.

[1] see for example OsteoFab® technology https://oxfordpm.com/osteofab-technology

The impact of PEKK composition, and especially the Terephthaloyl/Isophthaloyl ratio, is demonstrated in Table 2 and Figure 2.

	Norm	IMPEKK™ 3D-G	IMPEKK™ 1G
Appearance	/	Golden Yellow or White to cream solid	
Polymer type	/	Pseudo-amorphous	Semi-crystalline
% Tere/Iso	/	60/40	80/20
Melting point (°C)	DSC DIN EN ISO 11357	285 – 315	345 – 375
Glass Transition (°C)	DSC DIN EN ISO 11357	155-165	160-170
Tensile test at Break (MPa)	DIN EN ISO 527-1,	90	115
Tensile Modulus (GPa)	DIN EN ISO 527-1,	3,1	3,7
Impact Strength	DIN EN ISO 179-1eU	No break	180 kJ/m²
Impact Strength (notched)	DIN EN ISO 179-1eA	5,5 kJ/m²	5,7 kJ/m²
Density	DIN EN ISO 1183	1,27 g/cm³	1,30 g/cm³
Crystallization speed rate	/	Very Slow	Fast
Processing temperature (°C)	/	330°C	385°C

Table 2: Mechanical properties of IMPEKK™ range

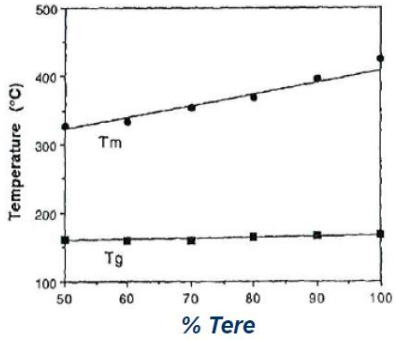

Figure 2: Impact of the ratio of Isophthaloyl and Terephthaloyl moieties on the melting and glass transition temperatures

Discussion:

The addition of Isophthaloyl groups lowers the melting temperature without impacting the Tg. Thus, when going from a semi-crystalline grade (IMPEKK™ 1G) - which behaves and is processed in a very similar way to PEEK - to a pseudo-amorphous grade (IMPEKK™3D), the crystallization rate drops very significantly. As a result, IMPEKK™ 3D is very suitable for processing by AM FFF, as the layers have the ability to inter-diffuse with each other, thus ensuring mechanical properties in the z-direction and filling unwanted porosities, before crystallization sets the system.

Seqens' IMPEKK™ (PEKK) will be commercially available for technical trials from Q2 in filament/granules to meet AM printing needs and in granules for injection molding/extrusion as early as Q3 22. Cleanroom batches of IMPEKK™ will also be available by Q3/Q4. Seqens has the capability to produce IMPEKK™ at industrial scale. At the same time, Seqens is pursuing biocompatibility studies, the results of which will be available by mid-2023.

Contamination and distortion free solidification of PEEK on a non-adherent substrate for 3D printing medical products

Popp, Uwe[1], Pfotzer, Lars[1]
[1]Apium Additive Technologies GmbH, Karlsruhe, Germany
Uwe.Popp@apiumtec.com, *Lars.Pfotzer@apiumtec.com*

Introduction: Polyetheretherketon (PEEK) is a well known material for its outstanding properties such as its general non-reactiveness resulting in its biocompatibility. In combination with additive manufacturing, in particular with material extrusion it is a cost and material saving method to create patient specific medical products such as cranial implants. However, there are multiple considerations that have to be taken into account to prevent any type of contamination to happen during the medical product creation process. Components that are in contact with the raw material should neither be reactive nor leave any kind of debris on the raw material, respectively should not change the biocompatibility of PEEK.

Since PEEK is in general non-reactive and sticks to very little materials, for industrial 3D-printing an adhesive agent is used to create a connection between printed PEEK and the substrate. The composition of the adhesive agent is most of the times unclear and an unknown substance within a medical workflow is always of concern. Therefore it is better to avoid using such an agent at all. Apium has chosen PEEK itself as a substrate to print parts upon. This kind of substrate is a so called raft to print on. But the raft also must be applied on something, and should be able to be removed. The method of choice to achieve such a condition is to create a form-fit of PEEK in the build plate.

The form-fit exhibits the conditions to have a strong connection of PEEK on the build plate and counters on top appearing inner stresses from a rapid cool down of PEEK when the first layers are printed on the build plate. The form fit is achieved by extruding PEEK into holes in the build plate and let the extruded material solidify. The holes are countersunk on one side providing the necessary space for the form fit.

In respect to the part size that should be 3D-printed a sufficiently big raft must be created. The size of the raft depends on the size the part covers when being projected perpendicular on the build plate, the parts so called foot print. The G-code calculation of the raft to cover the foot print is a two step process. In the first step in respect to the 3D-printing parts footprint an occupancy grid is determined by using a Bresenham algorithm. The systems determines, in respect to the occupied area of the footprint, the holes that need to be filled with material as form-fit connectors. In the second step the interface layers must be printed on the form-fit connectors to build the raft. In respect to the selected form-fit connectors a covering polygon is calculated. This polygon is filled up with material by using a sweep line algorithm. So the complete area within the calculated polygon will be fully covered by extruded material and form the basis on which the intended part can be printed on.

Methods and Materials:

As a build plate material for printing PEEK on, medical stainless steel had been chosen as a temperature resistant, non-reactive material which can be sterilized multiple times. To achieve the form-fit a symmetrical hole pattern with one side countersunk is applied on the build plate. As a substrate for medical PEEK, a raft out of PEEK is created. The raft is calculated and created within two steps. The first step is to cover the footprint of any printing object by determining the occupancy grid using a Bresenham algorithm. The selected holes are filled with PEEK resulting in connection points. The filled interface layers are created by calculating the boundary polygon based on the occupancy grid and a sweep line algorithm to fill the surface.

Discussion:

PEEK is a challenging material in the context of additive manufacturing. Especially when it comes to the creation of medical products the biocompatible properties must not be changed in any matter. Using a form fit to realize a connection of PEEK on the build plate has two main benefits. The biggest benefit is to be in a position to completely avoid the usage of an adhesive agent. On top of that, the appearing inner stresses of PEEK cooling down on a relatively cooler substrate can be compensated by the form fit. This counters the so called warping effect semi-crystalline polymers show in particular.

The mathematical methods to calculate an additional tool path for the 3D-printing part creation, the Bresenham and sweep line algorithm are reliable ways to generate a raft as a substrate for medical products.

As a critical part in the method of printing medical products free of contamination by using material extrusion technology, this concept has proven to be successful and is currently applied in more than 15 countries world wide and is reflected in of one of Apiums patents.

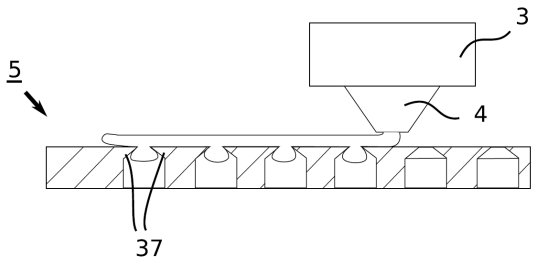

Fig.5

Perforated build plate with countersinks. The material is extruded in the holes, solidifies and generates a form-fit. Picture is taken from Patent DE102017131463A1.

Additive manufacturing of PEEK cranial implants: Powder Bed Fusion or Material Extrusion?

Y. Liu[1], N. Yi[1], R. Davies[1], P. McCutchion[1], O. Ghita[1]
College of Engineering, Mathematics and Physical Sciences, University of Exeter, Exeter, EX4 4QF, UK

Introduction: Poly(ether-ether-ketone) (PEEK) is an engineering thermoplastic of the poly(aryl-ether-ketone) (PAEK) family. PEEK has excellent mechanical properties and good thermal and chemical resistance and is widely used in harsh and demanding applications.[1] PEEK has also been widely applied to biomedical products for orthopedic, trauma and spinal implants due to its good biocompatibility.[2-3]

The last 10 years have seen a journey of discovery for many companies when it comes to processing or using PEEK in additive manufacturing (AM) processes; AM being attractive for medical applications as it can offer customized products. AM of PEEK uses mainly two techniques: powder bed fusion (PBF) process and material extrusion of polymers, commonly known as fused filament fabrication (FFF).[4-5]

Previous studies have reported the ability to fabricate PEEK cranial implants using both processes: PBF or FFF. El Halabi et al.[6] designed and compared the mesh PEEK cranial implants manufactured by PBF with two different scaffold geometries by numerical simulation. Berretta et al.[4] then experimentally investigated the PBF fabricated mesh PEEK cranial implants. The implants built in the inverted horizontal orientation showed the best overall mechanical properties. Several studies have also reported the possibility of using FFF to fabricate PEEK cranial implants and all the FFF printed implants[7-10] showed higher loading performance than the human parietal cranial bones.[11]

The problem with the existing materials is that they are not designed for the AM process, the AM process has a highly complex temperature profile which sits in between the isothermal and dynamic processes.[12] This doesn't necessarily favour the existing, highly crystalline polymers. Victrex PEEK 450 is the technical grade equivalent to OPTIMA LT1 – medical grade, and remains one of the few medical grades which could potentially be used in AM, although it is not commercially a product for either FFF or PBF processes.

The choice of technology is another dilemma the end-users and application specialists require more information on to fully understand. To exemplify the differences between the processes, this study chose printing of cranial implants using Victrex 450PEEK using filament/extrusion and powder bed technologies. The results provide insights into the mechanical behaviour of PEEK implants under the simulated compression and impact forces and future clinical implementation.

Methods and Materials: PEEK 450 (Victrex Plc, UK) was used for PBF in powder form and FFF as filament. The properties of the materials are listed in **Table 1**. The powder has an average particle size of 50 μm. The powder was heat treated at 250 °C for 24h to improve the powder flow.[13] The diameter of the filament is 1.75 mm.

Table 1. Material properties of Victrex PEEK 450.

Material	Melting temperature	Glass transition temperature
Victrex 450	343 °C	143 °C

Cranial implants were manufactured by PBF and FFF techniques using the same CAD model provided by Kumovis GmbH.

10 cranial specimens were manufactured by PBF in inverted horizontal orientation using the EOS P800 system (EOS, Germany) in reduced chamber mode. Because the PBF cranial implants built in inverted horizontal orientation showed the best mechanical performance in previous study.[4] The laser power and laser speed for contour are 9.35 W and 1000 mm/s. The laser power and laser speed for hatching are 16.5 W and 2550 mm/s. Other processing details for PBF specimens are listed in **Table 2**.

Table 2. PBF printing parameters.

Layer thickness	Hatching distance	Processing temperature
0.12 mm	0.2 mm	332 °C
Bed temperature	**Sidewall temperature**	
310 °C	315 °C	

10 cranial specimens were manufactured by FFF in vertical orientation using the Kumovis R1 3D printer (Kumovis GmbH, Germany). The FFF specimens were built in vertical orientation to minimise the support materials. The nozzle diameter is 0.6 mm. Other processing details for FFF specimens are listed in **Table 3**.

Table 3. FFF printing parameters

Layer thickness	Hatching distance	Chamber temperature
0.35 mm	0.4 - 0.6 mm	220 °C
Bed temperature	**Nozzle temperature**	
270 °C	440 °C	

The printed cranial implants were tested in static uniaxial compression loading using a Shimadzu AGS-20 kNX with a 20 kN load cell, test speed of 1 mm/min and a hemispherical indenter with a diameter of 10 mm. The specimens were placed on a custom-made laser sintered metallic sample holder.

The drop tower tests were performed on an Instron CEAST 9350 drop tower. A hemispherical nose impactor with a diameter of 20 mm as an instrumented striker, a load cell of 4.5 kN and a weight of 2.45 kg were employed. The

specimens were placed on the same metallic custom-made sample holder as the one used for quasi-static compression testing. Experiments were conducted at the same height and impact energy of 15 J. Five repeats were performed for the fabricated specimens.

Results and Discussions: Printed PBF and FFF cranial specimens are shown in **Figure 1** (a) and (b). The set-up of the quasi-static compression test for the PBF and FFF samples is shown in **Figure 1** (c) and (d). The specimens were fitted on a custom-made metal holder and the indenter started from the same height without any contact with the specimens. It was noticed that all the PBF specimens shattered into several pieces, suggesting a brittle failure (**Figure 1** (e)). For the FFF specimens, the indenter penetrated through the specimen and a hole was formed for four of the five FFF samples (**Figure 1** (f)), suggesting a tougher failure behavior. **Figure 2** shows all fractured cranial implants of PBF and FFF specimens. A more brittle fracture would be a potential risk for implant application because the shattered parts may damage the surrounding tissue.

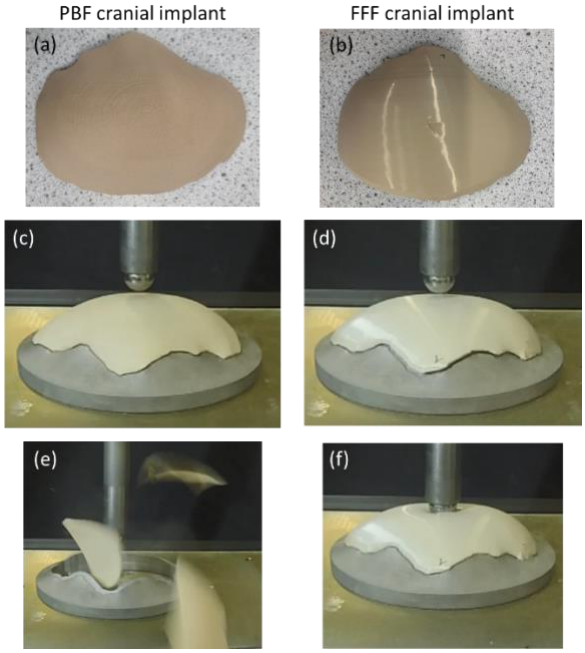

Figure 1. (a) The printed PBF cranial implant specimen; (b) the printed FFF cranial implant specimen; (c) – (d)

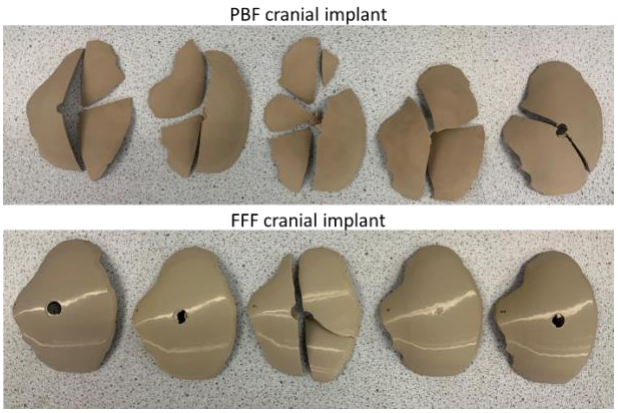

Figure 2. Fractured PBF and FFF cranial specimens after the quasi-static compression tests.

Table 4 shows the results of the quasi-static compression tests for the PBF and FFF cranial implant specimens. The maximum load is the highest load force applied on the samples during the test. Both PBF and FFF specimens show higher maximum load values compared to human parietal cranial bone, which is 793 N.[11] The displacement and total absorbed energy were higher for the FFF samples than the PBF specimens.

Table 4. Quasi-static compression test results for PBF and FFF cranial implant specimens.

Specimen	Maximum load (N)	Displacement (mm)	Total energy (J)
PBF cranial implant	1270.7 ± 68.5	3.44 ± 0.69	2.62 ± 0.85
FFF cranial implant	1164.9 ± 68.0	5.31 ± 0.91	3.47 ± 1.12

In addition to the compression tests, the drop tower impact tests were performed to replicate the behaviour of a sudden impact on the human skull, rather than a continuous load application. **Figure 3** shows the fractured specimens obtained from both processes after impact. All cranial samples shattered into several large parts and in a few cases, there was a significant number of small 2-5mm shards. The high impact velocity leads to full sample breakage across all specimens.

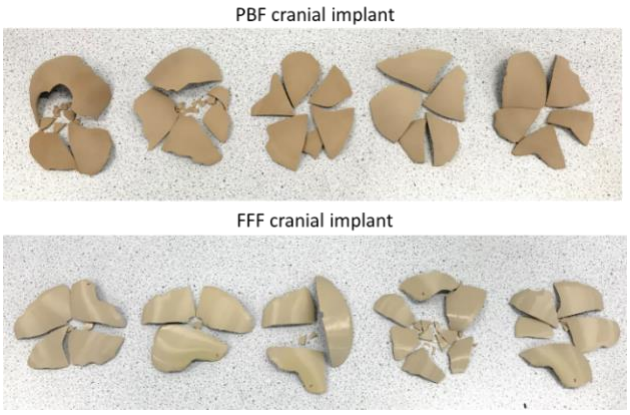

Figure 3. Fractured PBF and FFF cranial specimens after the drop tower impact tests.

Table 5 summaries the maximum force and total absorbed energy of PBF and FFF cranial specimens after the drop tower impact tests. A similar trend to the compression test has been observed during the impact tests. The PBF specimens had lower total energy than the FFF printed samples.

Table 5. Drop tower impact test results for PBF and FFF cranial implant specimens.

Specimen	Maximum force (N)	Total energy (J)
PBF cranial implant	1015.1 ± 133.2	2.90 ± 0.79
FFF cranial implant	1355.8 ± 379.5	4.72 ± 1.07

Figure 4 shows the microscope images of the fracture cross-section surfaces for the PBF and FFF cranial specimens after the quasi-static compression tests. The layered structure can be observed from the images. The cranial implant specimens were printed in different orientations for PBF and FFF samples. The printing layers of the PBF samples were observed from the image. Some particle-like features were observed in the PBF fracture surface, which may be related with the presence of partially molten PEEK particles. A layered hatching path was also observed in the FFF samples as well as a periodical pore structure, frequently noticed in FFF cross-sections as a result of filament deposition strategy. No obvious delamination phenomenon was observed during the tests suggesting the layer bonding for both PBF and FFF samples was good.

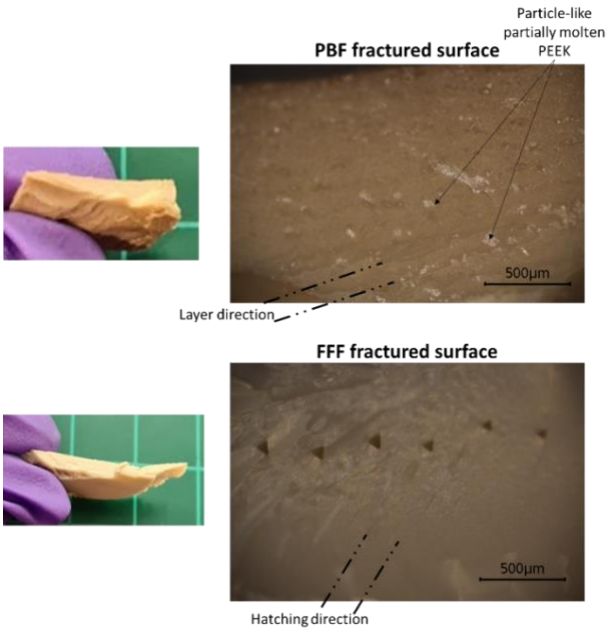

Figure 4. Microscope images of fractured surfaces for PBF and FFF specimen after the quasit-static compression tests.

Conclusions: The performance of PEEK cranial implants manufactured by PBF and FFF has been compared in this study. The mechanical properties performed in the quasi-static compression and drop tower impact tests show that FFF manufactured specimens can sustain higher energy than the PBF cranial implants. The FFF specimens deformed more during the compression test and showed more ductile failure; whereas a more brittle failure was observed on the PBF specimens.

This study has revealed that different AM process technologies significantly affect the mechanical behaviour of medical implants. AM of cranial implants provides a vast potential for craniofacial reconstruction applications. Further investigations on the reproducibility and biomechanical performance of the printed specimens would be essential for their medical applications.

Acknowledgements: The authors would like to acknowledge Dr Sebastian Pammer and his team from Kumovis GmbH for providing the FFF PEEK cranial samples. The authors would also like to thank the UK Research and Innovation (UKRI) for funding this study (Research in Residence).

References:

1. Comelli, C. A.; Davies, R.; van der Pol, H.; Ghita, O., PEEK filament characteristics before and after extrusion within fused filament fabrication process. *Journal of Materials Science* **2022,** *57* (1), 766-788.
2. Pérez-Martín, H.; Mackenzie, P.; Baidak, A.; Ó Brádaigh, C. M.; Ray, D., Crystallinity studies of PEKK

and carbon fibre/PEKK composites: A review. *Composites Part B: Engineering* **2021,** *223*, 109127.
3. Kurtz, S. M.; Devine, J. N., PEEK biomaterials in trauma, orthopedic, and spinal implants. *Biomaterials* **2007,** *28* (32), 4845-4869.
4. Berretta, S.; Evans, K.; Ghita, O., Additive manufacture of PEEK cranial implants: Manufacturing considerations versus accuracy and mechanical performance. *Materials & Design* **2018,** *139*, 141-152.
5. Yi, N.; Davies, R.; Chaplin, A.; McCutchion, P.; Ghita, O., Slow and fast crystallising poly aryl ether ketones (PAEKs) in 3D printing: Crystallisation kinetics, morphology, and mechanical properties. *Additive Manufacturing* **2021,** *39*, 101843.
6. El Halabi, F.; Rodriguez, J. F.; Rebolledo, L.; Hurtós, E.; Doblaré, M., Mechanical characterization and numerical simulation of polyether–ether–ketone (PEEK) cranial implants. *Journal of the Mechanical Behavior of Biomedical Materials* **2011,** *4* (8), 1819-1832.
7. Zhao, Y.; Zhao, K.; Li, Y.; Chen, F., Mechanical characterization of biocompatible PEEK by FDM. *Journal of Manufacturing Processes* **2020,** *56*, 28-42.
8. Sharma, N.; Aghlmandi, S.; Dalcanale, F.; Seiler, D.; Zeilhofer, H.-F.; Honigmann, P.; Thieringer, F. M., Quantitative Assessment of Point-of-Care 3D-Printed Patient-Specific Polyetheretherketone (PEEK) Cranial Implants. *International Journal of Molecular Sciences* **2021,** *22* (16), 8521.
9. Sharma, N.; Aghlmandi, S.; Cao, S.; Kunz, C.; Honigmann, P.; Thieringer, F. M., Quality Characteristics and Clinical Relevance of In-House 3D-Printed Customized Polyetheretherketone (PEEK) Implants for Craniofacial Reconstruction. *Journal of Clinical Medicine* **2020,** *9* (9), 2818.
10. Sharma, N.; Honigmann, P.; Cao, S.; Thieringer, F., Dimensional characteristics of FDM 3D printed PEEK implant for craniofacial reconstructions. *Transactions on Additive Manufacturing Meets Medicine* **2020,** *2* (1).
11. Motherway, J. A.; Verschueren, P.; Van der Perre, G.; Vander Sloten, J.; Gilchrist, M. D., The mechanical properties of cranial bone: The effect of loading rate and cranial sampling position. *Journal of Biomechanics* **2009,** *42* (13), 2129-2135.
12. Basgul, C.; Thieringer, F. M.; Kurtz, S. M., Heat transfer-based non-isothermal healing model for the interfacial bonding strength of fused filament fabricated polyetheretherketone. *Additive Manufacturing* **2021,** *46*, 102097.
13. Berretta, S.; Evans, K. E.; Ghita, O., Processability of PEEK, a new polymer for High Temperature Laser Sintering (HT-LS). *European Polymer Journal* **2015,** *68*, 243-266.

Biomechanically Tuning the Strength and Stiffness of an Open Pillar Implant Interface

Causey, GC[1]; Price, J[1]; Picha, GJ[1]; Pelletier, M[2]; Wang, T[2]; Walsh, WR[2], Mathey, E[3]; Carpenter, DR[3]
[1]Applied Medical Technology, Inc. Brecksville, OH.; [2]UNSW Australia; [3]Department of Mech. Eng, Univ. of CO Denver
greg.causey@appliedmedical.net

Intro: Osseointegration is paramount to the effectiveness of the implant system. Our research group has been exploring the mechanical performance and biologic response of an open surface morphology for orthopedic applications. In contrast to traditional porous surfaces in which the bone must grow into discrete pores, our macro-scale surface is comprised of discrete pillars which create an open space into which a continuous bony mass can easily grow. Engineering the pillars enables us to control the percent composition of implant and bone within the interface zone thereby providing the opportunity to control strength and stiffness and tailor the biomechanical response to best meet clinical requirements.

Objectives:

- Evaluate the biologic, biomechanical, and mechanical performance of an open pillar interface in-vivo and on the benchtop.
- Develop a finite element simulation of the biomechanical response of the pillar interface.

Methods: A combination of simulation, benchtop, and in-vivo testing has been employed in the development and characterization of the pillar morphology. In-vivo testing using a common ovine model was initially undertaken to assess the biologic and biomechanical response of the interface[1]. Benchtop testing was performed to further characterize the mechanical properties of the interface. Finite element simulation is underway to create an in-silico model of the bone/pillar interface[2] for product design and development use.

In-vivo: Following ethical clearance, cylindrical implants were placed in cortical (tibia) and cancellous (condyles) sites. Implant materials included PEEK, HA-PEEK, Ti coated PEEK, Titanium, and UHMWPE. Animals were sacrificed at 6 and 12 weeks with μCT and histologic evaluation of the biologic response and pushout characterization of biomechanical performance (shear stress, stiffness, and energy to failure).

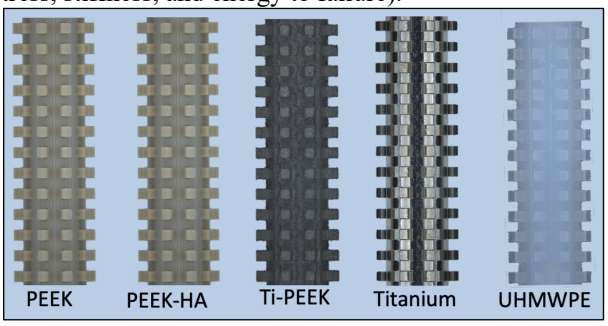

Figure 1: Ovine Implants

Benchtop: Generic lateral spinal cages were created which incorporated a pillar morphology on the top and bottom surfaces. Cages were subsequently tested using a standard expulsion test. In one series of experiments, pillar height was varied while keeping other variables consistent. In another, test implant material was changed while pillar morphology was kept the same. Average expulsion forces and interface stiffnesses were reviewed.

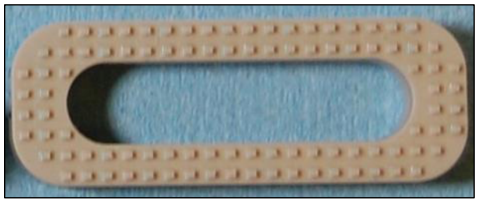

Figure 2: Lateral Spinal Cage (PEEK shown)

In-silico: Solid models of the cylindrical dowels (PEEK, Titanium) used in the in-vivo study were virtually placed into a simulated rectangular bone block. The model was reduced to 1/4 quadrant using symmetry and meshed using linear tetrahedral elements. The bone block was segmented into 3 regions: the bulk bone outside of the pillar interface zone, an outer pillar zone (100 micron layer), and an inner pillar zone. By varying the density in the various bone regions the simulation of ingrowing and maturing bone was replicated. The bottom of the bone block was fixed and a 0.5% global strain applied to the top of the implant. The the stiffness of the interface was calculated and the load sharing between the implant and bone computed. Physical pillared dowels were over-molded and benchtop tested with results used to refine and validate the FEA model.

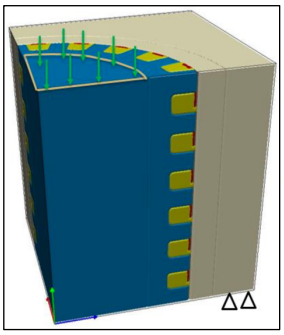

Results:

In-vivo: Review of bone growth into the intrapillar region revealed approximately 60% ingrowth at 6 weeks which increased to nearly 80% by the 12 week timepoint. No differences were noted among all implant materials.

Mechanical testing at the 6 week timepoint revealed no difference in shear stress between any group except for UHMWPE when compared to Titanium. At 6 weeks a trend of decreasing stiffness from the Titanium group to the PEEK groups to the UHMWPE group was noted. Titanium was significantly stiffer than PEEK, PEEK-HA, and UHMPWE while Ti-PEEK was significantly stiffer than the UHMWPE.

At 12 weeks there was no difference in shear stress between the Titanium and PEEK groups. The difference between UHMWPE and all other groups and was significant. The stiffness of Titanium was significantly greater than all groups. Ti-PEEK was significantly stiffer than UHMWPE. No other differences were noted.

Differences between timepoints for each group for both shear stress and stiffness was significant in all cases except Ti-PEEK and UHMWPE.

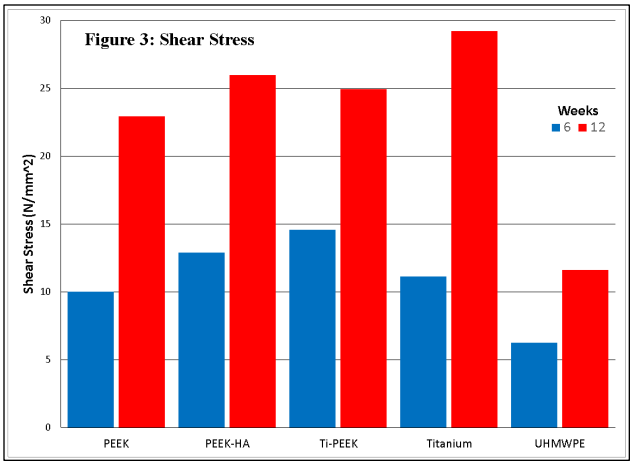

Energy to Failure increased in all groups from the 6 to 12 week timepoint. Titanium demonstrated the lowest energy to failure while the PEEK groups demonstrated the highest; UHMWPE fell between.

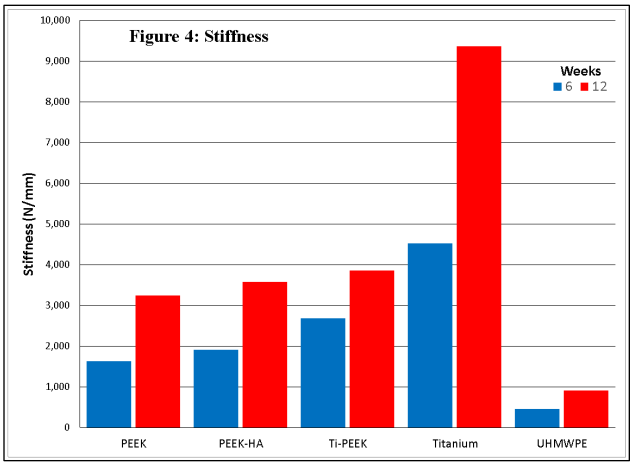

Benchtop: Comparison of different pillar heights (0.5, 1.0, 1.5, 2.0 mm) with the same pillar cross-section (0.5mm x 0.5mm) in a common material (PEEK) without initial embedding revealed an initial increase in shear stress which peaked and then decreased as height increased while stiffness decreased with height (Table 1).

Pillar Height	Average Expulsion Force (N)	Average Stiffness (N/mm)
0.5mm	1026	2467
1.0mm	1511	2015
1.5mm	1006	1389
2.0mm	572	1023

Table 1: Expulsion Force and Stiffness vs Pillar Height

Comparison of a similar pillar geometry (0.5mm x 0.5mm, 0.5mm height) in two different materials (PEEK, Titanium) without initial embedding revealed a difference in both strength and stiffness correlated with material properties (Table 2).

Material	Average Expulsion Force (N)	Average Stiffness (N/mm)
PEEK	1097	2257
Titanium	1141	3808

Table 2: Expulsion Force and Stiffness vs Material

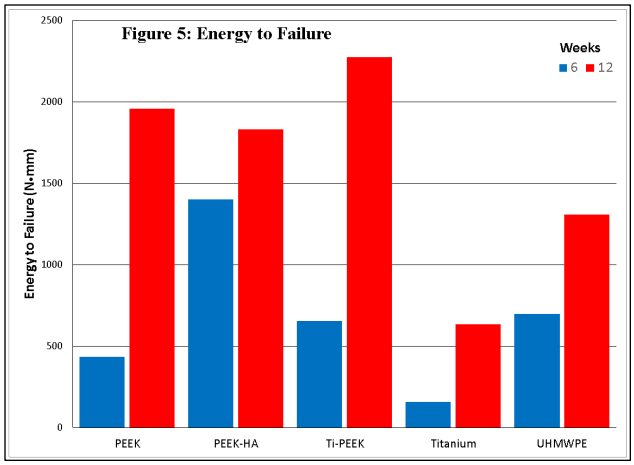

In-Silico: 3 timepoints were simulated by increasing the properties of the intra pillar zone from granular tissue to partial mineralization to full mineralization. Stiffness of the interface increased in both materials (PEEK, Titanium) as time progressed, however the stiffness of the Titanium implants were over 4X as stiff as the PEEK at the final timepoint.

Load sharing between the implants and surrounding bony tissue at the final timepoint demonstrated the bone carried an average of 12.2% greater load in the PEEK implant material as compared to the Titanium implant material with the same pillar geometry.

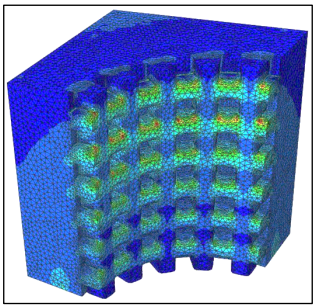

Discussion: Biomechanical performance of the bone/implant interface is crucial to the short-term fixation and long-term durability of any orthopedic implant. While testing is often focused on the strength of the interface as determined by mechanical pushout, the compliance of the interface is equally important but often overlooked. Achieving a stress sharing interface with the surrounding tissue can ensure the long-term durability of the interface. The interdigitation of the discrete pillars with the continuous mass of surrounding bone enables superior mechanical strength in polymeric materials yet still allows one to take advantage of the lower polymer modulus to reduce the interface stiffness. When comparing the shear stress, all PEEK groups had similar values as compared to Titanium. Yet PEEK exhibited 1/4 the stiffness which may demonstrate less propensity to stress shielding. Further, UHMWPE, a material not known to be bone friendly, demonstrated 3X the shear stress as compared to a common grit blast surface[3]. The stiffness, however, was approximately 1/4 the stiffness of the PEEK groups and 1/8 the stiffness of the Titanium group[4].

When examining the failure mode during pushout testing the Titanium always displayed a failure of the surrounding bone with no deformation of the pillars. The PEEK groups displayed a mixture of bone failure or pillar failure which may indicate a better matching of properties between the

implant and surrounding bone. The UHMWPE mostly failed in the pillars although a few demonstrated bone failure. Of note, however, was an unexpected failure mode seen in both the PEEK and UHMWPE groups. In some cases the body of the implant failed in compression without any disruption of the bone/implant interface. To our knowledge, this failure mode has not been previously seen in implants that are not 100% lattice structures without a solid body.

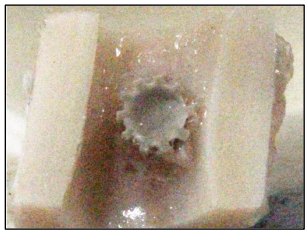

Benchtop pushout testing demonstrated the the ability to affect the strength and stiffness of the interface based on pillar geometry and implant material. While much work remains to be done, initial results demonstrate the potential to tune the interface interface.

A finite element model is under development to assist in designing the appropriate pillar geometry. While still actively in development, we have currently shown the ability of the pillar interface to provide better transmission of strain into the surrounding tissue as compared to a traditional porous surface[2]. Additionally, we have demonstrated pillars in PEEK can more effectively share stress with surrounding bone as compared to similar pillars in Titanium. Current work includes model refinement to increase fidelity and modeling of more clinically relevant scenarios. Ultimately our goal is to create a tool that can be used to assist and refine the pillar morphology for a given clinical scenario.

Conclusion:

- Successful ingrowth was seen in materials not generally considered to be "bone friendly" without subsequent on-growth coatings or surface treatments.
- The strength and stiffness response of the interface varied with pillar morphology and implant material.
- The interface strength often exceeded the bulk implant material properties in PEEK and UHMWPE implant materials.

Clinical Significance: The ability to design the biomechanical characteristics of the interface between the implant and surrounding bony tissue may enable more durable and robust implant systems. Tailoring the stiffness of the interface for the specific requirements based on patient's bone quality and clinical performance requirements may offer improved longevity of the bone/implant interface.

Utilizing a pillar interface that enables robust interdigitated bony ingrowth across a variety of implant materials can allow for the optimum material decision for specific application requirements.

[1] Causey, G.C., et.al., 2021. *The effect of a novel pillar surface morphology and material composition demonstrates uniform osseointegration*. https://doi.org/10.1016/j.jmbbm.2021.104775.
[2] Mathey, E., et.al., 2021. *Bone-Implant Stiffness and Load Sharing During Bone Ingrowth into a Novel Surface Topology*. ORS Annual Meeting 2021
[3] Causey, G.C., et.al., 2021. *In-Vivo response to a novel pillared surface morphology for osseointegration in an ovine model*. https://doi.org/10.1016/j.jmbbm.2021.104462.
[4] Causey, G.C., et.al., 2019. *Results of In-Vivo Testing of a Novel Macro-Scale Osseointegration Surface Morphology*, 4th Int. PEEK Symposium.

3D Direct-Printed PEEK Has Longer High-Cycle Fatigue Life to Machined 3D Printed PEEK

Bowsman, L[1], Du, H[1], Vakharia, A[2], Jasty, N[1], Kraay, M[2], Rimnac, C[1]
[1]Case Western Reserve University, Cleveland, OH, USA; [2]University Hospitals, Cleveland, OH, USA
leandra.bowsman@case.edu

Introduction: Additive manufacturing or 3D printing is of keen interest as a means by which to manufacture medical devices, including fused filament fabrication (FFF) of the biocompatible polymer polyether-ether-ketone (PEEK) [1]. Monotonic properties of 3D printed PEEK have been well-reported [2]. However, since orthopaedic implants (e.g., joint replacements) are often subject to complex cyclic loading [3] and are expected to have service lives of decades [4, 5], high-cycle fatigue life (stress-life (S-N)) is also important.

The objective of this study was to characterize the high-cycle fatigue life, percent crystallinity, peak melting temperature, and density of PEEK in two 3D-printed conditions; an injection molded control was also tested. Fracture surfaces were also observed to qualitatively assess print quality.

Methods and Materials: Fused filament fabrication (FFF) printing was conducted on an Apium P220 with 1.75 mm unfilled ThermaX PEEK filament (3DXTech). Filament was dried at 60C for a minimum of 12 hours prior to printing (PrintDry). All prints had 100% solid rectilinear infill at -45/+45 raster angles, 75% outline overlap, and speed of 1500 mm/min. (Table 1, Fig. 1). Cylindrically-waisted S-N specimens (gauge diameter: 3 mm; grip diameter: 4.75 mm; overall length: 29 mm) with dimensions guided by ASTM E466-07 were either machined from 3D printed rectangular "bricks" (PB) or directly 3D printed into S-N specimens (DP). 3D printed bricks were individually printed and machined into specimens using a benchtop CNC lathe (Sherline). DP specimens were printed two at a time; grip and gauge regions were sanded to nominal dimensions. Gauge regions of both groups were finish-sanded to nominal dimensions. Neither group underwent post-thermal treatment (e.g., annealing). Machined injection molded controls (IM) were also prepared similarly to the machined PB group.

High-cycle fatigue (S-N): S-N tests (n = 3-10/group and stress) were conducted to determine high-cycle fatigue life at 5 nominal cyclic stresses: 55 MPa; 64 MPa; 68 MPa; 72 MPa; and 80 MPa. Tests were conducted to failure or run-out (10M cycles) using two custom cantilever rotating bending testing frames with specimens submerged in a physiologically relevant 37C PBS bath (Fig. 2) [3]. When plotted on a log-log scale, the stress amplitude, σ, and high-cycle fatigue life, N_f, can be related with the equation $\sigma = A(N_f)^b$, where coefficient, A, and exponent, b, are constants [3]. Coefficient A and exponent b were determined from a log-log transform and least squares fit of data from all failed specimens from each printed group (MATLAB 2020b) [3]. Median life and range were plotted. Fracture surfaces of selected specimens from each printed group were documented via scanning electron microscopy (Tescan Vega3).

Percent crystallinity, peak melting temperature, and density: Using a double-melt method, first and second heat percent crystallinities, $\%\chi$, and peak melting temperatures, T_m, were determined via differential scanning calorimetry (DSC, Mettler Toledo) per ASTM D3418-15. Samples were taken from the grip and gauge regions and the data were combined (n = 12/group). Density (n = 5-15/group) was measured using ASTM D792-20 as a guide.

Statistical analysis: For S-N behavior, regression analysis was conducted to compare coefficient, A, and exponent, b, between printed groups (Minitab 20). No fit was generated for the IM group due to the number of run-out samples. $\%\chi$ differences between first and second heats and groups were compared with two-sample t-tests. Two-sample Mann-Whitney U tests were used to compare T_m differences between first and second heats and groups and group densities. Significance was taken at $p < 0.05$.

Results: At each cyclic stress, DP S-N specimens had longer median life than PB S-N specimens. All DP S-N specimens tested at 55 MPa and one at 64 MPa achieved run-out (Fig. 3). There was no difference between the coefficient, A ($p = 0.95$) and exponent, b ($p = 0.77$) between the two printed groups. For the PB group, fracture either propagated transversely with respect to the layer's surface along the raster angle, or the surface was relatively flat and fracture propagated transversely with respect to the layer's surface with no distinction along the raster angle. DP specimen fractures propagated transversely with respect to the layer's surface on the top and bottom (i.e., where the layers forming the top and bottom of the gauge region were not continuous) and also indicated torsional influence toward the center (Fig. 4).

There was no difference in $\%\chi$ (Table 2) between first and second heats for each group, or between groups for the second heat. Only the PB group showed a difference in T_m between first and second heats ($p = 0.039$); for second heats, there was no difference in T_m between printed groups, but there were differences when each printed group was compared to the control PB v. IM ($p < 0.001$) and DP v. IM ($p = 0.001$). The median (IQR) densities were: PB 1.18 (0.101 g/cm^3); DP 1.28 (0.012 g/cm^3); IM 1.30 (0.003 g/cm^3). Density differences were significant: PB v. DP ($p = 0.009$); IM v. PB ($p = 0.001$); IM v. DP ($p = 0.001$).

Discussion: Directly printing S-N specimens resulted in qualitatively better S-N fatigue behavior than if one were to treat 3D printed material in a more traditional manner (i.e., subtractive manufacturing via machining, PB group), but the injection molded control generally still had greater median life. The large p-values may be due to the large range of cycles at each stress. Regardless of method of printed manufacture, all printed specimens showed evidence of layer separation on the fracture surfaces. The

PB fracture surfaces with relatively shorter life fractured along the raster angle, further supporting poor or inadequate layer adhesion. In contrast, though separation of layers was also evident in the DP group, the frequent observation of a torsional center-spiral fracture indicates overall better resistance to fracture than the PB group, suggesting that layer adhesion was somewhat better in the DP group.

Percent crystallinities of both printed groups were similar to the injection molded control, and median peak melting temperatures were only slightly lower than the control, suggesting that fatigue life was influenced more by printing quality than by material changes. DP had a tighter range and density closer to the control than the PB group. The lower density and larger range in the PB group may be due to variations in processing parameters during printing that remain to be determined.

Some limitations of this study include: the use of non-medical grade filament; an injection molded control group of the same resin was not available for comparison; only build orientation relative to the print bed was examined; and influence of post-annealing was not examined.

These initial findings provide a basis for demonstrating the feasibility of characterizing the high-cycle fatigue life of FFF printed PEEK. Direct-printed results at lower and likely more physiologically relevant stresses (i.e., $\leq$ 55 MPa as seen in bone [3]) show particular promise, with further print setting optimization and/or post-process annealing possibly improving fatigue life by relieving internal stresses and/or facilitating enhanced layer adhesion.

References

[1] Basgul, C et al. J Mater Res, 2018. [2] Shanmugam, V et al. I J Fatigue, 2020. [3] Islam, A et al. CORR, 2016. [4] Evans, J et al. Lancet, 2019; 393: 647-54. [5] Evans, J et al. Lancet, 2019; 393: 655-63. [6] Wu, W et al. Mater, 2015.

Acknowledgements

Gordon and Mary Harnett Fund for Joint Replacement and Preservation (MJK); W. J. Austin Chair (CMR).

Table 1. Notable print settings.

Setting	PB	DP
Print bed adhesive	Nanopolymer	DimaFix (pen)
Print bed T (C)	140	130
Nozzle T (C)	470	440

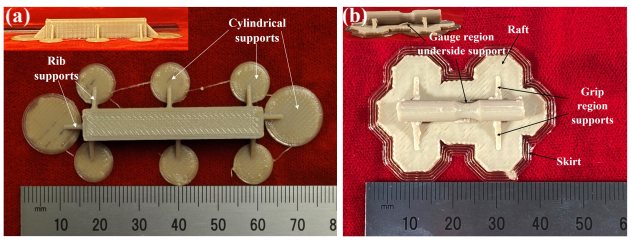

Figure 1. (a) Printed brick prior to machining and (b) DP specimen prior to polishing.

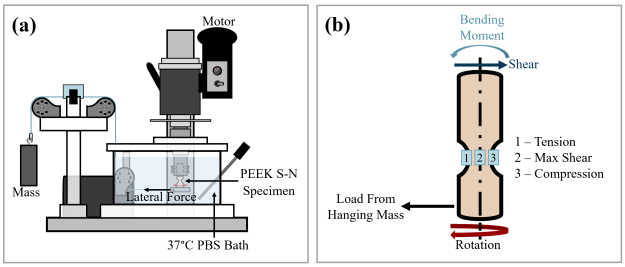

Figure 2. (a) Custom cantilever rotating bending testing frame and (b) stresses delivered to specimen during a single 360° rotation.

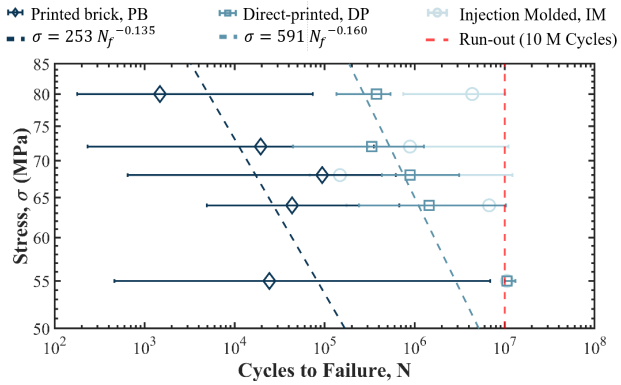

Figure 3. PB and DP range and median life S-N data with least squares regression fit of pooled data. Fit excluded DP run-out data, i.e., all data at 55 MPa and one at 64 MPa. IM range and median life provided for reference.

Table 2. Mean (standard deviation) of first and second heat percent crystallinities (%χ) and median (IQR) of first and second peak melting temperatures (T_m).

	1st %χ	2nd %χ	1st T_m (C)	2nd T_m (C)
PB	39.0 (7.7)	33.0 (7.0)	335.5 (0.79)	336.1 (0.21)
DP	40.2 (8.3)	34.5 (6.9)	335.8 (0.75)	335.9 (0.71)
IM	38.5 (4.2)	36.5 (5.2)	338.5 (1.3)	338.0 (0.54)

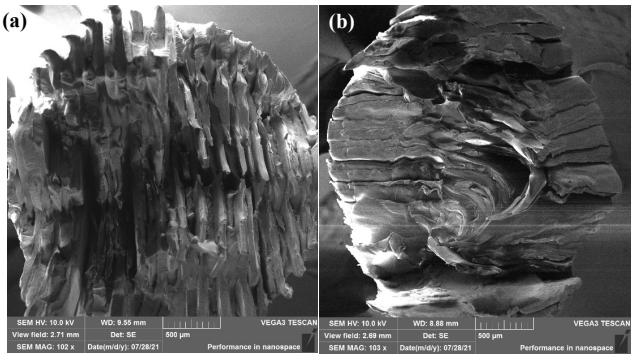

Figure 4. Fracture surfaces of (a) PB and (b) DP showing layer separation.

MDR-compliant Medical Device Production System for PEEK CMF-implants

Leonhardt, Stefan; Pammer, Sebastian
Kumovis GmbH – a 3D Systems company, Munich, Germany
stefan.leonhardt@3dsystems.com, sebastian.pammer@3dsystems.com

Introduction: 3D-prinitng with implantable high-performance polymers, like PEEK, still is facing challenges that must be taken to finally become the standard process to manufacture patient specific implants. Advantages like cost- and time-savings are well known. However, there are only a few companies that can proof equal mechanical properties compared to machined implants using 3D-printing technology. Furthermore, often there is no full biological validation available and no clear regulatory pathway in place. In this presentation we will show an end-to-end solution for the manufacturing of patient specific cranial. Additionally, we will present results from an intensive biological validation as well as the performance of printed worst-case design in impact testing and compression testing.

Methods and Materials: The presented end-to-end workflow consists out of the following steps:

- Segmentation using D2P (3D Systems)
- Implant and support design using Freeform (3D Systems)
- Assigning of prosses parameters based on implant analysis
- 3D-printing using proprietary Kumovis technology
- Process-monitoring using Oqton
- Post-processing
- Cleaning and Sterilization

The automated segmentation and partly-automated implant design process will be presented during the presentation. Based on an analysis of the implant size a pre-defined parameter set is assigned.
In an extensive performance study all pre-defined parameter sets were used to print worst-case designs. The designs varied in size and thickness and were showing a worst-case pattern of perfusion holes. The worst-case geometries and acceptance criteria used for the performance study were derived from a comprehensive literature research.
For the printing process the Kumovis R1 and Evonik i4 3DF-T filament was used. All samples were cleaned using IPA and sterilized two times (134°C, 4 min). Afterwards the samples were mounted on a counterpart using commercially available titanium cranium fixation plates and screws (KLS Martin).
Impact-testing was carried out in a stepwise manner: First, the drop height was adjusted to an impact energy of 3 J. Then, the weight was released. After the impact, the plate was inspected for any visible failure. In case there was no failure detectable, the drop height was increased. Testing was stopped as soon as either failure of the plate was detected, or the maximum applicable impact energy of 40 J was reached.
Static compression testing was performed using a Zwick Z020 with a 20kN load cell. The load was applied via the force actuator of the material testing machine using a plunger. Each implant was positioned in the static material testing machine and an initial axial load of 5 N was applied. During the test, each implant was loaded axially, starting at the initial axial load, with an increasing force and at a constant loading rate of 5 mm/min until the implant failed or a maximum applicable load of 20 kN was reached. Furthermore, the breaking behavior (if occurred) from all samples (static compression and impact) were evaluated.
To proof the biological safety of the defined process all required end-points according to the standard DIN EN ISO 10993 for long-term implants have been performed. This also included a 90-day implantation in the calvarial bone of rats.

Results: The static compression tests showed that maximum loads between 1kN and 9kN could be applied to the printed implants, depending on the size and thickness of the sample. The thinnest and largest implants (lowest load) showed a deformation up to 11 mm before breaking occurs.
Impact testing showed that all acceptance criteria were hit. For large, thick implants impact forces up to 20J could be obtained.
All implants showed a good breaking behavior. No delamination or breaking between the layers could be observed. Furthermore, no shuttering of the implants could be observed. Therefore, it can be stated that the printed samples still show a ductile behavior.
The biological evaluation showed that printed samples using worst-case printing parameters passed. The chemical analysis studies showed that the printing process leads to no contamination or degradation. Implantation studies showed that no mortality occurred during the implantation period. Clinical and ophthalmological observation including functional/detailed behavioral examination revealed no specific findings. All animals showed weight gain on the day of necropsy when compared to the day of implantation. The calvarial implantation sites of the test item and control showed no specific macroscopic findings in all animals.

Discussion: The performed study showed that all printed worst-case designs using Evonik i4-3DFT and the Kumovis printing technology passed the acceptance criteria for static compression and impact testing. Furthermore, all required biological end-pointes for long-term implants were passed. In next steps a clinical bench testing will be performed investigating the usability and fitting of the implant. Therefore, representative cases will be used to perform the full end-to-end solution to manufacture patient specific PEEK implants. Afterwards surgeons will use a host model and commercially available fixation hardware to perform a bench-implantation.

Optimizing Flexural Strength of CF-PEKK for Fracture Fixation

Rabinowitz, Aliza[1]
[1]Drexel University, Philadelphia, PA
ar3765@drexel.edu

Introduction: There has been growing interest and success in 3D printing polymers and composite materials for medical applications. One such composite, carbon fiber poly-ether-ketone-ketone (CF-PEKK), offers biocompatibility, comparable elastic modulus to bone, and radiolucency, making it a strong candidate for fracture fixation applications.

Fracture fixation plates must have adequate flexural strength to promote proper bone healing. The aim of this research is to determine the optimal printing parameters to maximize the flexural strength of CF-PEKK. In addition, a comparison was made between the flexural strength of 3D printed CF-PEKK and 3D printed and pressed CF-PEKK.

Methods and Materials: A Design of Experiments (DOE) was created based on the Taguchi method. The input parameters varied in this experiment were nozzle diameter, layer height, print speed, raster angle, and nozzle temperature. There was a total of 8 experimental groups with n=5 for each group.

The material used in this experiment was CF-PEKK A manufactured by 3DX Tech. The filament was dried at 60ºC for 12 hours and printed on a Kumovis-HTRD-1.3 printer to create flexure specimens with dimensions 12.7x2x144 mm. The printed and pressed specimens were printed at 9T labs in Zurich, Switzerland utilizing a temperature controlled mechanical press.

The specimens were mechanically tested in 3-point bending in accordance with ASTM D790 to determine how printing parameters impact flexural strength. The fracture surfaces were investigated using the Zeiss Supra SEM to determine differences in internal structure.

Results: The flexural strength results were determined for all the specimens and the mean was determined for each group. A Taguchi statistical analysis was performed and the SN ratio for each input parameter was found to be Nozzle diameter 3.33, Layer Height 6.22, Print Speed 1.01, Raster Angle 2.06, Nozzle Temperature 2.32. SN ratios were analyzed with a one-way ANOVA, and it was determined that the nozzle diameter, layer height, and raster angle have a statistically significant impact on the flexural strength ($p<0.05$). A Taguchi statistical analysis was performed to maximize the mean and response values are Nozzle Diameter 6.45, Layer Height 11.50, Print Speed 2.20, Raster Angle 12.15, Nozzle Temperature 1.05. Mean response values were analyzed with a one-way ANOVA, and it was determined that a 0.8 Nozzle diameter, 0.25 Layer Height, and 0/90 infill pattern have a significant impact on increasing the flexural strength of the specimens.

The optimal 3D printed specimens had a (mean ± SD) flexural strength of (107.9 ± 3.6) MPa and a mean flexural modulus of 3.5 GPa. The 3D printed and pressed specimens had a (mean ± SD) flexural strength of (252.7 ± 19.6 MPa) and a mean flexural modulus of 7.8 GPa. These values were compared to known values for the flexural modulus of Femur bone (2.2 GPa) and flexural strength of Femur bone (84.03 $\pm$ 9.91). Friedman Dunn test was used to determine that there is a significant difference between the Flexural Strength of the 3DP+P CF-PEKK and femur bone but not between 3DP CF-PEKK and femur bone ($p<0.05$). Tukey's multiple comparison was used to determine that SS316L and TI6Al4V have a higher significant difference in flexural modulus when compared to bone than both 3DP CF-PEKK and 3DP+P CF-PEKK.

The SEM images of the fracture surfaces are shown below in figure 1. The 3DP CF-PEKK specimens have pores and void spaces when compared to the 3DP and pressed specimens. The 3DP and pressed specimens exhibit better fiber matrix adhesion.

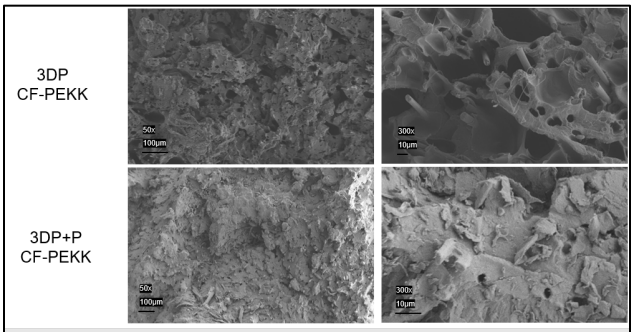

Figure 1: Fracture Surface Comparison

Discussion: In this study, we created a DOE to determine the best printing parameters for optimizing 3D printed CF-PEKK flexural strength. This will be useful for understanding the process-structure-property relationship to help guide future medical and industrial applications.

Extraordinary Interfacial Behaviors of Osteofab™ (Powder Bed Fusion of PEKK (PolyEtherKetoneKetone) Polymer) Orthopedic Devices - Anti-Microbial and Bone Apposing Effects Observed in the Absence of Surface Modification – an Overview

DeCarmine, A[1] and DeFelice, S[1]
[1]Oxford Performance Materials, South Windsor, CT USA

tdecarmine@oxfordpm.com

Introduction: The family of PAEK high performance polymers (encompassing PEEK, PEKK and others) has served well in the permanent implant world for many years. During that time, observations suggest the interface behaviors of PEEK may not be optimal for all uses – while inert and directly harmless, this inertness also seems to defeat (or at the very least, not aid) the body's mechanisms for defense against microbial ingression. Also suffering this inertness are mechanisms driving bony apposition facilitating incorporation of permanent reparative devices. While PEKK is classified as a PAEK family system by virtue of general structure, PEKK has substantial and important specific differences enabling fabrication via Powder Bed Fusion as well as providing substantially different surface chemistry behaviors that contribute to the defeat of microbial infection and enhance apposition of living bone directly to a device. An overview is presented revealing examinations of laboratory work performed to enlighten understanding of surface energy and resolve the relationship between composition and topography.

Methods and Materials:
As this presentation will be a light overview of published and unpublished work, it seems more fitting to offer a *sampled* bibliography to provide representation of the work quality than assembling the span of minutia herein.

1. Cheng, B., Jaffee, S., Averick, S., Swink, I., Horvath, S., & Zhukauskas, R. (2020). A comparative study of three biomaterials in an ovine bone defect model. *The Spine Journal*, *20*(3), 457-464. doi: 10.1016/j.spinee.2019.10.003

Results: PEKK implants demonstrated bone ingrowth, no radiographic interference, no fibrotic tissue membrane formation, significant increase in bony apposition over time, and significantly higher push-out strength compared to standard PEEK. The PEKK implant displayed bone growth characteristics comparable to Ti-coated PEEK with significant improvements in implant integrity and radiographic properties.

Conclusion: This study found that PEKK displayed preferable characteristics when compared to PEEK and Ti-coated PEEK, and is therefore a potential alternative to their use.

2. Lin, Y., Umebayashi, M., Abdallah, M., Dong, G., Roskies, M., & Zhao, Y. et al. (2019). Combination of polyetherketoneketone scaffold and human mesenchymal stem cells from temporomandibular joint synovial fluid enhances bone regeneration. *Scientific Reports*, *9*(1). doi: 10.1038/s41598-018-36778-2

In vitro results showed that hSF-MSCs attached, proliferated, and were osteogenic on PEKK. *In vivo* results indicated that PEKK seeded with hSF-MSCs regenerated twice the amount of newly formed bone when compared to PEKK seeded with osteogenically-induced hSF-MSCs or PEKK scaffolds alone. These results suggested that there was no need to induce hSF-MSCs into osteoblasts prior to their transplantations *in vivo*. In conclusion, the combined use of PEKK and hSF-MSCs was effective in regenerating critical-sized bone defects.

3. Roskies, M., Fang, D., Abdallah, M., Charbonneau, A., Cohen, N., & Jordan, J. et al. (2017). Three-dimensionally printed polyetherketoneketone scaffolds with mesenchymal stem cells for the reconstruction of critical-sized mandibular defects. *The Laryngoscope*, *127*(11), E392-E398. doi: 10.1002/lary.26781

Results: All scaffolds were well integrated into adjacent bone. Bone-to-tissue volume increased from 30.34% (+/- 12.46) to 61.27% (+/- 8.24), and trabecular thickness increased from 0.178 mm (+/- 0.069) to 0.331 mm (+/- 0.0306) in the 10- and 20-week groups, respectively, compared to no bone regrowth on the control side ($P < 0.05$). Histology confirmed integration at the bone–implant interface. Biomechanical testing revealed a compressive resistance 15 times that of bone alone ($P < 0.05$).

Conclusion: 3D-printed PEKK scaffolds combined with ADSCs present a promising solution to improve the bone–implant interface and increase the resistance to forces of mastication after mandibular reconstruction.

4. Wang, M., Bhardwaj, G., & Webster, T. (2017). Antibacterial properties of PEKK for orthopedic applications. International Journal Of Nanomedicine, Volume 12, 6471-6476. doi: 10.2147/ijn.s134983

In this study, a nanostructured surface was fabricated on poly-ether-ketone-ketone (PEKK), a new orthopedic implant chemistry, comprised of nanopillars with random interpillar spacing. Specifically, after 5 days, when compared to the orthopedic industry standard poly-ether-ether-ketone (PEEK), more than 37% less *Staphylococcus epidermidis* were found on the PEKK surface. *Pseudomonas aeruginosa* attachment and growth also decreased 28% after one day of culture, with around a 50% decrease after 5 days of culture when compared to PEEK. Such decreases in bacteria function were achieved without using antibiotics. In this manner, this study demonstrated for the first time, the promise that nanostructured PEKK has for numerous anti-infection orthopedic implant applications.

Results:
Benchmarking against both PEEK and Titanium, we find the bio-response of PEKK resins potently beneficial. These benefits exhibit in positive bone tissue response in the form of apparently load bearing apposition as well as infection response defeating adhesion, proliferation, and colony formation in bacterial and viral organisms. These responses, while enhanced by the nanosurface native to the 3D printed form, are an intrinsic behavior of devices composed of PEKK resin.

Discussion:
PAEK (PolyArylEtherKetone) family resins have provided welcome alternatives to metallics in the orthopedic space for some 20 years. Avoiding stress shielding, subsidence and enabling diagnostic imaging are boon to the medical community and patients alike. With time and experience, we learn what seemingly workable solutions yield unintended consequences – apposition failure and metallosis are examples of (bio)chemical interfacial behaviors causing avoidable suffering when employing ‘accepted’ materials. With time and progress, we expect improvements in efficacy, safety and cost. Adding layers and materials to salvage ‘accepted’ solutions, historically, adds cost, failure mode expansion and overall risk. Shifting to a base material that embodies the correct behavior set is the simplest, safest option. PEKK exhibits the correct technical property set for such a base material. Medical use materials must also have the bona fides - PEKK thermoplastic resins have been in the commercial orthopedic implant market since the mid-2000s under the OXPEKK™ banner. In that time, tens of thousands of serial spine fusion cages as well as thousands of patient specific cranial devices have been implanted without meaningful incident. This statement covers devices both machined from rod and 3D printed (Osteofab™). Over 15 US FDA 510(k) Documents have been issued covering OXPEKK™ and Osteofab™ devices.

3D-Printed Silicon Nitride-PEEK Composite Promotes In Vitro Osteogenic Activity and Mineralization

Paul DeSantis[1], Ryan Bock[2], Sean Ronayne[2], Bryan McEntire[2], Noreen J. Hickok[3], Steven M. Kurtz[1,4]
[1]Drexel University, Philadelphia, PA, [2]SINTX Technologies Corporation, Salt Lake City, UT,
[3]Thomas Jefferson University, Philadelphia, PA, [4]Exponent, Inc., Philadelphia, PA
pauldesantis@drexel.edu

Introduction: Treatment for intervertebral disc degeneration often involves the complete removal of the disc and the fusion of two adjacent vertebrae via a biocompatible implant. Molded or machined polyetheretherketone (PEEK) cages are often used due to PEEK having a similar elastic modulus to bone [2]. PEEK's surface, however, is chemically inert and hydrophobic, which can interfere with the implant's ability to osseointegrat]. An alternative material to metal and polymer-based implants is silicon nitride (Si_3N_4), which is a synthetic non-oxide ceramic. Silicon nitride implants have been shown to support bone growth and resist bacterial infection *in vivo*, but are unfortunately susceptible to brittle fracture due to its ceramic nature. A composite material made from both PEEK and Si_3N_4 could have the potential to combine the favorable biomechanical properties of PEEK with the antimicrobial and osseointegrative properties of Si_3N_4. Finally, such a composite material could allow for the creation of custom orthopedic implants, as PEEK is a thermoplastic that is able to be 3D printed into custom shapes through the process of fused filament fabrication, a process that pure Si_3N_4 is not compatible with.

Methods and Materials: Samples with dimensions of 10x10x1 mm were printed using SiN-PEEK composite containing 30% Si_3N_4 (Apium P220). Samples were imaged using scanning electron microscopy (SEM) (Zeiss Supra 50VP) in order to verify the presence of Si_3N_4 on the surface of the samples. Samples of 3D printed PEEK, machined Ti6Al4V, and machined pure Si_3N_4 were also prepared and imaged using SEM. Samples were sterilized via immersion in 70% ethanol and exposure to UV light, and placed in ultra-low attachment 24-well plates. A positive control of tissue culture plastic (TCP) was used. MC3T3E1 pre-osteoblast cells (ATCC) were cultured in Minimum Essential Media α (α-MEM) supplemented with 10% fetal bovine serum and 1% penicillin/streptomycin, and seeded at a density of 30,000 cells per well (n=6). At Day 7, media was supplemented with 5mM β-glycerophosphate and 5 µg/mL ascorbic acid in order to support the mineralization process. MTT and ALP assays a Days 7, 14, and 21 acted as markers for cell proliferation and osteogenic activity, respectively. Normalized ALP was calculated to measure osteogenic activity relative to cell number. An alizarin red assay was used on Day 21 to determine the amount of cumulative mineralization. A two-way ANOVA with multiple comparisons test was performed to compare normalized ALP results, and a one-way ANOVA with multiple comparisons test was used to compare alizarin red results (n=6).

Results: SEM images of composite SiN-PEEK samples show characteristic Si_3N_4 structures (Figure 1). Normalized ALP activity found that the SiN-PEEK composite showed the highest activity at Days 7 and 14, but was only significantly greater than the Ti6Al4V and positive control groups at Day 14. At Day 21, the SiN-PEEK group was not significantly different from the positive control and was significantly less than the Ti6Al4V, PEEK, and pure SiN groups. According to alizarin red stain results after 21 days, the SiN-PEEK composite had the highest amount of stain with 0.0982±0.0171 mM and the pure SiN sample had the lowest amount of stain at 0.0595±0.00699 mM.

Discussion: SEM imaging of composite samples show that SiN structures are present on the surface of 3D printed samples, indicating that cells would be able to interact with SiN without the need for post-processing of the surface. Materials used in orthopedic implants need to both support cellular proliferation and osteogenic differentiation for osseointegration to occur. The normalized ALP results suggest that the SiN-PEEK composite material provided a good surface for osteogenic activity in the first 14 days when compared to other materials, but was outpaced by the Ti6Al4V, pure SiN, and pure PEEK samples by 21 days. This could indicate that the surface better supports osteogenic differentiation as opposed to cellular proliferation in the short term. The alizarin red results suggest that over the period of 21 days, the SiN-PEEK composite material supported the formation of the most bone-like mineral, further supporting the idea that the composite material strongly supports osteogenic activity. In the future, the SiN-PEEK composite material could be tested *in vivo* to understand how the material performs in a more clinically relevant scenario.

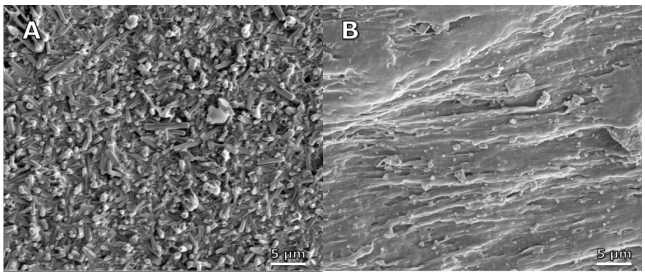

Figure 1: SEM image of **(A)** pure Si_3N_4 and **(B)** 3D-printed SiN-PEEK composite containing 30% Si_3N_4.

Will cement in your cup cause dramatic failure?
A Geometric Analysis of Polyethylene Liners Exposed to Acrylic-based Bone Cement

Thompson, Z[1], Hothi, H[2], Brillantes[1,3], Khoshbin, A[1,3], Atrey, A[1,3]

[1]University of Toronto, 27 King's College Cir, Toronto, ON M5S, Canada
[2]The Royal National Orthopaedic Hospital, Brockley Hill, Stanmore HA7 4LP, UK
[3]St. Michael's Hospital, University of Toronto, 30 Bond St., Toronto, ON M5B 1W8, Canada

zoe.thompson@mail.utoronto.ca

Introduction: Acrylic-based bone cement (PMMA) is a common material used in orthopaedic surgeries, however in preparing PMMA a highly exothermic reaction occurs. The heat released in this process has the potential to damage nearby materials that are poorly heat resistant such as highly crosslinked polyethylene. Both PMMA and highly crosslinked polyethylene are used in total hip arthroplasty (THA) and although not intended to come into contact intraoperatively these two materials could interact during femoral stem fixation.

Objective: To determine if the exothermic PMMA polymerisation reaction can alter the surface characteristics of highly crosslinked polyethylene acetabular liners used in THA.

Methods: Six XLPE liners were assigned to one of four experimental categories and had varying volumes of cement applied in a manner that mimicked how the two materials would come into contact intraoperatively. Cement was removed using digital sweep as it might be intraoperatively. Measurements of the liners were taken both pre- and post-intervention using a coordinate measuring machine (CMM) for geometric and gravimetric analysis. Light microscopy was conducted post-intervention to examine liners for surface damage.

Results: CMM measurements showed minimal global wear in all six liners but there was evidence of isolated surface deposits in four out of six liners, the largest measuring 140.7µm in height. The average maximal surface deviations, when compared to the control, for liners exposed to 1 cc of cement, 2 cc of cement or 1 cc of cement with a femoral head implant attached were 26.6µm, 77.2µm and 26.4µm respectively. Subtle surface scratches were identified using light microscopy on all six liners. All but one liner showed an increase in volume following cement application when compared to the control condition.

Conclusion: Highly cross-linked polyethylene shows areas of isolated surface deformation in a dose-dependent manner but with minimal global wear after coming into contact with highly exothermic PMMA. Nevertheless, these deposits have the potential to increase the rate of third body wear on articulating surfaces leading to THA failure.

Migration of the femoral component and clinical outcomes after total knee replacement: a narrative review

Zinno, RA[2], Di Paolo, ST[2], Alesi, DO[1], Zaffagnini, ST[1,2], Barone, GI[2], Bragonzoni, LA[2]

[1]IRCCS Istituto Ortopedico Rizzoli, Bologna, Italy
[2]University of Bologna, Italy

domenicoalesi@ymail.com

Introduction: Total knee replacement (TKR) represents a valid solution for the treatment of end-stage knee osteoarthritis. With the right indications and a reliable and reproducible surgical technique, TKR has an average lifetime of nearly 20 years with in vivo use before revision surgery becomes a necessity. A recent systematic review suggests that the rate of survival at 25 years of TKR is 82%. Anyway, there is still a considerable percentage of TKR failure whose consequent revision surgery might occur earlier than 20–25 years. Loosening is considered as a main cause of implant failure in TKR. Among the predictive signs of loosening, migration is the most investigated quantitative parameter. Several studies focused on the migration of the tibial component in TKR, while no reviews have been focused on the migration of the femoral component and its influence on patients' clinical outcomes. The aim of this narrative review was (1) to provide information about of the influence of migration in femoral component of TKR prostheses, (2) to assess how migration may affect patient clinical outcomes and (3) to present alternative solution to the standard cobalt-chrome prostheses.

Methods and Materials: A database search was performed on PubMed Central® according to the PRISMA guidelines for studies about Cobalt-Chrome femoral component migration in people that underwent primary TKR published until May 2020. All articles published until August 2020 were included in this review. During the screening procedure, only full-text available items, written in English language, were considered; pre-clinical and 'other animal' studies were included; moreover, reviews were added to the list. Subsequently, the authors further screened title and abstract of the papers, in order to exclude the irrelevant ones for this review. Then, the authors full-screened the remaining papers to leave out those not concerning femoral micromotion analysis, while papers concerning femoral components materials alternative to most used CoCr were included. In the end, 21 papers were included in the review. Furthermore, 17 papers (gray) mentioned in the selected works were added, since they did not appear in the first screening. Overall, 38 articles matched the selection criteria and were included in the study.

Results: Few studies investigated the femoral component through the migration, and no clear migration causes emerged. The Roentgen Stereophotogrammetric Analysis (RSA) has been mostly used to assess the migration for prognostic predictions. An annual migration of 0.10 mm seems compatible with good long-term performance and good clinical and functional outcomes.

Discussion: Only a limited number of studies evaluated micromotion of the TKR femoral component. There is no total agreement regarding the migration causes; at the same time, there are contrasting opinions about patients' clinical outcomes after surgery. At the present time, the RSA technique is the most commonly used, as well as the most accurate tool to evaluate migration. Indeed, it is recognized by the scientific literature as an instrument to predict the stability and the lifetime of the prosthetic implant, both for femoral and tibial components. Furthermore, the study raised up possible alternative solutions, such as polyethylene and ceramics. Though the latter showed good long-term results, no recent studies were retrieved (less than 10 years). This aspect could be symptomatic of an obsolescence of such alternative. PEEK material seems a suitable solution because of reduced material stiffness, which may lead to a limited stress shielding. However, further studies on patients are needed to evaluate the benefits and long-term survival of such alternative in a real clinical scenario. Given the successful use of RSA for the assessment of migration and material deformation in presence of alternative materials in other body districts, such application could be extended to a TKR context as well.

Causes of stiffness after total knee arthroplasty: a systematic review

Zaffagnini, ST[1,2], Di Paolo, ST[2], Meena, AM[3], Alesi, DO[1], Zinno, RA[2], Barone, GI[2], Pizza, NI[1], Bragonzoni, LA[2]

[1]IRCCS Istituto Ortopedico Rizzoli, Bologna, Italy
[2]University of Bologna, Italy
[3]Vardhman Mahavir Medical College & Safdarjung Hospital, New Delhi, India

domenicoalesi@ymail.com

Introduction: Total knee arthroplasty (TKA) is a well-established treatment for end-stage osteoarthritis that effectively reduces pain and improves knee functionality. The primary patient's expectations are usually related to pain and joint mobility improvement.
However, about 20% of patients remain "unsatisfied" by the procedure. The main complaints are discomfort or pain referred to the operated joint. A heterogeneous list of possible causes has been proposed. Excluding the most frequent and evident causes, i.e., aseptic or septic loosening and implant failure, there are several other causes with less clear categorization and treatment path. Knee stiffness after total knee arthroplasty (TKA) often leads to pain and discomfort, failing to meet patients' expectations on the surgical procedure. Despite the growing debate on the topic, a comprehensive literature analysis of stiffness causes has never been conducted. Thus, the purpose of the present study was to systematically review the literature regarding the main causes of stiffness after TKA.

Methods and Materials: Pubmed Central, Scopus, and EMBASE databases were systematically reviewed according to the Preferred Reporting Items for Systematic Reviews and Meta-analysis (PRISMA) guidelines for studies on stiffness and pain or discomfort after TKA through November 2020. Overall, 25 articles matched the selection criteria and were included in the study. Clinical relevance and strength of evidence of the included studies were graded using the risk of bias and the methodological index for non-randomized studies quality assessment tools. Two authors (G.B., R.Z.) independently performed the quality assessment for each article. A third author (L.B.) was consulted in case of disagreement.

Results: The main causes of pain and discomfort due to stiffness were surgery-related issues, i.e., component malpositioning and over-voluming, implant loosening, psychological distress, and obesity, which could be considered "modifiable" factors, and expression of profibrotic markers, high material hypersensitivity-related cytokines level, male gender, previous contralateral TKA, and high pre-operative pain, which could be considered "non-modifiable" factors.

Discussion:
Stiffness after TKA might occur for different and, sometimes, multifactorial causes. Possible solutions should be looked for into alternative aspects, e.g., different component material properties and anatomy-based TKA designs. The use of alternative technologies such as surgical robots, anatomy-based devices, and more inert and less stiff component materials could help in reducing stiffness caused by both modifiable and even some non-modifiable factors. Furthermore, early diagnostic detection of stiffness onset could consistently support surgeons in patient-specific decision-making.

Retrieval Analysis of Vitamin E Doped Total Knee Arthroplasty Inserts and Comparison Between Incorporation by Blending versus Diffusion

Tabitha Derr[1], Hannah Spece[1], Daniel W. MacDonald[1], Gregg R. Klein[2], Michael A. Mont[3], Arthur L. Malkani[4], Steven M. Kurtz[1]

[1]Drexel University, Philadelphia, PA, [2]Rothman Institute, Montvale, NJ, [3]Lenox Hill Hospital at Northwell Health, New York City, NY, [4]University of Louisville, Louisville, KY

td627@drexel.edu

Introduction: Vitamin E doping is a popular strategy for reducing free radicals and improving the oxidation resistance of highly crosslinked polyethylene (HXLPE) for orthopaedic devices. The antioxidant can be incorporated either by blending, in which vitamin E is mixed with polyethylene resin powder prior to compression molding, or by diffusing vitamin E into the polyethylene following crosslinking. The purpose of this study was to provide an update to a previously published retrieval analysis of vitamin E polyethylene (VEPE) inserts for total knee arthroplasty (TKA). A secondary goal was to compare the in vivo performance of VEPE components created by diffusion versus blending.

Methods and Materials: 174 TKA inserts were retrieved during revision surgery as part of a multi-institutional implant retrieval program. The cohort represented VEPE formulations from 4 manufacturers with n = 153 manufactured via diffusion and n = 21 via blending. The inserts were evaluated for 7 surface damage mechanisms according to the semiquantitative Hood scoring method. Sample slices approximately 200 µm in thickness were then created using a microtome, and the samples were boiled in heptane for 6 hours and sonicated in water to remove lipids that may have diffused into the material in vivo. The samples were then analyzed for oxidation using Fourier-transform infrared spectroscopy. To compare vitamin E incorporation methods, blended and diffused components were matched on the basis of implantation time, BMI, and age at insertion, resulting in 21 matched pairs for statistical analysis.

Results: The cohort had an average implantation time of 1.1 ± 1.3y and average patient of BMI 32.3 ± 6.6 kg/m2. The components were revised most often for infection (n = 40/174), instability (n = 37/174), and loosening (n = 19/174) and pain (25/174). Across the entire cohort, at least minimal pitting was observed on 99% (n = 146/148) of inserts, at least minor scratching was observed on 97% (n = 143/148), and at least minor burnishing was observed on 95% (n = 140/148). We found a correlation between implantation time and UCLA score (Correlation Coefficient=0.188, p=0.036), condyle articulating OI (Correlation Coefficient=0.533, p<0.001), max OI (Correlation Coefficient=0.322, p<0.001) and total wear (Correlation Coefficient=0.174, p=0.029). Max UCLA score was associated with total wear (Correlation Coefficient=0.246, p=0.006). Comparison between matched blended and diffused components showed no significant difference in total damage score (p=0.53) or scores for the most common damage modes of scratching (p=0.21), pitting (p=0.58), and burnishing (p=0.33). We found no statistical difference in oxidation index (OI) at the A/P surface (p=0.09) or articulating surface (p=0.33). OI at the backside and maximum overall OI were statistically greater in the blended components (p<0.01 and p<0.05), but the actual difference were minimal (mean difference at backside=0.05,mean difference for maximum OI=0.03, p=0.48).

Discussion: In this study we found that infection, instability, pain, and loosening were the primary revision reasons for VEPE TKA inserts. We examined the *in vivo* damage for the retrieved VEPE blended and diffused components and found that certain damage mechanisms (i.e., scratching, pitting, and burnishing) were highly prevalent and did not differ between the vitamin E incorporation methods. Mean oxidation for the entire cohort was below the clinically relevant threshold of 1. We found a weak positive correlation for implantation with oxidation. The differences in OI between blended and diffused components were not statistically or clinically significant.

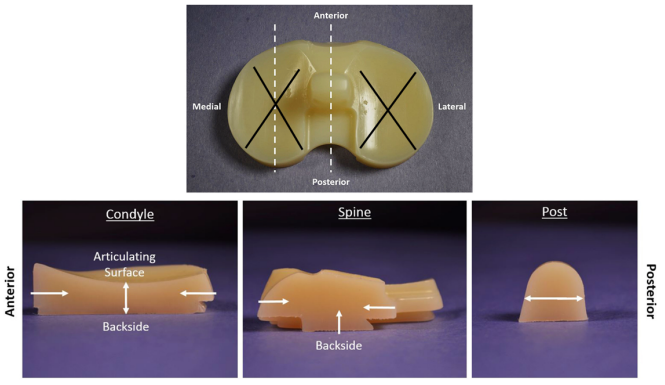

Figure 1: Regions of interest for oxidation index evaluations.

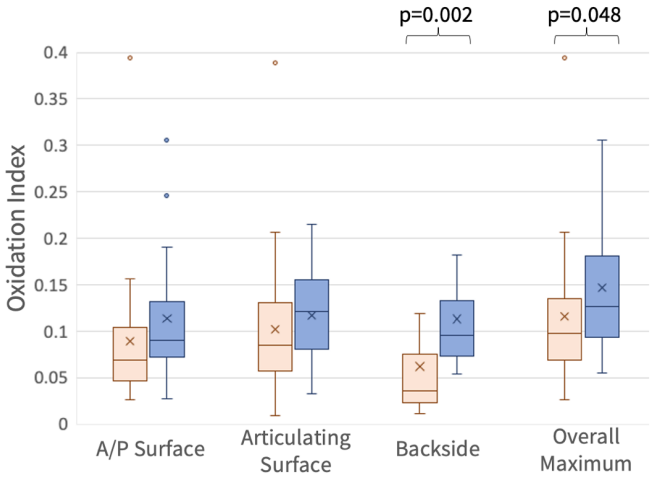

Figure 2: Oxidation index values for diffused (pink) and blended (blue) inserts at different regions of interest.

Fatigue Crack Propagation Assessment of Unfilled and Carbon Fiber Reinforced PEEK using a Compliance Approach

Catherine Mohme, Jay Bensusan, Clare Rimnac
Case Western Reserve University, Cleveland, OH, USA
clare.rimnac@case.edu

Introduction

With PEEK and related formulations being incorporated more frequently into orthopaedic implant devices, such as in spinal applications, and proposed for other applications such as total knee replacement components, it is important to understand how this material behaves in terms of static and cyclic fracture, particularly in the presence of design-related stress concentrations (1). As new medical formulations of PEEK are developed, the comparative fatigue crack propagation behavior of unfilled neat-PEEK and filled-PEEK formulations will be one of the important characteristics to document. Due to its opacity and relatively high stiffness, PEEK is not amenable to a visual approach for tracking crack growth during an FCP test (and such methods are also labor intensive); rather, a more suitable approach is to use a compliance-based methodology.

The objective of this study is to report on a compliance testing approach developed for use with unfilled and filled PEEK formulations.

Materials and Methods

Materials and specimens: Two "exemplar" materials were used in the development of the compliance method approach for FCP characterization of PEEK: extruded and unfilled Ketron 1000 (1000 PEEK); and 30% carbon fiber reinforced Ketron LSG CA30 (LSG CA30 PEEK).

Square and notched compact tension specimens were machined from each material (W= 40 mm, b = 10 mm). The initial normalized notched length (a/W) was 0.30.

Serial sharpening method to establish compliance relationship: To generate the compliance relationship between normalized fatigue crack length (a/W) and normalized compliance (U), serial sharpening was conducted on one specimen from each group. Crack mouth opening displacement (CMOD) was attained with an extensometer attached on the front face of the specimen using rubber bands. The specimen was cycled at a constant ΔP and for blocks of approximately 100 cycles. The notch was then repeatedly manually extended with a custom machined punch in increments of 0.5mm, each time being cycled for about 100 cycles. This procedure was continued until the notch had been extended approximately 10mm. With the recorded data, the normalized compliance was calculated and plotted versus a/W. Using the Instron software WaveMaker, a program was developed to record the compliance: every 1,000 cycles between 0 - 10,000 cycles; every 10,000 cycles after 10,000 cycles; or, each time the compliance changed by 1.5 x 10^{-5} (for 1000 PEEK) or 1.0 x 10^{-6} (for LSG CA30 PEEK).

FCP testing: Specimens were razor sharpened at least 24 hours prior to testing. FCP tests (n= 3 per group) were conducted on an Instron servo-hydraulic test system (2). Testing was conducted in air at 3 Hz, with a sinusoidal waveform and an R-ratio = 0.1. CMOD was monitored during testing with an attached extensometer, from which the normalized compliance was calculated (3). Using the compliance curve generated from serial sharpening, the fatigue crack growth rate, da/dN, was found. The fatigue crack growth rate, da/dN vs. the cyclic stress intensity factor, ΔK, was then determined. Linear regression of the log-log transformed data was used to determine the coefficient (C) and exponent (m) of the Paris relationship ($da/dN = C\Delta K^m$). The Paris regime was defined from a crack growth rate (da/dN) of 10^{-4} mm/cycle to 10^{-2} mm/cycle. $\Delta K_{inception}$ was visually estimated from the pooled da/dN v. ΔK curves for each group.

The fracture surface appearance for each group was documented using scanning electron microscopy (20kV).

Results

Using the compliance method, the da/dN vs. ΔK vs. behavior was successfully generated for both materials with good consistency between specimens in each group (Fig. 1). The carbon fiber reinforced PEEK (LSG CA30 PEEK) demonstrated initially better FCP resistance compared with the unfilled PEEK (1000 PEEK) material in the low ΔK and intermediate (Paris) regimes, with reduced resistance in the high ΔK regime. For the unfilled PEEK, the power-law relationship in the Paris regime was determined to be $da/dN = 1.1x10^{-7}(\Delta K)^7$. The low ΔK region was also nicely captured, with $\Delta K_{inception}$ estimated as 2.5 $MPa(m)^{1/2}$. For the carbon fiber reinforced PEEK, the power-law relationship in the Paris regime was determined to be $da/dN = 1.9x10^{-11}(\Delta K)^{14}$. Though the low ΔK regime was not well-captured for this group, a $\Delta K_{inception}$ around 2.9 $MPa(m)^{1/2}$ is suggested from the data.

The fracture surface of the unfilled PEEK was flat, with characteristic parabolic markings associated with crack front pinning at inclusions or particles (Fig. 2). For the carbon fiber reinforced PEEK, randomly oriented carbon fibers can be seen on the fracture surface, resulting in a rougher, more tortuous fracture path (Fig. 3), as-expected. The interface between the carbon fibers and the polymer matrix was not uniform; the carbon fibers were often not strongly attached to the polymer matrix.

Discussion

PEEK is not amenable to a visual approach for tracking crack growth during an FCP test; in addition, visual crack growth methods are labor intensive. In this study, we established that an automated compliance-based approach

can be successfully employed to determine the FCP behavior of unfilled and filled PEEK materials, even in the low ΔK regime. The procedure should be applicable to any PEEK formulation, regardless of manufacturing method, provided that a specimen can be devoted to serial sharpening. (We have also found that sufficient compliance data can also be obtained from the same specimen used to generate fatigue crack growth.) Limitations of this study include the use of non-medical PEEK materials as "exemplars" in this study.

This approach could be particularly useful in the evaluation of FCP behavior of 3D-printed PEEK constructs; we have successfully accomplished this, though side-grooves are needed in some build orientations to keep crack growth in-plane.

References

(1) S Kurtz, PEEK Biomaterials Handbook, 2012; (2) ASTM E647; (3) ASTM E1820.

Acknowledgements

W.J. Austin Chair (CMR).

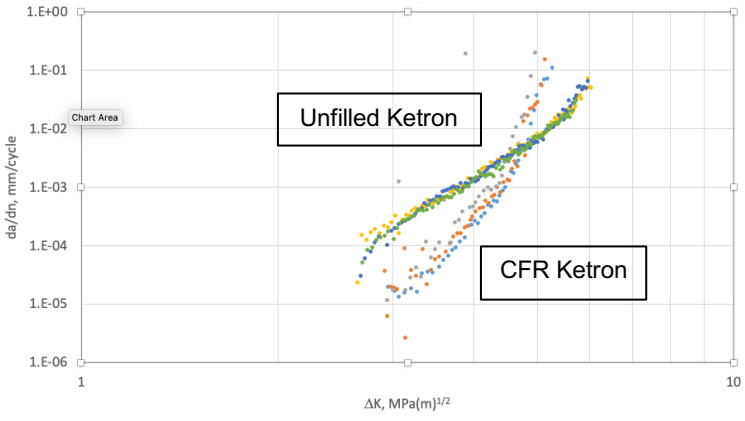

Figure 1. FCP Behavior of unfilled (1000 PEEK) and carbon fiber reinforced (LSG CA30 PEEK) PEEK.

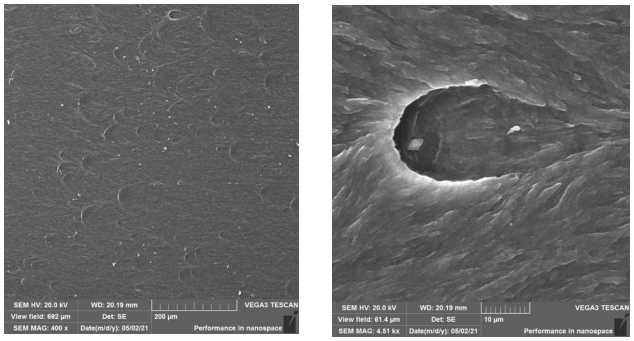

Figure 2. Scanning electron fractography images of unfilled PEEK showing (Left) flat fracture surface and characteristic parabolic markings associated with (Right) pinning of the crack front around particles or inclusions. Crack growth is from left to right.

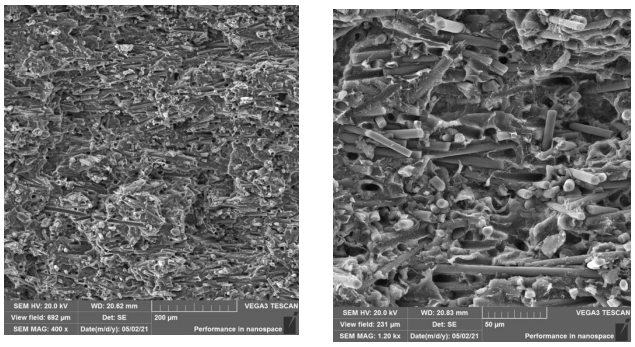

Figure 3. Scanning electron fractography images of carbon fiber reinforced PEEK showing (Left) rough fracture surface associated with randomly oriented carbon fibers having (Right) heterogeneous and often poor adhesion to the polymer matrix. Crack growth is from left to right.

Enhanced Pre-Clinical Wear Simulation of an All-Polymer Total Knee Replacement

Cowie RM[1], Schwiesau J[2], Briscoe A[3], Jennings LM[1]
[1]Institute of Medical and Biological Engineering, University of Leeds, UK. [2]Aesculap AG, Tuttlingen, Germany. [3]Invibio Ltd., Lancashire, UK.
r.cowie@leeds.ac.uk

Introduction: Experimental wear simulation of an all-polymer, PEEK-OPTIMA™-polymer on-UHMWPE total knee replacement has shown comparable wear rates to conventional implant materials under a walking gait cycle.[1] The aim of this study was to expand the envelope of test conditions to investigate wear under activities of daily living and under third body wear conditions.

Methods and Materials: PEEK-OPTIMA™ polymer (Invibio ltd, UK) and cobalt chrome (CoCr) (Maxx Orthopedics, Inc), cruciate retaining, fixed bearing femoral components of similar initial surface topography and geometry against all-polyethylene tibial components (GUR1020, conventional, EO sterile, Maxx Orthopedics, Inc) were investigated in two 6 station ProSim electromechanical knee simulators. The lubricant used was 25% bovine serum + 0.03% sodium azide and the studies carried out under room temperature conditions. Wear of the UHMWPE tibial components was determined by gravimetric analysis.

Activities of daily living: 5 million cycles (MC) of wear simulation was carried out under displacement controlled, Leeds high kinematic conditions representative of a walking gait cycle,[1] the same implants were subsequently investigated under a stair ascent profile for 2 MC,[2] N=6.

Third body wear simulation: Third body particles of interest were porcine cortical bone and PMMA sieved within a size range of 500-1000 μm.[3] Initially, 1MC simulation was carried out under a gait cycle to set a baseline wear rate for this implant (N=3 for PEEK and CoCr). 1MC of wear simulation was then carried out with bone particles added to the lubricant followed by an additional 1MC with PMMA particles. Gravimetric analysis of the UHMWPE tibial components was carried out every 0.3MC and particles were replenished at each measurement point.

Statistical analysis compared PEEK to CoCr using ANOVA with significance taken at $p<0.05$.

Results: The wear of the UHMWPE tibial components under the different conditions is shown in Figures 1 & 2. Under walking gait conditions in clean and contaminated lubricant, there was no significant difference ($p>0.05$) in UHMWPE wear between the different implant materials; under stair ascent conditions, the wear of UHMWPE was higher against PEEK than CoCr although the wear rates were low (<5mm^3/MC). Scratching was visible on the PEEK components for all the conditions investigated. When contaminated with PMMA particles, the lubricant in the metal-on-polyethylene study had a darker appearance, no visible change was apparent in the all-polymer study.

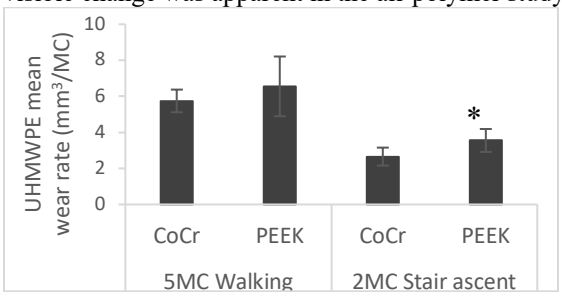

*Figure 1: Mean wear rate ± 95% confidence limits of UHMWPE tibial components after 5MC walking and 2 MC stair ascent (N=6). * denotes p<0.05.*

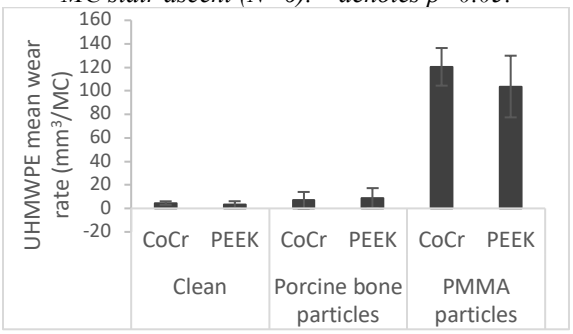

Figure 2: Mean wear rate ± 95% confidence limits of UHMWPE following third body wear simulation (N=3).

Discussion: There was no significant difference in UHMWPE wear rate components articulating against PEEK or CoCr under a walking gait cycle. Under stair ascent, the wear rate was higher against PEEK but the wear rates remained low. Scratching on the PEEK implants had no influence on wear rate which remained linear over the duration of the study.

The introduction of bone particles into the test cell resulted in a similar wear of UHMWPE to clean lubricant; with harder PMMA particles, there was an increase in wear rate for both material types. There was no significant difference in wear rate of UHMWPE articulating against the different femoral component materials when contaminated with either particle. The change in lubricant for the metal-on-polyethylene study when challenged with PMMA particles suggests release of metal particles, the release of PEEK particles is unknown.

Under the majority of conditions investigated, the wear of UHMWPE was similar against PEEK and CoCr femoral components.

References: [1]Cowie RM, et al. 2016, JEIM, 230(11):1008-1015. [2]Abdelgaied A, et al. J Mech Behav Biomed Mater, 78, 282-291. [3]Schroeder C, et al. 2013, J Mater Sci: Mater in Med 24(5):1319-1325

In Vitro Wear Performance of X-ray Cross-Linked Vitamin E Blended Polyethylene

M.A. Mulliez[1,2,*], R.M. Bargon[1], B. Fritz[1], M. Holderied[1], C. Schilling[1], T.M. Grupp[1,2]
[1]Aesculap AG, Research & Development, 78532 Tuttlingen, Germany
[2]Ludwig Maximilians University, Department of Orthopaedics Surgery, Physical Medicine & Rehabilitation, Campus Grosshadern, 81377 Munich, Germany

Introduction: Radiation crosslinking of UHMWPE has been introduced by Oonishi to improve the wear performance of hip prostheses.[1] Since the early attempts to improve the wear behaviour of UHMWPE different approaches have been undertaken to improve wear properties of UHMWPE by different physical (gamma radiation or electron beam) and chemical crosslinking methods.[2,3] One problem after crosslinking are remaining radicals that can entail severe oxidation and brittleness of the polymer and implant.[4] Instead of remelting after crosslinking of the virgin UHMWPE the blending with Vitamin E or the diffusion of Vitamin E have been introduced to trap free radicals after crosslinking.[5,6] However, conventional radiation methods like electron beam and gamma involve disadvantages: The penetration depth of electron beam radiation which is a particle radiation and leads to scattering of the electrons inside the polymer is limited to circa 40 mm.[7] Larger dimensions of moulded or extruded parts must be discarded rendering in some cases this technique less economical. Gamma crosslinking implies a limited ^{60}Co source and has comparatively the lowest dose rate among the three radiation methods that can not be adjusted due to the origin of the radiation.[8] X-ray crosslinking is an upcoming method that lies in terms of crosslinking density at comparable dose in between electron beam and gamma radiation.[9,10] We were interested to examine the wear properties of Vitamin E blended UHMWPE hat has been crosslinked by X-ray irradiation at different temperatures.

Methods and Materials: Titanium Plasmafit® Poly Cups size 54 (Aesculap AG, Tuttlingen, Germany) were taken as acetabular cups and articulated against cobalt chromium (CoCr) femoral heads (taper 12/14). UHMWPE processing was modified regarding the radiation dose (80 kGy vs. 100 kGy) and the processing temperature (room temperature vs. warm). Prior to testing, inserts have been subjected to accelerated ageing according to ASTM F2003 for two weeks The tests were performed with the largest (40 mm diameter) and thinnest (5 mm) inserts to simulate a worst case. The acetabular inserts have been tested on a customized 6 + 2 (loaded soak controls) stations servohydraulic hip simulator (Endolab GmbH, Thansau, Germany) with kinematic and load patterns according to ISO 14242-1 for 5 million cycles (mc) at a frequency of 1 Hz in diluted newborn calf serum with a protein content of 30 g/l and incubated at 37 °C. Following accelerated aging the inserts were soaked in the test medium to achieve fluid saturation. Additionally loaded soak controls were subjected only to axial load to detect fluid absorption during the test. The wear of the remaining specimens was determined gravimetrically in relation to the loaded soak controls. The measurement of the gravimetrical changes was performed after 0.5, 1, 2, 3, 4 and 5 million cycles. The wear rates were calculated as per ISO 14242-2 using the least squares linear fit relationship between the net mass loss after 5 million cycles and the number of loading cycles (5 million) excluding the zero time point. The articulation surface and the back side of the polyethylene inserts underwent an optical analysis after 5 million cycles using a digital microscope (VHX-5000, Keyence Corporation, Osaka, Japan) with a 30-fold magnification for the former and a 20-fold magnification for the latter. The geometrical alterations due to creep and wear after 5 million cycles were assessed by means of a 3D measuring machine (UMM850, Carl Zeiss AG, Oberkochen, Germany) in a tactile measuring mode (1500 points per scan). The geometrical changes were displayed vertically to the transversal plane of the polyethylene inserts with a pseudo-color mode. The uni-axially loaded soak controls exhibited a creep deformation which was responsible for the initial three dimensional changes. The creep was subtracted from the overall deformation to obtain the linear wear. For each insert the deformation was calculated as the mean value of the color range at the deepest position.

To determine the wear amount and the wear rates an analysis of variance ANOVA was carried out ($p < 0.05$) followed by a post hoc test to differentiate between the five material groups (Tukeys HSD-Test, $p < 0.05$). Prior to analysis, the normal distribution (p-p plots) and the homogeneity of variance (Levene Test) were verified (Statistica R13, TIBCO Software Inc.). A p value < 0.05 was considered as significant.

Results: The wear simulation test revealed a wear rates of 11.3 ± 0.7 mg/mc for X(80 kGy)-RT, 7.5 ± 0.3 mg/mc for X(100 kGy)-RT, 5.1 ± 0.8 mg/mc for X(80 kGy)-warm, and 2.6 ± 0.1 mg/mc for X(100 kGy)-warm respectively, corresponding to a 34% (at RT) and 50% (warm) lower wear rate for the material cross-linked with 100 kGy compared to 80 kGy. A similar observation could be made with the irradiation temperature with less wear for the warm irradiated material. X(80 kGy)-warm exhibited 55% less wear than X(80 kGy)-RT and X(100 kGy)-warm 66% less than X(100 kGy)-RT respectively (see Figure 1).

Figure 1. Gravimetric wear rate of the four X-ray cross-linked UHMWPE groups compared to e-beam irradiated Vitelene® as clinical established reference interpolated from data between 0.5 and 5 million cycles.

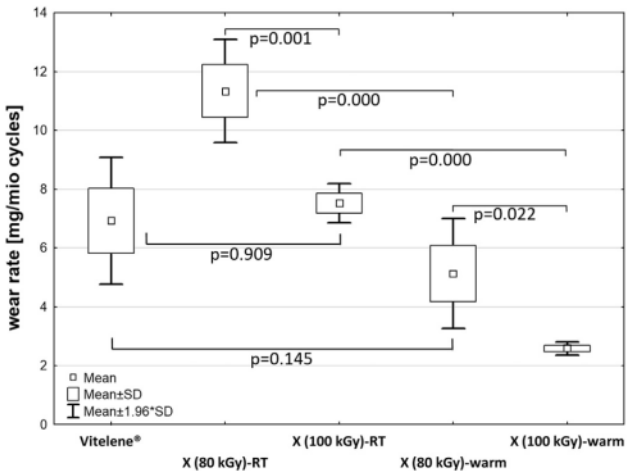

Discussion: The irradiation temperature and the dose have been found to affect significantly the wear behavior of the vitamin E blended X-ray cross-linked polyethylene, with the temperature having a bigger effect than the dose. Enhancing the dose and increasing the temperature led to a reduced wear rate. This outcome corroborated the observations of Oral et al.[11] that electron beam radiated vitamin E blended polyethylene at elevated temperature resulted in improved wear resistance.

References

1 Oonishi H, Takayama Y, Tsuji E. Improvement of polyethylene by irradiation in artificial joints. *International Journal of Radiation Applications and Instrumentation. Part C. Radiation Physics and Chemistry* 1992; **39:** 495–504. https://doi.org/10.1016/1359-0197(92)90102-L.

2 Bistolfi A, Giustra F, Bosco F, et al. Ultra-high molecular weight polyethylene (UHMWPE) for hip and knee arthroplasty: The present and the future. *J Orthop* 2021; **25:** 98–106. https://doi.org/10.1016/j.jor.2021.04.004.

3 Grupp TM, Holderied M, Mulliez MA, et al. Biotribology of a vitamin E-stabilized polyethylene for hip arthroplasty - Influence of artificial ageing and third-body particles on wear. *Acta Biomater* 2014; **10:** 3068–78. https://doi.org/10.1016/j.actbio.2014.02.052.

4 Muratoglu OK, Harris WH. Identification and quantification of irradiation in UHMWPE throughtrans-vinylene yield. *J. Biomed. Mater. Res.* 2001; **56:** 584–92. https://doi.org/10.1002/1097-4636(20010915)56:4<584::AID-JBM1131>3.0.CO;2-Y.

5 Bracco P, Oral E. Vitamin E-stabilized UHMWPE for total joint implants: a review. *Clin Orthop Relat Res* 2011; **469:** 2286–93. https://doi.org/10.1007/s11999-010-1717-6.

6 Gigante A, Bottegoni C, Ragone V, Banci L. Effectiveness of Vitamin-E-Doped Polyethylene in Joint Replacement: A Literature Review. *J Funct Biomater* 2015; **6:** 889–900. https://doi.org/10.3390/jfb6030889.

7 Mittendorfer J, Niederreiter M. Intrinsic dose characteristics in electron beam irradiation. *Radiation Physics and Chemistry* 2020; **177:** 109124. https://doi.org/10.1016/j.radphyschem.2020.109124.

8 Chmielewski AG, Al-Sheikhly M, Berejka AJ, Cleland MR, Antoniak M. Recent developments in the application of electron accelerators for polymer processing. *Radiation Physics and Chemistry* 2014; **94:** 147–50. https://doi.org/10.1016/j.radphyschem.2013.06.024.

9 Mulliez MA, Schilling C, Grupp TM. Equivalent mechanical properties of X-ray and E-beam cross-linked vitamin E blended ultrahigh molecular weight polyethylene. *J Biomed Mater Res B Appl Biomater* 2020; **108:** 2131–40. https://doi.org/10.1002/jbm.b.34552.

10 Bracco P, Brunella V, Zanetti M, Luda MP, Costa L. Stabilisation of ultra-high molecular weight polyethylene with Vitamin E. *Polymer Degradation and Stability* 2007; **92:** 2155–62. https://doi.org/10.1016/j.polymdegradstab.2007.02.023.

11 Oral E, Neils AL, Rowell SL, Lozynsky AJ, Muratoglu OK. Increasing irradiation temperature maximizes vitamin E grafting and wear resistance of ultrahigh molecular weight polyethylene. *J Biomed Mater Res B Appl Biomater* 2013; **101:** 436–40. https://doi.org/10.1002/jbm.b.32807.

Experimental and Computational Modelling Assessment of Edge Loaded Marathon Total Hip Replacement Liners.

Cooper, N[1]; Etchels L[1]; O'dwyer Lancaster-Jones, O[2]; Williams, S[1]; Wilcox, R[1]
[1]Insitute of Medical and Biological Engineering, University of Leeds, Leeds, UK. [2]DePuy Synthes Joint Reconstruction, Leeds, UK.
mnnco@leeds.ac.uk

Introduction: Non-optimal clinical alignment of components in total hip replacements (THRs) may lead to edge loading of the acetabular cup liner. In particular, high cup inclination angles or cup centre mismatch result in the separation between the head and liner during the swing phase[1]. This has the potential to cause changes to the liner rim that are not accounted for in standard wear models. A greater understanding of the material behaviours could be beneficial to inform design and surgical guidance for THR devices. The aim of this research was to combine both finite element (FE) modelling and experimental simulation including microstructural assessment by Raman Spectroscopy to examine material behaviour changes during edge loading.

Materials and Methods: A dynamic deformable FE model (Abaqus v6.14, Dassault Systémes, France), matching the experimental conditions, was created to simulate the stress strain environment within liners. An elastic-plastic material model representing Marathon UHMWPE properties (linear elastic modulus 677 MPa, yield stress 8.4 MPa) was applied to the liner. Mesh convergence and mass scaling sensitivity studies were performed. Five Marathon Pinnacle liners (36 mm, neutral) (DePuy Synthes Joint Reconstruction, Leeds, UK) were tested for 4 Mc (million cycles) of standard loading (ISO14242:1) followed by 3 Mc of edge loading with dynamic separation (ISO14242:4) in an Electromechanical Prosim hip simulator (Simsol, Stockport, UK). Microstructural measurements by Raman spectroscopy (inVia, Renishaw, Wotton-under-Edge, UK) were taken at unloaded and highly loaded rim locations informed by the FE results. Amorphous and crystalline phase percentages were determined using peaks located at 1303 cm^{-1} and 1414 cm^{-1}, respectively, normalized against an internal standard at 1295 cm^{-1}. The intermediate phase is determined by the remaining mass fraction. Gravimetric (XP205, Mettler Toledo, Columbus, Ohio, US) and geometric measurements (Legex CMM, Mitutoyo, Kawasaki, Kanagawa, Japan) were taken every 1 Mc.

Results: Under edge loading, peak Mises stress and plastic deformation occur below the surface of the rim during heel strike (Figure 1A). After 7 Mc, microstructural analysis determined edge loaded regions had an increased crystalline mass fraction compared to unloaded regions ($P<0.05$) (Figure 1B). Both amorphous and intermediate phases decreased in percentage, but differences were not determined to be statistically significant ($p>0.05$). Gravimetric wear rates of 12.5 mm^3/Mc and 22.3 mm^3/Mc were determined for standard and edge loading periods, respectively. A liner penetration of 0.37 mm was measured after 7 Mc.

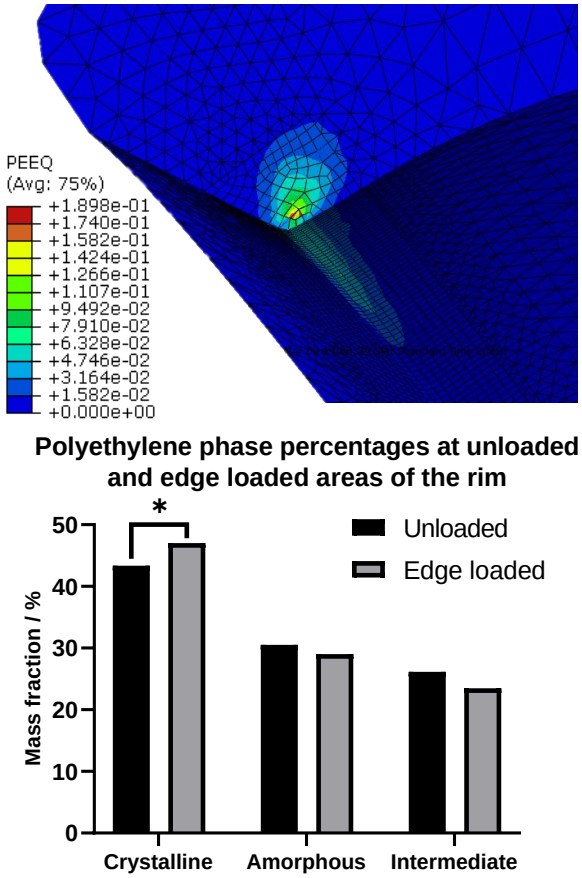

Figure 1. (A) Equivalent plastic strain accumulation during one cycle. (B) Microstructural analysis of unloaded and edge loaded regions on the rim (*$P<0.05$).

Discussion: Edge loading led to an increase in gravimetric wear rate indicating a different wear mechanism is occurring. The FE and Raman results suggest that changes to material behaviour at the rim could be possible. These methods will now be used to assess more liners and over a larger number of cycles of edge loading. All the tools presented are capable of non-destructively assessing the progression of material changes in liners. They have potential to explore the impact of edge loading on different surgical and patient variables.

References:

1. Partridge, S. et al. Evaluation of a new methodology to simulate damage and wear of polyethylene hip replacements subjected to edge loading in hip simulator testing. J. Biomed. Mater. Res. - Part B Appl. Biomater. 106, 1456–1462 (2018).

Conflicts of interest:

Authors on this publication receive research funding or are employed by DePuy Synthes Joint Reconstruction.

Evaluation of mechanical properties of PEEK filled materials and nanoscale observations

Siskey, RL[1] and Davis, MS[1]
[1]Exponent, Philadelphia, PA
rsiskey@exponent.com

Introduction: Filler materials are commonly added to polyetheretherketone (PEEK) to improve material performance across a variety of industries, from aerospace, automotive, and biomedical applications. In this work, PEEK was examined with mechanical testing techniques such as tensile, impact, and fatigue testing. Then, samples were observed with optical microscopy, SEM, and subsequently probed for nanoscale behavior using microhardness and nanoindentation. The matrix-filler interactions provide the increased strength properties for the filled materials, and cross-sections were imaged to view these relationships. Understanding the response of PEEK materials, particularly when filled with carbon fiber or glass, will aid in failure analyses and failure prevention across industries, especially the biomedical field where materials are subjected to various loading conditions.

Methods and Materials: Neat PEEK, carbon fiber-filled PEEK, and glass-filled PEEK were purchased as raw material in plaque form. Samples were created from each set of material with proper ASTM dimensions for tensile, impact, and fatigue crack propagation testing. Each material was subsequently tested using standard methods and the results were analyzed. Following testing, fracture surfaces were viewed with optical microscopy and SEM. Additionally, specimens were polished using standard metallographic techniques to view bulk structure and the area of fracture for each materials type and failure mode. Samples were then probed with Vickers microhardness and nanoindentation.

Results: The various testing performed for each material type (neat, carbon fiber-filled, and glass-filled PEEK) showed that fillers added to PEEK material improved strength properties and increased fatigue resistance. Observations of the fracture surfaces showed fiber-matrix interactions that were dependent on failure mode, although fatigue is not as clear as it appears in neat PEEK and is continued to be studied. Cross-sections showed how the filler materials affect the fractured surface behavior; in general, filler material directionality greatly affects crack behavior as a strengthening mechanism when cracks follow paths of lowest energy. Figure 1 shows a cross-section of carbon fiber-filled PEEK after tensile testing. The lighter areas on the image show the carbon fiber, which has an inherent anisotropy based on the sample preparation and directionality chosen for test specimens. The fracture surface tends to follow the path of the filler materials. Similar visual trends were seen for impact and fatigue samples. Microhardness proved only useful for neat PEEK; the size of the indent showed that there were interactions with matrix and filler material with the indenter tip, attributing to sample error. Figure 2 shows a comparison of the indents after testing. A Vickers indent should leave a diamond-shaped impression on the material, which is then used in the hardness calculations. Analyzing the microscale is difficult because the fiber-matrix interactions are at a smaller scale than the Vickers indent. However, probing at the nanoscale elucidated differences in properties for the filler materials separate from the bulk.

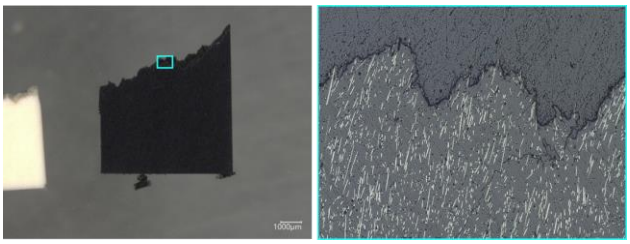

Figure 1. Carbon fiber-filled PEEK specimen after tensile testing and prepared as a cross section (left); higher magnification image of the fracture surface of the PEEK material indicating the filler materials and fracture path (right).

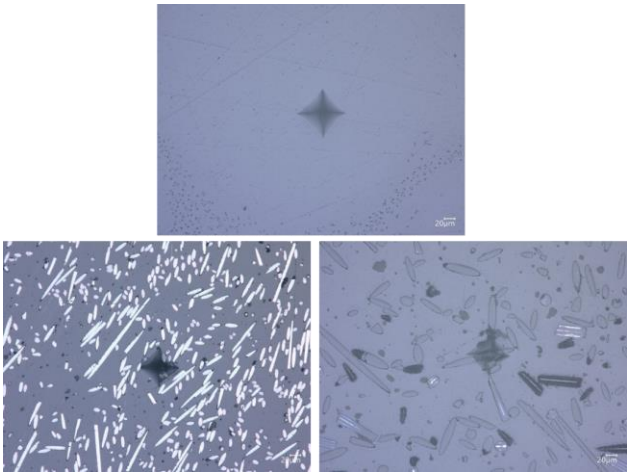

Figure 2. Microhardness indentation on neat (top), carbon fiber-filled (left), and glass-filled PEEK (right).

Discussion: Filled materials are selected based on improved mechanical properties, but to fully characterize material behavior, the nanoscale interactions must be considered. Mechanical testing of PEEK with filler materials showed the improved properties with carbon fiber or glass. Fractography of the fatigue surfaces continues to be investigated because the filled material does not respond with typical beach marks and striations as seen in neat PEEK. Cross-sectional analysis and additional mechanical testing provide an understanding of the mechanisms occurring at the micro- and nanoscale that translate to the bulk material properties. In all, this work continues to provide an atlas of fracture surfaces for PEEK materials through different failure modes and adds to the overall investigation by showing the nanoscale fiber interactions when examined in cross-sectional views.

Additive Manufactured PEEK Scaffold: Understanding the AM Process Capability

Seyed Ataollah Naghavia[1], Changning Sun[2], Ling Wang[2], Chaozong Liu[1*]
[1] Institute of Orthopaedic & Musculoskeletal Science, University College London, London, UK
[2] State Key Laboratory for Manufacturing Systems Engineering, Xi'an Jiaotong University, Xi'an, China
Chaozog.Liu@ucl.ac.uk

Introduction: PEEK is a biomaterial that has good resistance and stability of PEEK allowing it to be implanted into human body and stay for long period. Its elastic modulus (3 GPa) and yield stress (110 MPa) are closer to those of human bone compared to biomedical metal materials such as titanium-based alloys, cobalt-based alloys and stainless steel, effectively reducing the stress shielding with sufficient load-bearing capacity. PEEK is radiolucent so that there are no artefacts on X-rays which can be detrimental to post-operative examination. With these advantages, PEEK have emerged as the promising biomaterials for the reconstruction of large bone defects, such as skull, maxillofacial reconstruction, rib and spinal cages, as well as joint implants, by using additive manufacturing technology. However, in-depth understanding the effect of AM process capability on the results implants to achieve precision "implant" is an important aspect in translation. This paper examined the morphological deviation of AM PEEK porous scaffold from the design and analysed its impact on the mechanical property. It provides an insight in design, manufacturing, and clinical translation of AM technology.

Methods and Materials: Porous PEEK scaffolds were fabricated by using a fused filament deposition technique (Engineer 200, Jugao AM, China). All scaffolds were built by the same orthogonal structure with a unit cell size of 0.8 mm, a pore size of 0.4 mm and struct size of 0.4 mm, thus the porous part of the scaffolds had a nominal porosity of 50%. The fabricated PEEK samples were scanned and their morphology was characterized using a Nikon XTH 225 ST micro-computed tomography (micro-CT). Mechanical properties including compressive, tensile, 3-points bending and torsional strength were performed according to ISO 13314:2011 procedures. The FE modelling of compression, tension and three-point bending, and torsional scaffolds were performed to determine the theoretical mechanical properties.

Results: The morphological characterization of the resultant scaffold by micro-CT revealed that that the averaged measured strut thicknesses (0.31 ± 0.01) are thinner than the designed value of 0.4 mm and have a percentage error of approximately 22 % between the two values due to the struts shrinkage after printing and getting fully solid. The shrinkage in strut thickness results in a larger pore size of the printed scaffolds. The averaged measured pore size (0.46 ± 0.03) is thicker than the designed value of 0.4 mm. This reduction of strut thickness and increase of pore size resulted in a higher porosity (61%) than the designed porosity (50%). Surface to volume ratio of the printed scaffold was also measured to be 8.08 mm^(-1) which is larger by less than 7% compared to the designed scaffold (7.56 mm^{-1}).

The mechanical testing and FE modelling demonstrated that the printed PEEK scaffolds have lower mechanical properties than that of FE values (Fig 1). FE modelling revealed a smooth transition of forces from the vertical structs to the horizontal struts in all mechanical testing.

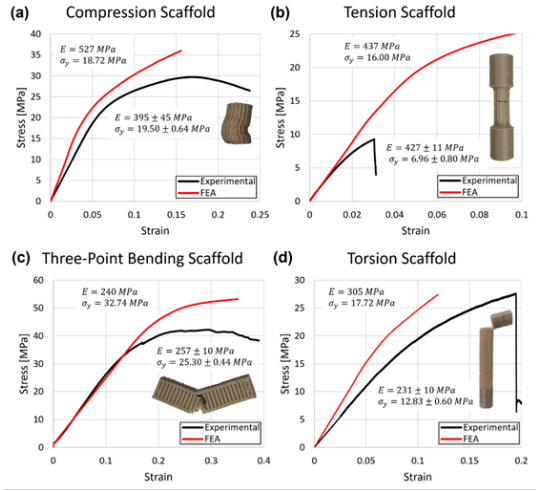

Fig 1. Stress-strain curve of experimental and FE model in compression (a), tension (b) and three-point bending scaffolds (c), torsion (d)

Discussion and Conclusion: Overall, a good consistency in the mechanical testing data for all samples with a smooth transition from elastic to plastic region. With filament 3D printing, there will always be a small gap between the outer edge of any two overlaying layers which can act as stress concentrators and initiate crack. The good consistency in the mechanical testing data for all samples with a smooth transition from elastic to plastic region. This suggests FEA provides a viable method for predicting the mechanical properties of PEEK porous structure for different designed porosity and unit cells. The mechanical properties of the PEEK porous structure specimens designed with 50% porosity were in similar range of cancellous bone of human body, and all the PEEK specimens exhibited ductile fracture modes under different loading patterns. The porous structure is beneficial of improving osseointegration of PEEK implant, but the weak mechanical properties present a challenge for the design and AM.

Acknowledgement: The study was financially supported by EU via the H2020-MSCA-RISE-2016 program (734156).

Adjustment of simulation models for essential work of fracture tests of polymeric materials intended for biomedical applications

Pascual, F.J.[1,2], Jiménez, R[1]., Ibarz, E.[2,3], Gracia, L.[2,3], Puértolas, J.A.[2]
[1]*Centro Universitario de la Defensa de Zaragoza, Spain.*
jpascual@unizar.es
[2]*Instituto Universitario de Investigación en Ingeniería de Aragón, I3A, Universidad de Zaragoza, Spain*
[3]*Departamento de Ingeniería Mecánica, Universidad de Zaragoza, Spain*

Introduction: This work is intended to correlate experimental results obtained from Essential Work of Fracture (EWF) tests with the numerical modeling of the problem by the Finite Element Method (FEM), allowing the fine adjustment of the model and subsequent extrapolation to more complex situations. The work focuses on ultrahigh molecular weight polyethylene (UHMWPE), commonly used as an interposition material in TKR and THR surgeries.

In contrast with more complex J-based methods, EWF method in expected to provide an alternative route for providing an accurate metric for toughness, because of its simple experimental development. In addition, to assure a robust and efficient FEM model could lead to more accurate simulations. Nowadays, commercial UHMWPE grades are usually modified by gamma irradiation and subsequent heat treatments to reach a compromised balance between wear resistance, oxidation stability and mechanical properties, including toughness.

In this work, a cautious selection of UHMWPE based materials is used to check the proposed FEM model considering the aforementioned factors in order to contrast the proposed numerical model.

Methods and Materials: Medical grade UHMWPE is considered for the experimental section. Specifically, Celanese's GUR 1050 is used with molecular weights between 5-6 Mg/mol, with low calcium content. The material was supplied in plate form by Orthoplastics (UK). The heat treatments were carried out in an LTE Qualivac (UK) vacuum oven. DDENT specimens were machined at the Precision Mechanics Service of the University of Zaragoza. Its dimensions were 85x25x3 (mm3) in length, width and thickness, respectively, with a ligament width that varies from 5-12 mm, in increments of 1 mm.

The EWF test system was implemented on an INSTRON 5565 universal test machine. Because of toughness is a highly sensitive property to crosslinking and stabilization treatments, the correlation with the basic properties obtained from the uniaxial tensile test is very significant. From the specimens tested by EWF, 3 mm diameter cylinders were extracted for study by differential scanning calorimetry (DSC).

For the simulation using FEM, a three-dimensional geometric model is generated with the dimensions of the test specimens. Subsequently, a meshing is carried out by means of three-dimensional elements, being progressive in the area of stress concentration at the edge of the crack (Figure 1), and the contour conditions corresponding to the test arrangement (fixation in a jaw and imposed displacement on the contrary) are specified. A bilinear elastoplastic model is used and adjusted to experimental results from tensile tests on standardized specimens.

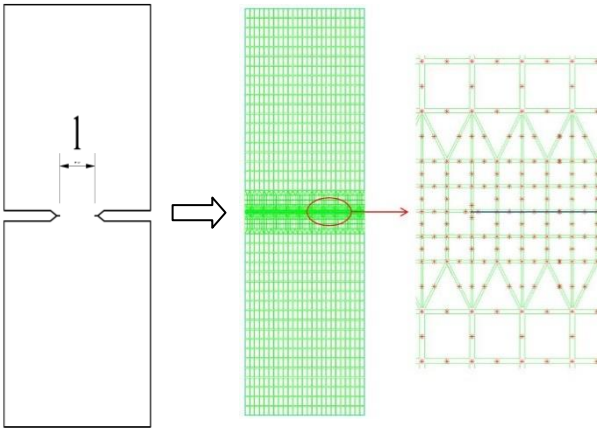

Figure 1. DDENT sample and proposed FEM geometric model.

Results: The size of the plastic zone and the value of the integral J for each specimen model can be determined using numerical simulations. The degree of adjustment between the results obtained in the numerical simulations with those available from the experimental tests is then verified. Based on the results obtained, the correlation coefficients are determined, establishing a minimum threshold value, below which the numerical models are reviewed until an adequate adjustment is obtained.

Figure 2 shows the maps of vertical displacement and strain on the deformed one (amplified by a factor of 5) of the 5 mm ligament specimen. In addition to the opening of the crack, there is a noticeable loss of thickness just at the edge of the crack, which increases as the test progresses. The opening shape of the crack is of parabolic type, with a vertex located on the edge itself.

Regarding the stress field, the expected concentration occurs at the edge of the crack, causing a localized yield

that evolves during the test. In addition, the results support the use of two-dimensional flat tension models, given the uniformity of tensions and equivalent plastic deformation obtained in the crack front.

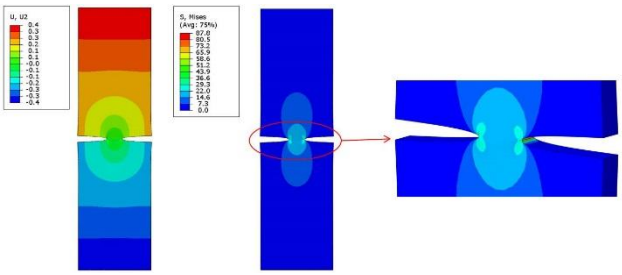

Figure 2. Strain and stress fields near the crack tip.

Once the models have been calibrated, they can be used for specimens with different sizes of ligament and thickness, to verify the fulfillment of the flat tension conditions required in the test.

Discussion: An adequate correlation between the experimental and the numerical displacement field is verified, which allows to infer the areas of greater plasticity. The validity of this hypothesis is checked, in addition to comparing the numerical values, by image analysis.

The main novelty of the work is to use the simulation by FEM applied to EWF tests schemes, to obtain behavioral models for different UHMWPE based materials.